GWPF - STATE OF THE CLIMATE 2023

Ole Humlum

Manuscript version, February 5, 2024.

Ole Humlum is former Professor of Physical Geography at the University Centre in Svalbard, Norway, and Emeritus Professor of Physical Geography, University of Oslo, Norway.

Contents:

31: Written references, Links to data sources

General overview 2023

This report has its focus on observations, and not on output from numerical models, with few exceptions (e.g., Figure 47). References and data sources are listed at the end of the report. The observed data series presented here reveals a vast number of natural variations. The existence of such natural climatic variations is not always fully acknowledged, and therefore often not considered in contemporary climate conversations.

Air temperatures

Average air temperatures measured near the planet's surface (surface air temperatures), or rather their deviation from the average calculated for a chosen reference period, are central to many climate deliberations. However, the significance of any short-term warming or cooling recorded in these datasets should not be overstated. Firstly, focusing on averages tends to hide the fact that we all deal with much larger temperature variations daily. Secondly, whenever Earth experiences warm El Niño or cold La Niña episodes, major heat exchanges take place between the Pacific Ocean and the atmosphere above, eventually showing up as a signal in the global air temperature. However, this does not reflect similar changes in the total heat content of the atmosphere-ocean system. In fact, global net changes can be small, and such heat exchanges may chiefly reflect redistribution of energy between ocean and atmosphere. Evaluating the dynamics of ocean temperatures is therefore equally important as evaluating changes of surface air temperatures.

Relative to the whole period since 1850/1880, 2023 was very warm, and all databases used in the present report has 2023 as the warmest year on record. A strong El Niño episode established itself during the year, rationalizing the high annual global temperature, and underlining the remarkable importance of ocean-atmosphere exchanges.

Many Arctic regions experienced record high air temperatures in 2016, but since then conditions generally have turned toward somewhat cooler conditions. However, this changed again in 2023, which feasibly may mark another temperature peak. The Arctic temperature peaks in 2016 and 2023 presumably were affected by ocean heat released from the Pacific Ocean during strong El Niño's and subsequently transported towards the Arctic region. This underscores how Arctic air temperatures may be affected, not only by variations in local conditions, but also by variations playing out in geographically remote regions.

Many diagrams in this report focus on the time from 1979 and ahead, reflecting the commencement of the satellite era, and the advent of a wide range of observations with nearly global coverage, including temperature. These data provide a detailed view into temperature changes over time at different altitudes in the atmosphere. Among other phenomena, these observations reveal that a Stratospheric temperature plateau has prevailed since 1995.

Since 1979, lower troposphere temperatures have increased over both land and oceans, but most clearly over the land. The most straightforward explanation for this observation is that much of the warming is caused by solar insolation, but there may well be several supplementary reasons, such as differences in heat capacity and changes in cloud cover and land use.

Oceans

The Argo program has now achieved 20 years of global coverage, growing from a relatively sparse global array of 1000 profiling floats in 2004, to more than 3900 in December 2023. Since their inception these have provided

a unique ocean temperature dataset for depths down to 1900 m. The data is currently updated to December 2021. Although the oceans are much deeper than 1900 m, and the dataset is still relatively short, interesting features are now emerging from these observations.

Since 2004, the upper 1900 m of the oceans have globally experienced net warming of about 0.037°C. The maximum net warming (about 0.2°C) affects the uppermost 100 m of the oceans. This is seen mainly in regions near the Equator, where the greatest amount of solar radiation is received. At greater depths, a small (about 0.025°C) net warming has occurred between 2004 and 2021.

This development in the global average ocean temperatures is generally reflected across the Equatorial oceans, between 30°N and 30°S, which, with exception of slight cooling at 300-500 m depth. A temperature peak may possibly have been passed around 2019-2020. Because of the spherical form of the planet, the Equatorial oceans represent a huge surface area, and have correspondingly great impact on global surface air temperatures. Simultaneously, the northern oceans (55–65°N) have on average experienced a marked cooling down to 1400 m depth, and slight warming at greater depths. Just now a temperature recovery may be in process in the North Atlantic. The southern oceans (55–65°S) have on average seen some warming at most depths since 2004, but mainly near the surface, above 200 m depth. However, averages may be misleading, and quite often better insight is obtained by studying the details, as is discussed later in this report.

The record of El Niño and La Niña episodes since 1950 is influenced by a significant 3.6-year cycle, and feasibly also by a 5.6-year cycle.

Sea level

Sea level is monitored by satellite altimetry and by direct measurements using tide-gauges situated along coasts. While the satellite-derived record suggests a global sea level rise of about 3.4 mm per year or more, data from tide-gauges all over the world suggest a smaller average global sea-level rise, about 1–2 mm per year. The tide-gauges measurements do not indicate any clear recent acceleration (or deceleration), but the record is characterised by recurrent variations. The marked difference (a ratio of about 1:2) between the two datasets still has no universally accepted explanation, but it is known that satellite observations of sea level are complicated in areas near the coast (see, e.g. Vignudelli et al. 2019). Either way, for local coastal planning the tide-gauge data is preferred, as explained later in this report.

Sea ice

In 2023 the global sea ice cover extension remained well below the average for the satellite era (since 1979), but now with a stable or even rising global trend indicated. At the end of 2016 the global sea ice extent reached a marked minimum, at least partly caused by the operation of two different natural variation pattern characterising sea ice in the Northern- and the Southern Hemisphere, respectively. Both variations had simultaneous occurring minima in 2016, with resulting consequences for the global sea ice extension. The opposite development, towards stable or higher ice extent at both poles, probably began around 2018, and has since been augmented especially in the Northern Hemisphere. The marked Antarctic 2016 sea ice reduction was also affected by special wind conditions.

Snow cover

Variations in the global snow cover extent is mainly caused by changes in the Northern Hemisphere, where all the major land areas are located. The Southern Hemisphere snow cover extent is essentially controlled by the Antarctic Ice Sheet, and therefore relatively stable. The Northern Hemisphere average snow cover extent has

also been more or less static since the onset of satellite observations, although local and regional interannual variations may be large. Considering seasonal changes since 1979, the Northern Hemisphere snow cover autumn extent is slightly increasing, the mid-winter extent is basically stable, and the spring extent is slightly decreasing. In 2023, the Northern Hemisphere seasonal snow cover extent was near the 1972–2022 average.

Global precipitation

Annual precipitation (rain, snow) varies from more than 3000 mm/year in wet regions to almost nothing in desert regions. The global average precipitation however undergoes variations from one year to the next, and regional annual variations up to ±30 mm/year from the long-term global average are not unusual. The global precipitation was especially high around 1956, 1973 and 2010, and especially low around 1941, 1965, 1987 and 1992. Fourier frequency analysis shows the global precipitation anomaly to be influenced by 3.6- and 5.6-year cycles. This bear resemblance to observed cyclic behaviour for the Southern Oscillation (SOI) and the Pacific Decadal Oscillation (PDO), respectively.

Storms and hurricanes

The most recent data on global tropical storm and hurricane accumulated cyclone energy (ACE) is well within the range seen since 1970. The global ACE data display a variable pattern over time, but without any clear trend towards higher or lower values. A Fourier analysis indicates important oscillations of about 11.5- and 6.5-years' duration, but the data series is too short to draw firm conclusions on this. A longer ACE series for the Atlantic Basin (since 1850), suggests natural rhythms of 61.5 years' duration, and possibly also a 5.6-year period. Modern data on the number of hurricane landfalls in the continental United States remains within the normal range throughout the entire observation period since 1851.

The spatial pattern of global surface air temperatures 2023

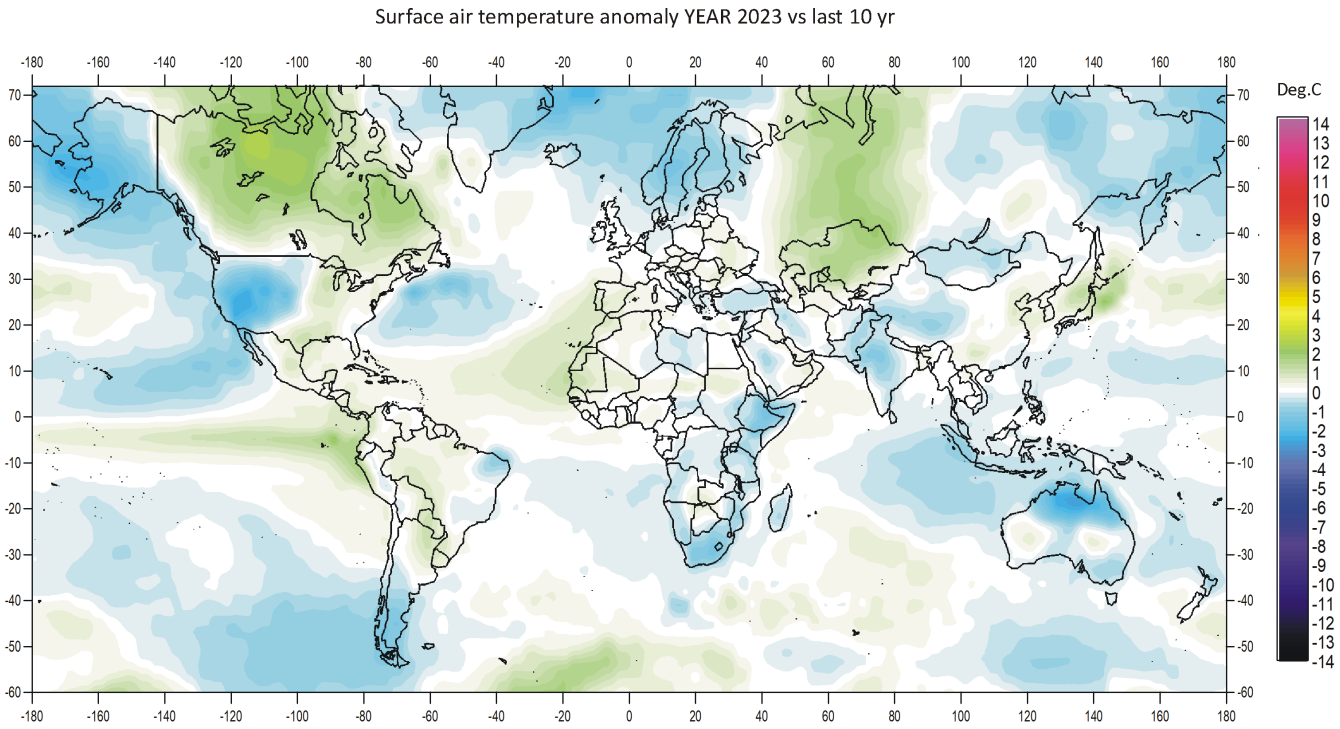

FIGURE 1: Year 2023 surface air temperatures compared to the average for the previous 10 years. Green-yellow-red colours indicate areas with higher temperature than the average, while blue colours indicate lower than average temperatures. Data source: Remote Sensed Surface Temperature Anomaly, AIRS/Aqua L3 Monthly Standard Physical Retrieval 1-degree x 1-degree V006 (https://airs.jpl.nasa.gov/), obtained from the GISS data portal (https://data.giss.nasa.gov/gistemp/maps/).

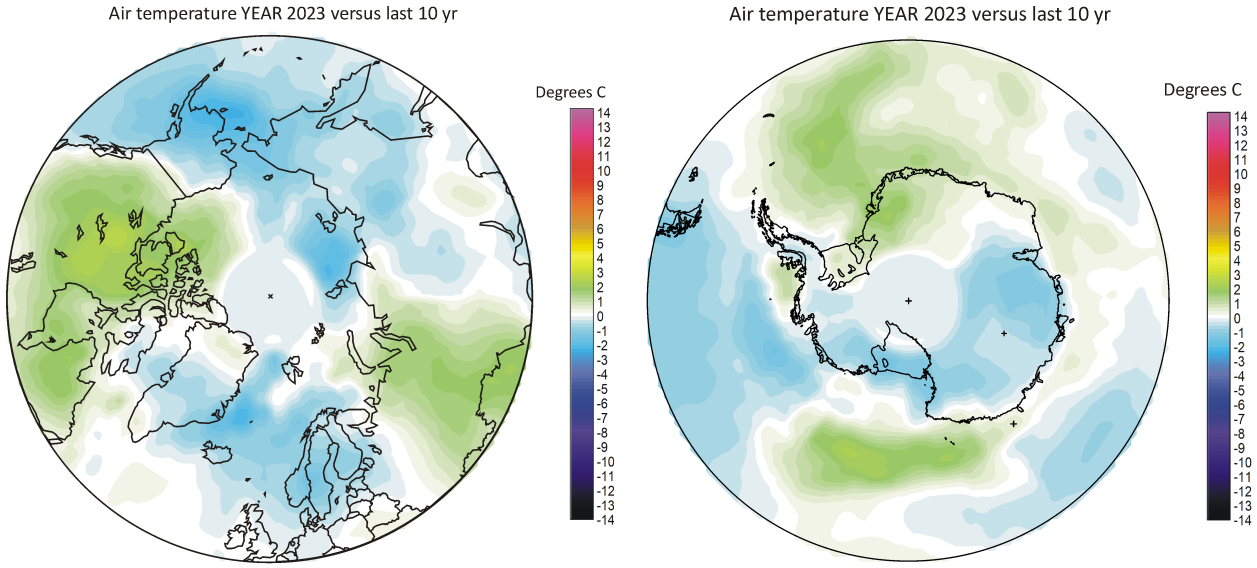

FIGURE 2a-b: Year 2023 Polar regions surface air temperatures compared to the average for the previous 10 years. Green-yellow-red colours indicate areas with higher temperature than the average, while blue colours indicate lower than average temperatures Data source: Remote Sensed Surface Temperature Anomaly,

AIRS/Aqua L3 Monthly Standard Physical Retrieval 1-degree x 1-degree V006 (https://airs.jpl.nasa.gov/), obtained from the GISS data portal (https://data.giss.nasa.gov/gistemp/maps/).

Remarks to the spatial pattern of global surface air temperatures 2023:

Global average surface air temperature for 2023 was the highest on record for all databases considered in this report. The year 2023 was affected by a warm El Niño episode (Pacific Ocean, see Figure 29 and 30).

The Northern Hemisphere was characterised by regional temperature contrasts, especially north of 30°N. The most pronounced temperature events in 2023 were high average temperatures in Canada and in parts of western Russia. In contrast, western USA, much of North Atlantic, northern Europe, Siberia, Alaska had relatively low temperatures in 2023 (compared to the last 10 years).

In the Arctic, the Canada and Russian sectors were relatively warm, while the Greenland, Atlantic and Siberian sector were relatively cool.

Near the Equator, surface air temperatures were generally above the average for the previous 10 years, reflecting the ongoing El Niño episode in the Pacific Ocean. This is a fundamental explanation for the high 2023 average global temperature, as no less than 50% of the planet's surface is located between 30°N and 30°S.

In the Southern Hemisphere annual surface air temperatures in 2023 were near or below the average for the previous 10 years. Especially South America and most of southern Africa and Australia were cool compared to the previous 10 years. Ocean wise, temperatures were near or below the 10-yr average, with exception of the southern parts of the South Atlantic, which were relatively warm.

The ocean around the Antarctic continent was generally characterised by relatively high annual surface air temperatures in 2023. Only the ocean beyond parts of West Antarctic was relatively cold. Most of the Antarctic continent was relatively cold. Only parts of the Atlantic sector of East Antarctic were relatively warm.

Summing up for 2023, global average air temperatures were very high relative to a long instrumental timescale (since 1850), a result of the still ongoing El Niño episode. In contrast, the two previous years 2021 and 2022, were influenced by a cold La Niña episode in the Pacific Ocean. Thus, the global surface air temperature record in 2023 continues to be significantly influenced by oceanographic phenomena.

Global monthly lower Troposphere air temperature since 1979

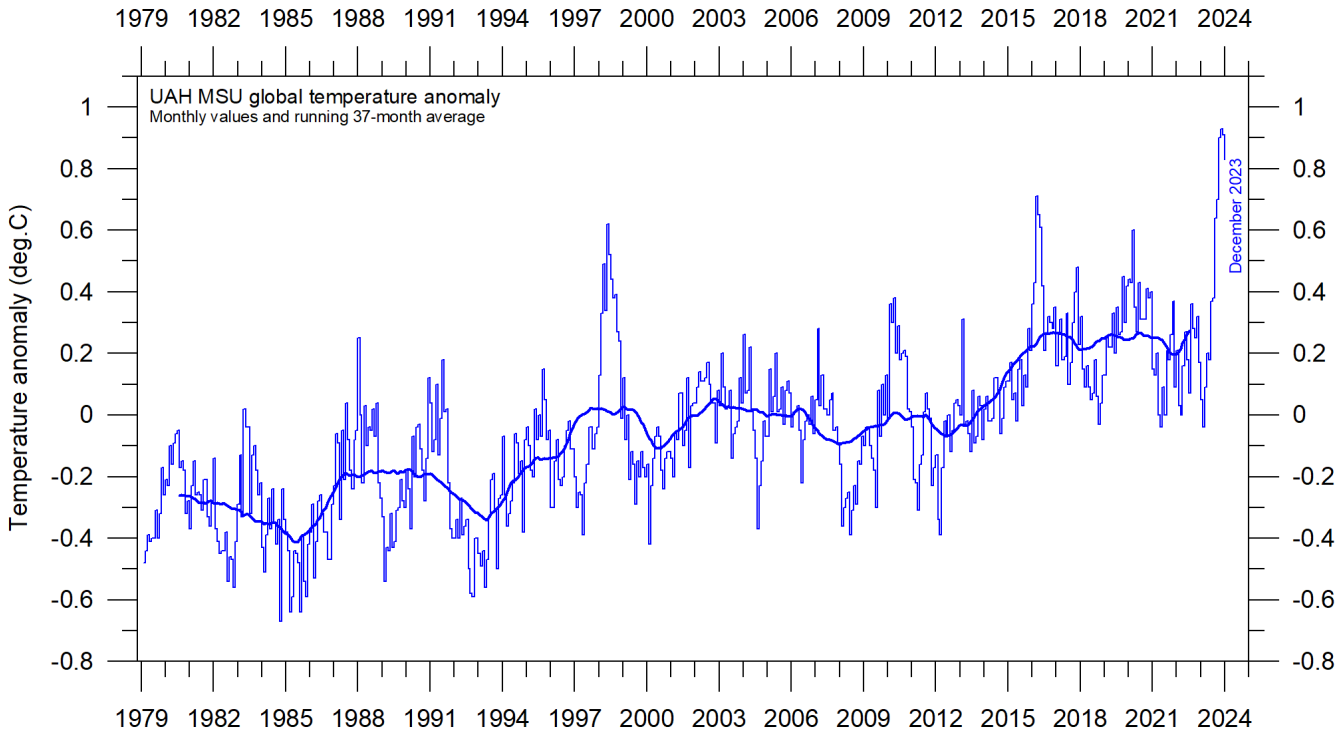

FIGURE 3: Global monthly average lower Troposphere temperatures since 1979, representing conditions at about 2 km altitude. Satellite data interpreted by University of Alabama at Huntsville (UAH), USA. The thick line is the simple running 37-month average, nearly corresponding to a running 3-year average.

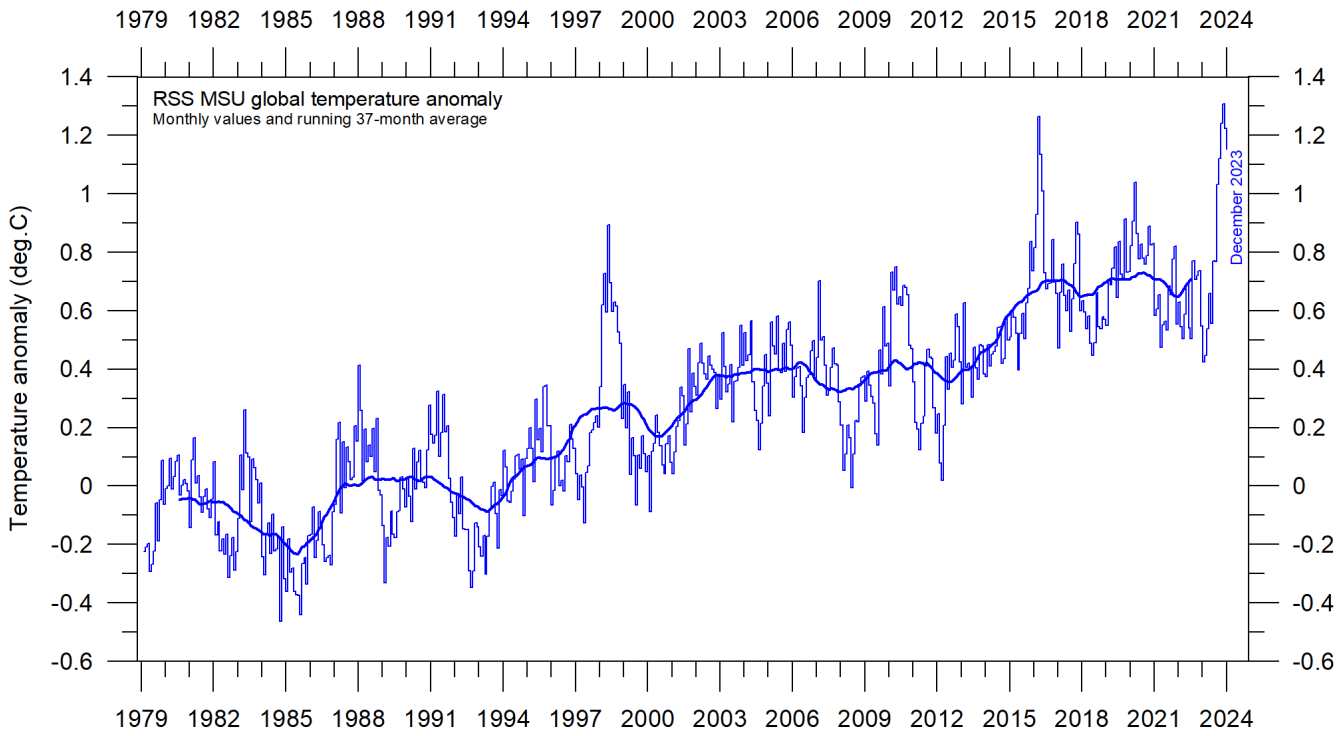

FIGURE 4: Global monthly average lower Troposphere temperatures since 1979, representing conditions at about 2 km altitude. Satellite data interpreted by Remote Sensing Systems (RSS), USA. The thick line is the simple running 37-month average, nearly corresponding to a running 3-year average.

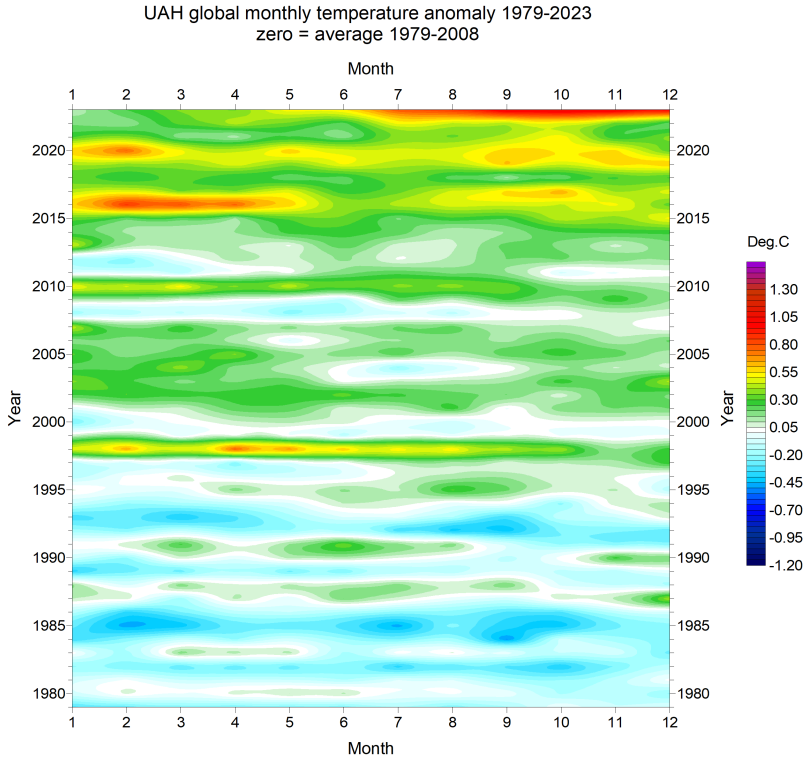

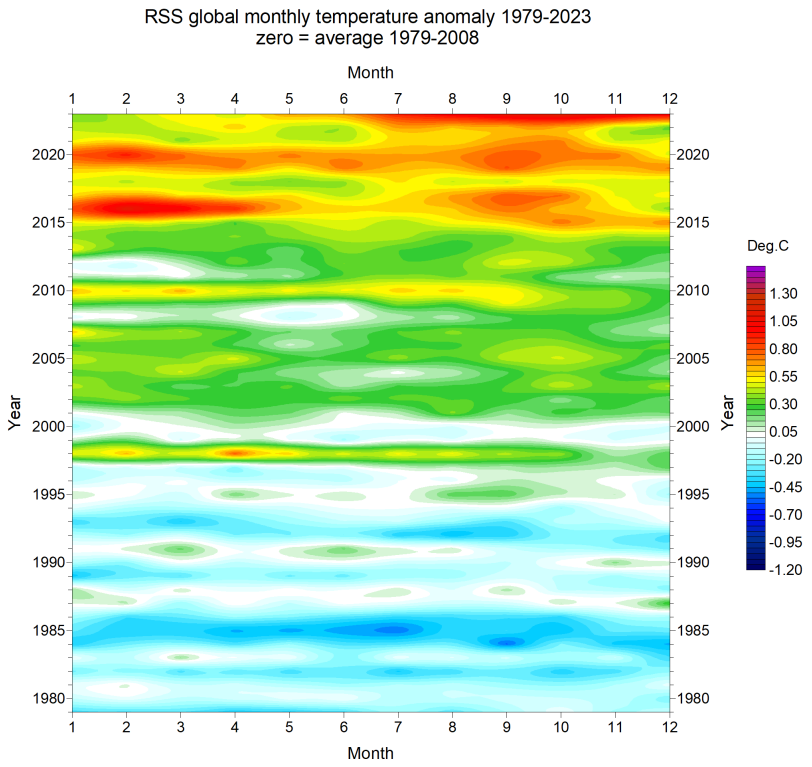

FIGURE 5: Temporal diagrams showing global monthly lower Troposphere temperatures since 1979, according to UAH and RSS, respectively, from top to bottom. The effects of the El Niño's 1998, 2010,2015-2016 and 2023 are clearly visible as "warm" bands, as are the tendency for many El Niño's to culminate during the Northern Hemisphere winter. As the different temperature databases are using different reference periods, the series have been made comparable by setting their individual 30-year average 1979-2008 as zero value.

Both satellite records for the lower Troposphere temperature clearly show a temperature spike associated with the 2015-16 and the 2019-20 El Niño's, with subsequent temperature drops due to intervening La Niña's. The latest development is a renewed temperature increase since May-June 2023 due to a new and still ongoing El Niño episode in the Pacific Ocean. See also Figure 29. There is a tendency for many El Niño's to culminate during the Northern Hemisphere winter. From the two diagrams in Figure 5, however, it looks as if the present El Niño perhaps culminate somewhat earlier, during the Northern Hemisphere autumn and early winter.

The overall temperature variation in the diagrams (Figures 3-5) is similar for the two data series, but the overall temperature increase from 1979 to 2023 is larger for RSS than for UAH (Figures 6-7). Before the rather significant adjustment of the RSS series in 2017 the temperature increase was almost identical for the two data series.

Global mean annual lower Troposphere air temperature since 1979

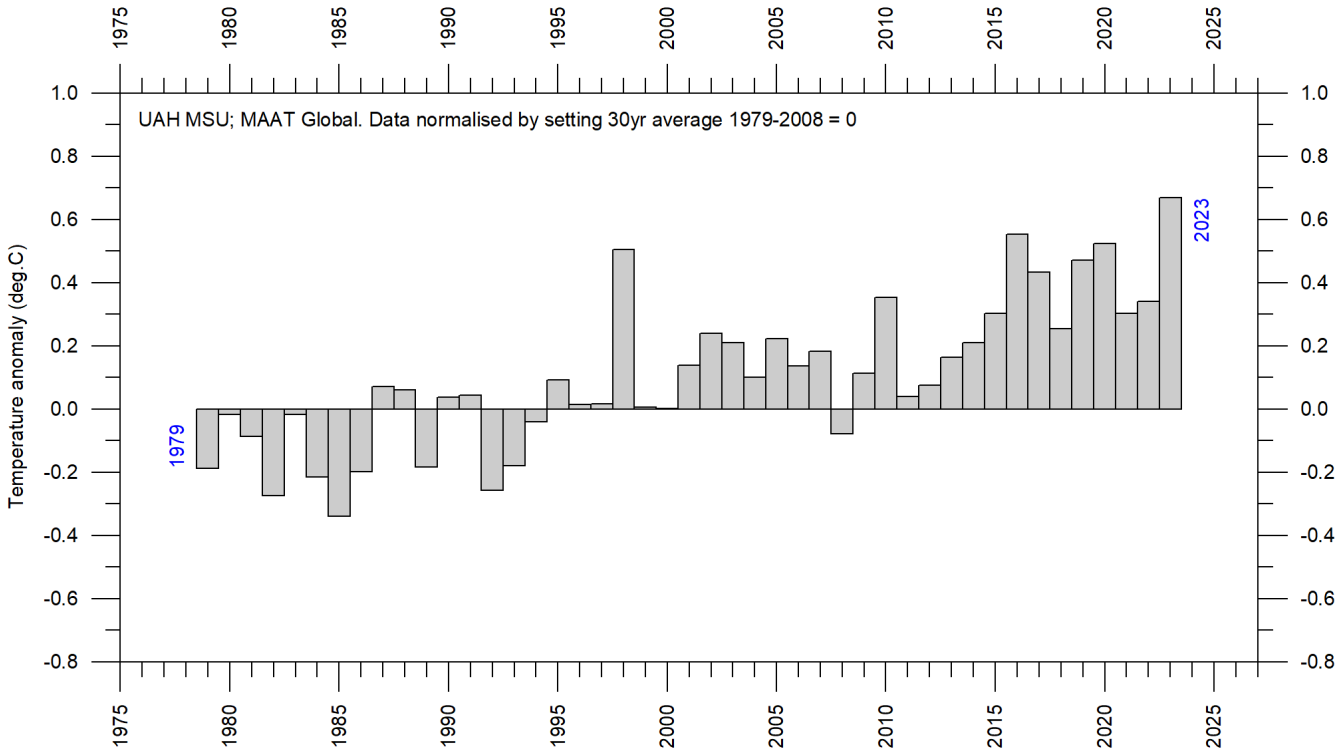

FIGURE 6: Global mean annual lower Troposphere air temperatures since 1979. Satellite data interpreted by University of Alabama at Huntsville (UAH), USA.

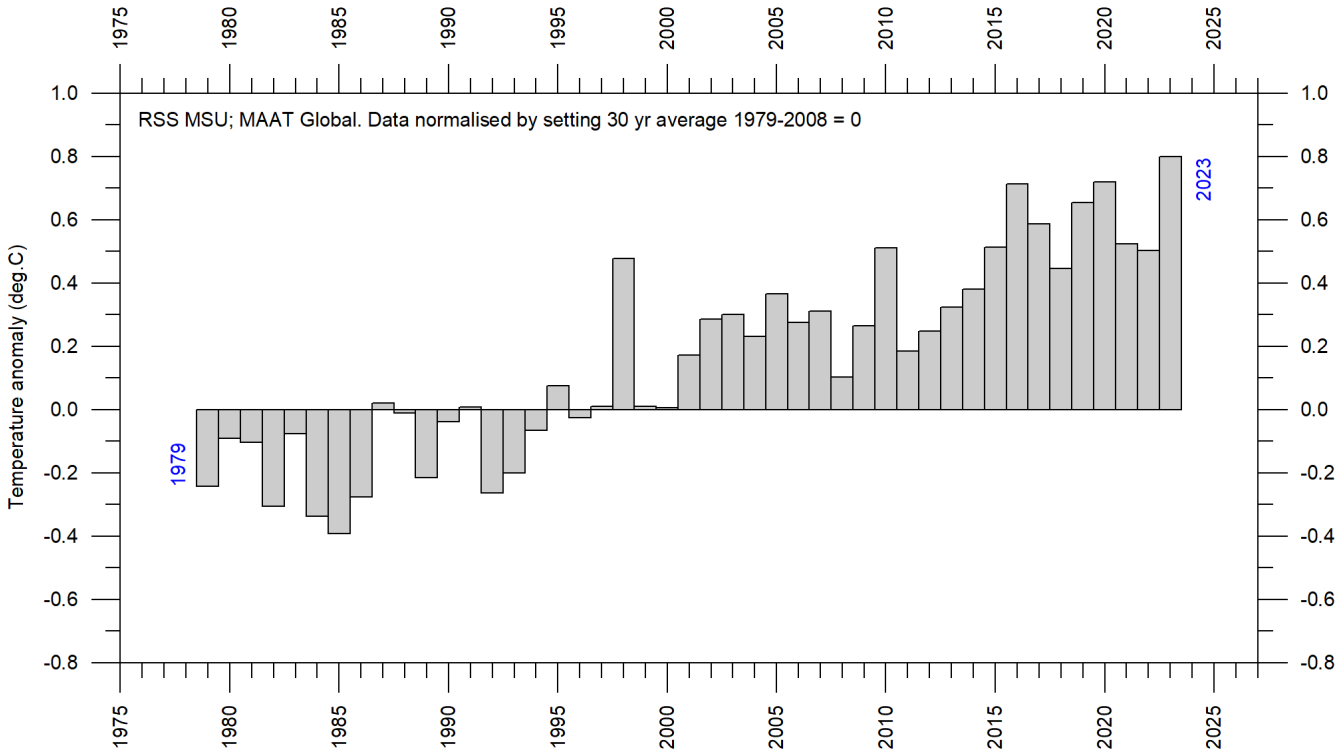

FIGURE 7: Global mean annual lower Troposphere air temperatures since 1979. Satellite data interpreted by Remote Sensing Systems (RSS), USA.

Global monthly surface air temperature since 1979

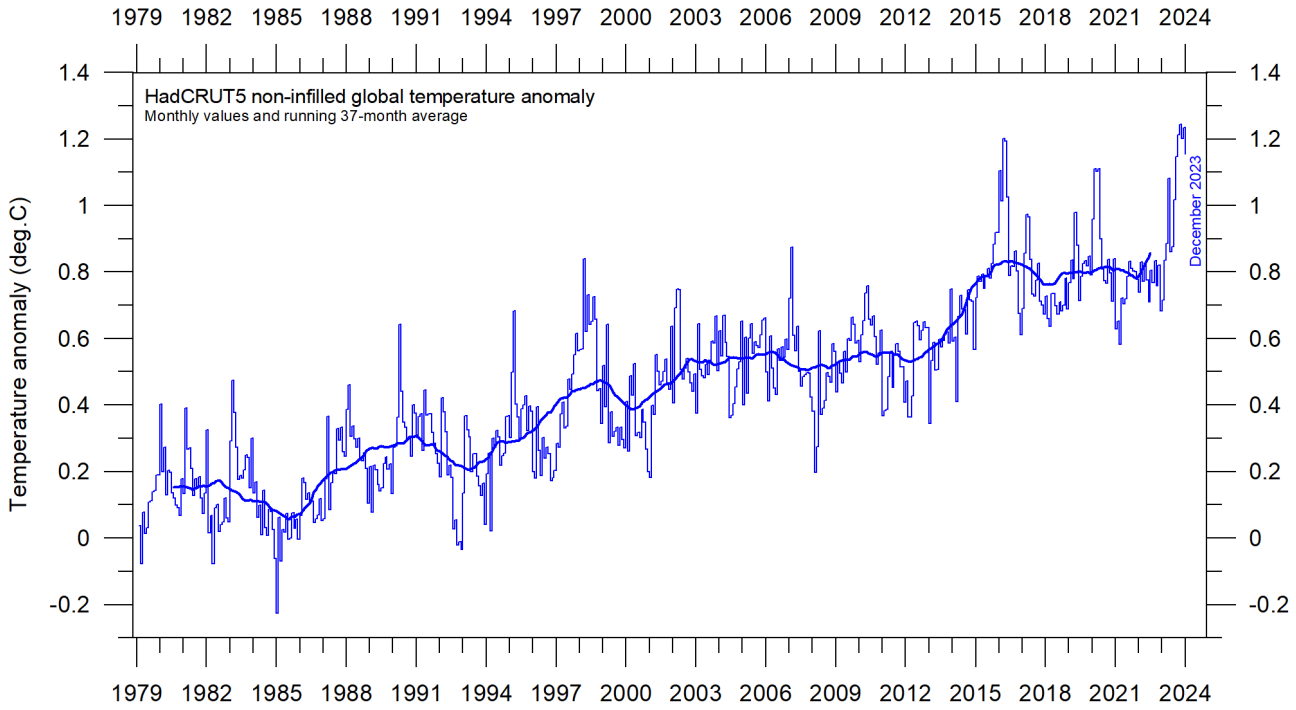

FIGURE 8: Global monthly average surface air temperature since 1979 interpreted by Hadley CRUT, a cooperative effort between the Hadley Centre for Climate Prediction and Research and the University of East Anglia's Climatic Research Unit (CRU), UK. The thick line is the simple running 37-month average, nearly corresponding to a running 3-year average.

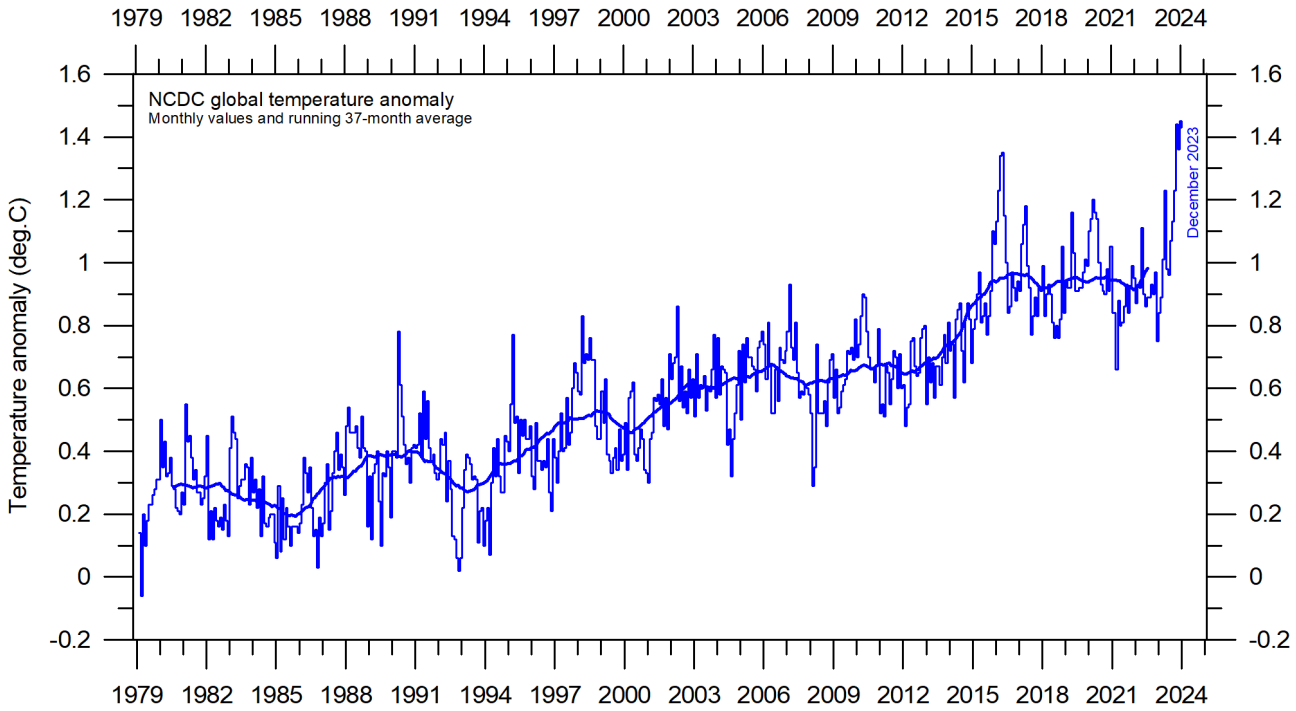

FIGURE 9: Global monthly average surface air temperature since 1979 interpreted by the National Climatic Data Center (NCDC), USA. The thick line is the simple running 37-month average, nearly corresponding to a running 3-year average.

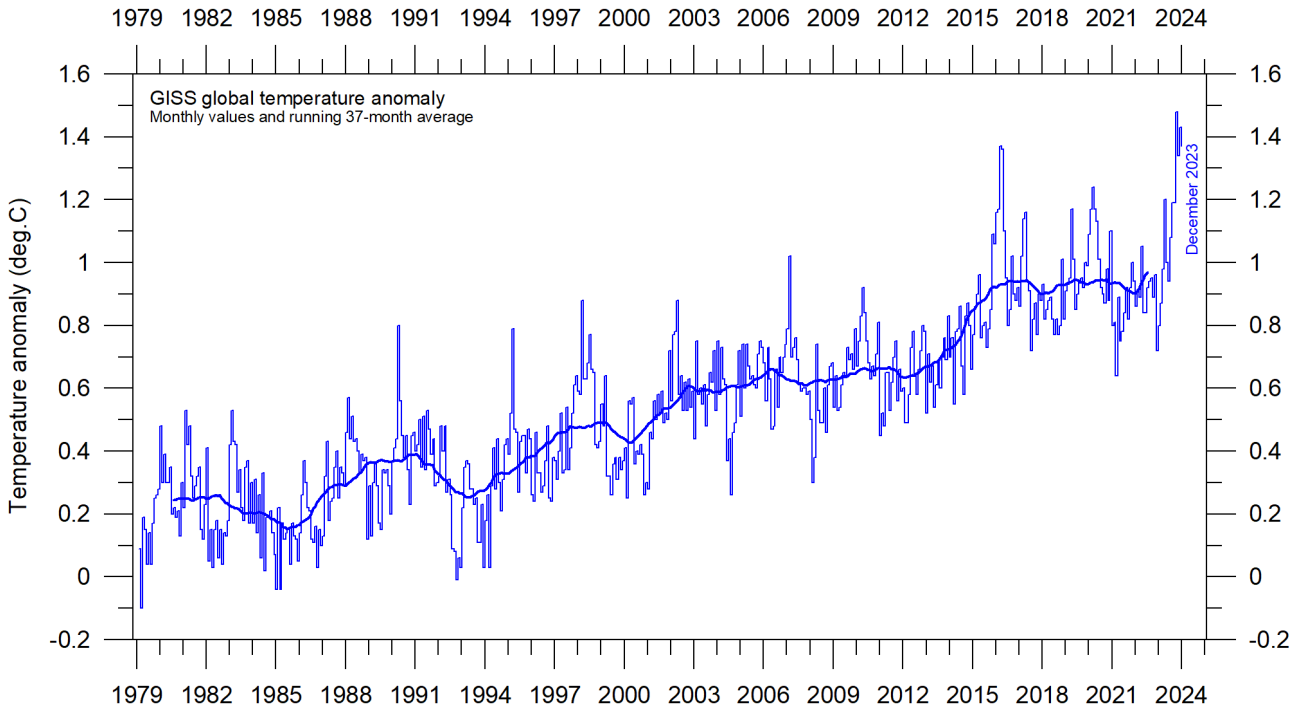

FIGURE 10: Global monthly average surface air temperature since 1979 interpreted by the Goddard Institute for Space Studies (GISS) USA. The thick line is the simple running 37-month average, nearly corresponding to a running 3-year average.

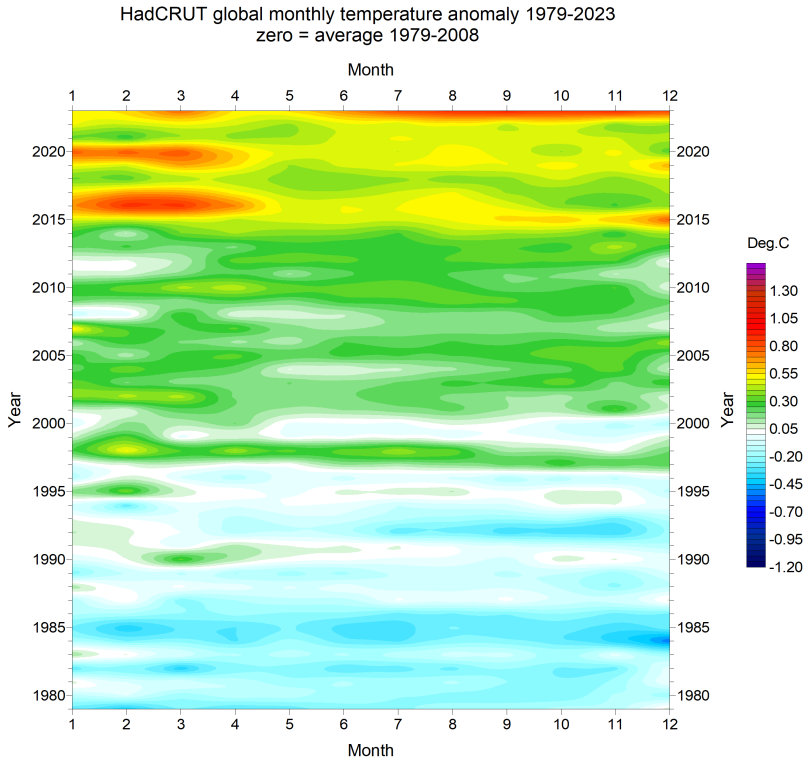

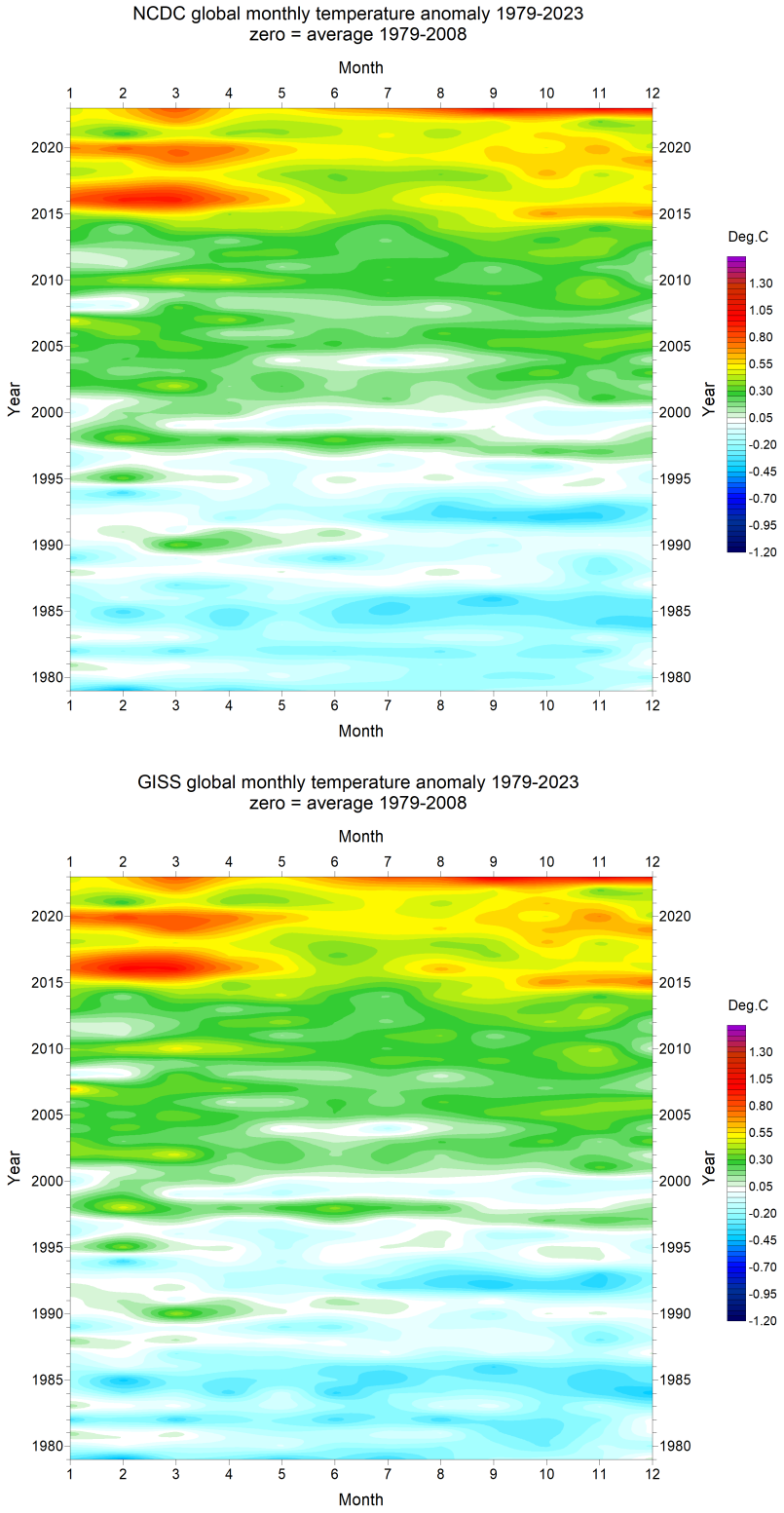

FIGURE 11: Temporal diagrams showing global monthly surface air temperatures since 1979, interpreted by HadCRUT, NCDC and GISS, respectively, from top to bottom. As the different temperature databases are using different reference periods, the series have been made comparable by setting their individual 30-year average 1979-2008 as zero value.

All three surface air temperature records clearly show variations in concert with El Niño's and La Niño's playing out in the Pacific Ocean (Figure 28). The latest development is a renewed temperature increase since May-June 2023 due to a new and still ongoing El Niño episode. Global surface air temperature is greatly influenced by this oceanographic phenomenon.

Global mean annual surface air temperature

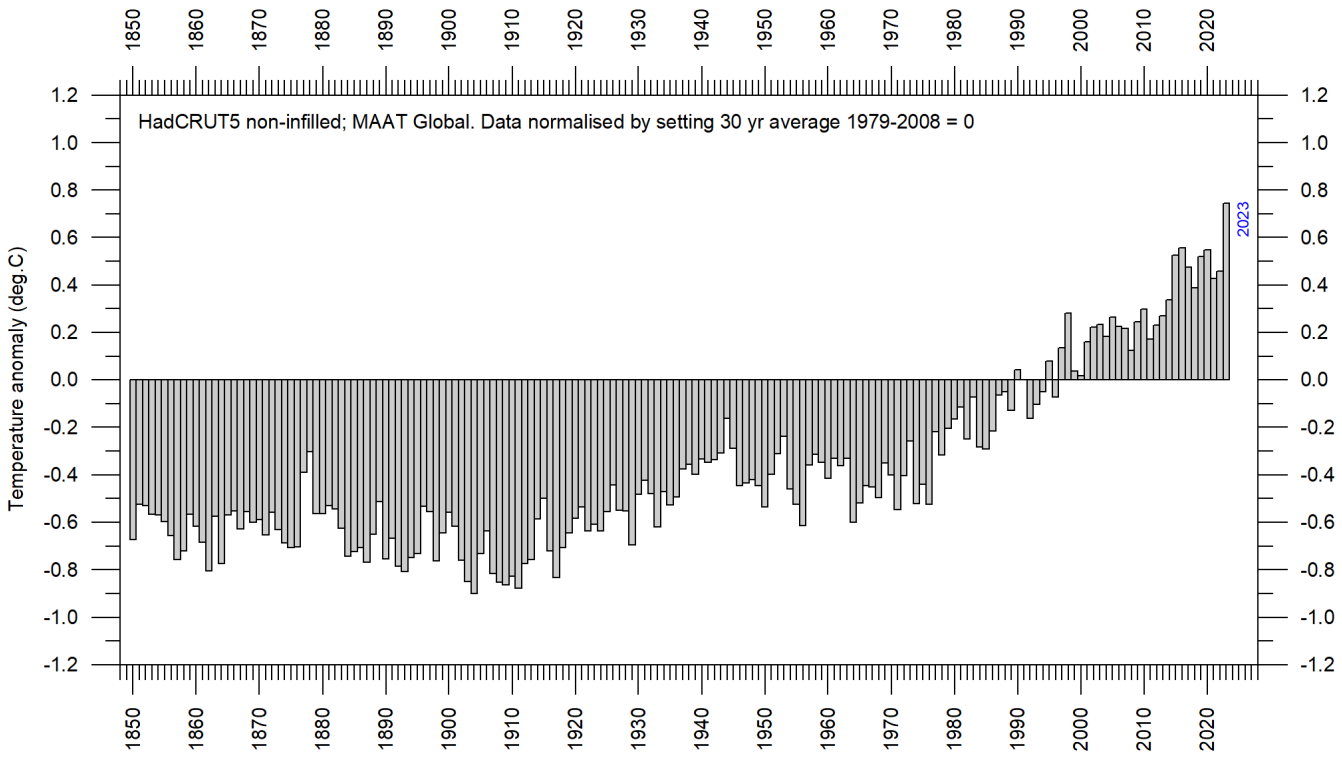

FIGURE 12: Global mean annual surface air temperatures since 1850. Data interpreted by Hadley CRUT, UK.

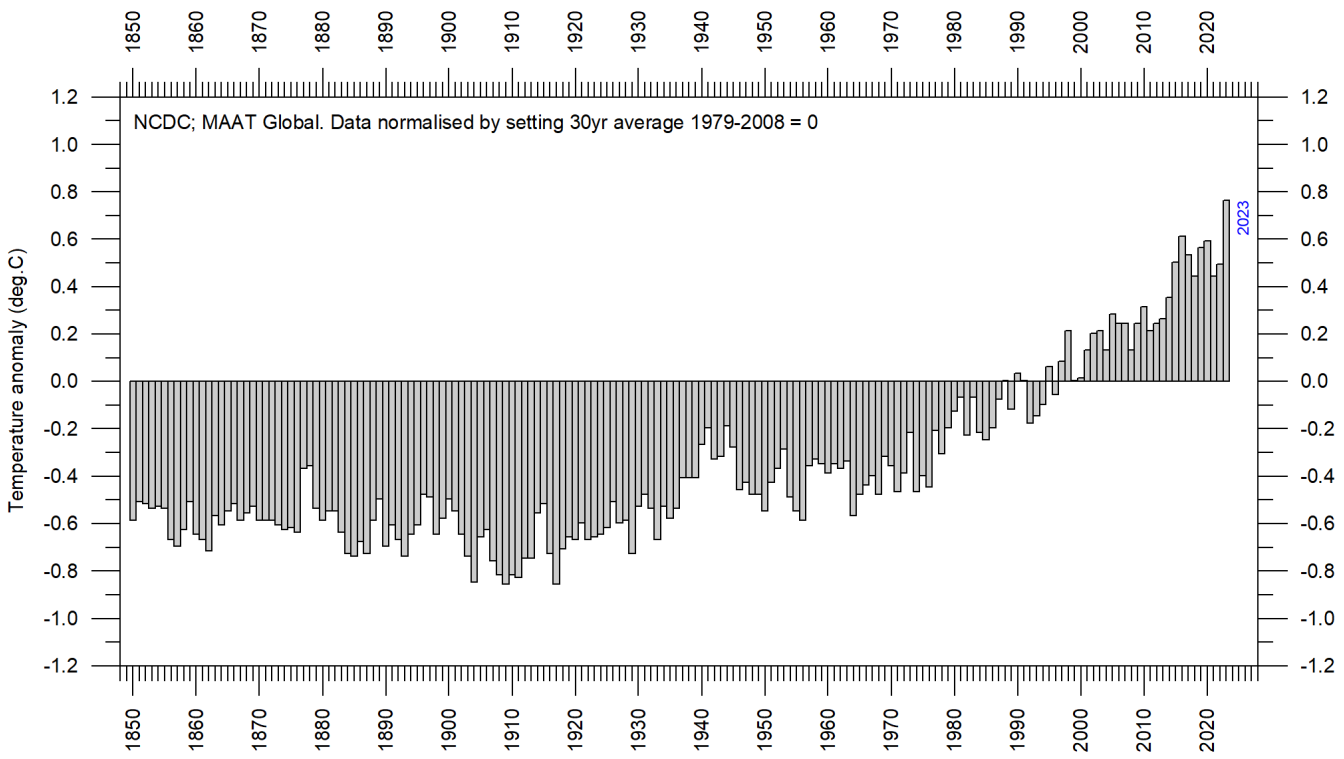

FIGURE 13: Global mean annual surface air temperatures since 1880. Data interpreted by NCDC, USA.

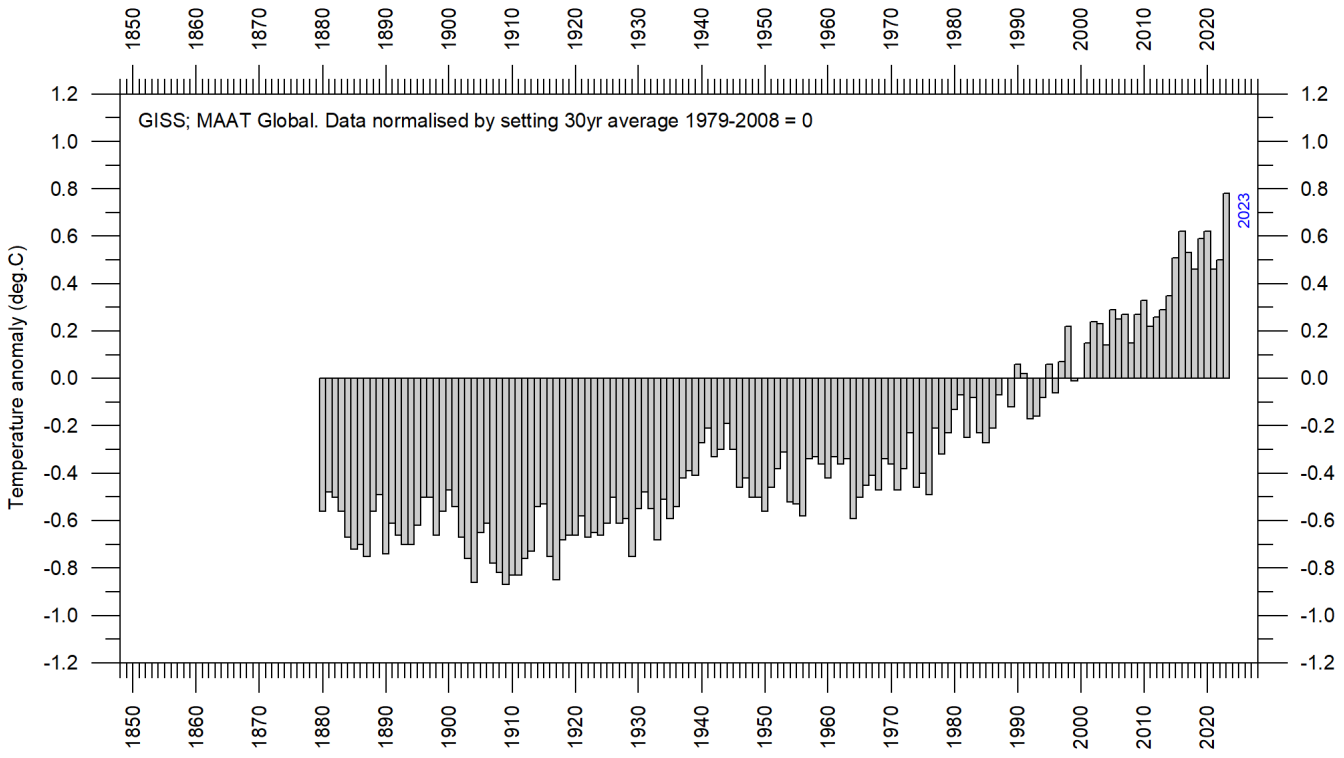

FIGURE 14: Global mean annual surface air temperatures since 1880. Data interpreted by GISS, USA.

All three average surface air temperature estimates show the year 2023 to be the warmest year on record. Year 2023 was influenced by a strong El Niño episode playing out in the Pacific Ocean (see figure 28).

Reflections on the margin of error, constancy, and quality of temperature records

According to the various air temperature records (since 1850/1880/1979) 2023 was the warmest year on record.

The surface records represent a blend of sea-surface data, collected by moving ships or by other means, and data from land stations, of partly unknown quality and unknown representativeness for their region. Many of the land stations have also been moved geographically during their period of operation, instrumentation has been changed, and most have been influenced by ongoing changes in their surroundings (vegetation, buildings, and so on).

The satellite temperature records have their own problems, but these are generally of a more technical nature and therefore are probably easier to rectify. In addition, the temperature sampling by satellites is more regular and complete on a global basis than for the surface records. It is also important to note that the sensors on satellites measure temperature directly, by emitted radiation, while most modern surface temperature measurements are indirect, using electronic resistance.

All temperature records are affected by at least three different sources of error, which differ between the individual station records used for calculation of a global average temperature estimate. 1) The *accuracy* is the degree of closeness of measurements to the actual (true) values. 2) The *precision* is the degree to which repeated measurements under unchanged conditions show an identical value, true or not. In addition, we 3) have the measurement *resolution*, which is the smallest change in temperature that produces a response in the instrument used for measurement. Combined, these represent the *margin of error* for temperature records. The margin of error has been intensively discussed over time and is probably at least ±0.1°C for surface air temperature records, and possibly higher. This often makes it statistical impossible to classify any year as representing a temperature record, as several other years may be within the ±0.1°C range of the value considered.

In addition, two other issues relating to the margin of error for surface records have not been similarly widely discussed: First, as an example, it will not be possible to conclude much about the actual value of the December 2023 global surface air temperature before March-April 2024, when data not yet reported (in January 2024) eventually are incorporated in the surface air temperature databases. This is what might be described as the effect of *delayed reporting*. Secondly, surface air temperature records furthermore often display *administrative changes* over time, which makes it even more difficult to conclude about the significance of any recently reported monthly or annually surface air temperature.

The second (administrative) issue arises from the apparently perpetual changes of monthly and annual temperature values carried out for several temperature databases, with the consequence that what in one particular year was reported as the average global temperature for previous years will later change due to

ongoing administrative "corrections". These appear to have little or nothing to do with delayed reporting of missing data: particularly with the GISS and NCDC databases, changes are made to monthly temperatures for periods far back in time, even before the year 1900, for which the possibility of reporting delays is exceedingly small. Most likely, such administrative changes are the result of alterations in the way average monthly values are calculated by the various databases, in an attempt to enhance the resulting record.

As an example, Figure 15 show the accumulated effect since May 2008 of such administrative changes in the GISS global surface air temperature record, extending back to 1880, although any of the other datasets could be used instead. The overall net effect of the administrative changes introduced in the GISS record since May 2008 is a warming of the early and modern part of the record and cooling of the period in between, roughly from 1900 to 1970. Several of the net changes introduced since 2008 are quite substantial, ranging from about +0.20 to -0.20°C.

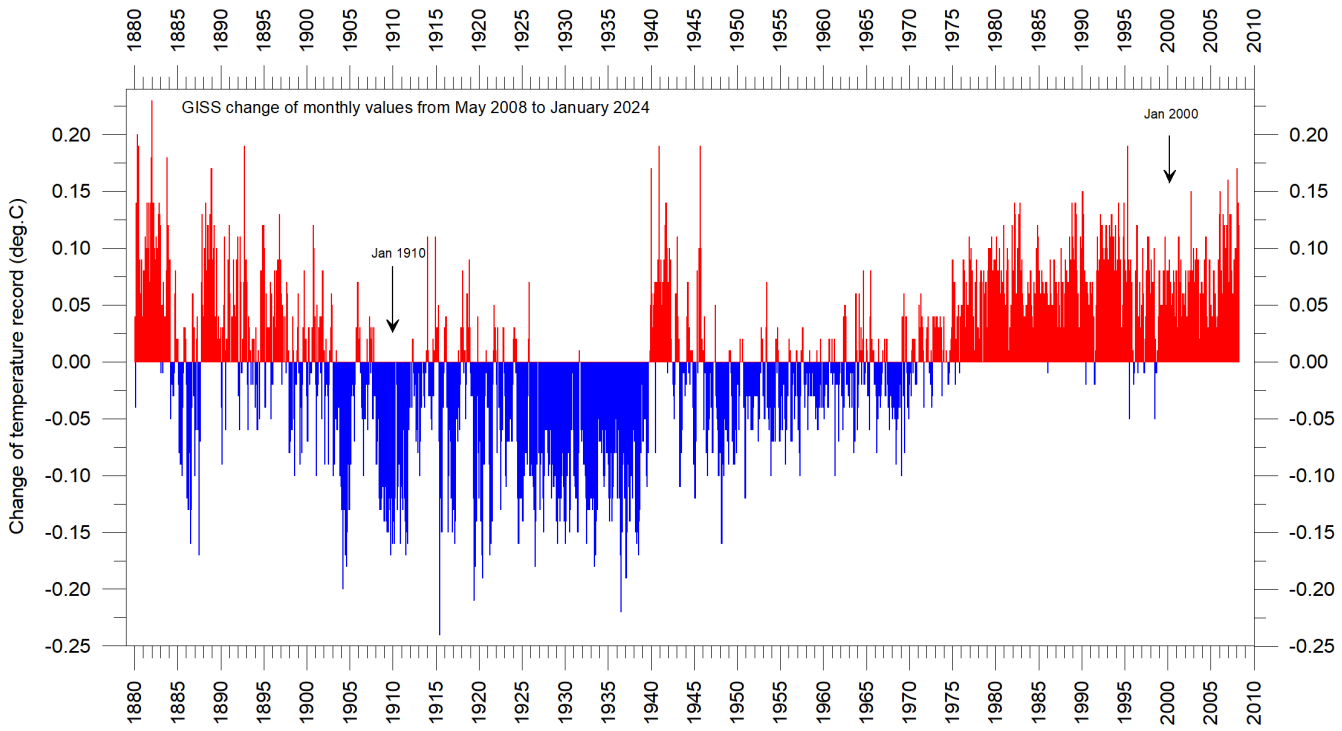

FIGURE 15. Diagram showing net administrative changes since 17 May 2008 in the global monthly surface air temperature record prepared by the Goddard Institute for Space Studies (GISS), at Columbia University, New York City, USA.

To illustrate the effect of administrative changes in a different way, figure 16 show how the global surface air temperature for January 1910 and January 2000 (months indicated in Fig. 15) has changed since May 2008, again exemplified by the GISS record.

The administrative upsurge of the global surface air temperature increase (GISS) from January 1915 to January 2000 has grown from 0.45 (reported May 2008) to 0.67°C (reported January 2024). This represents an about 49% administrative temperature increase over this period, meaning that about half of the apparent global temperature increases from January 1910 to January 2000 (as reported by GISS in January 2023) is due to

administrative changes of the original data since May 2008. Clearly such administrative changes are important to consider when evaluating the overall quality of various temperature records, along with other standard sources of error. In fact, the magnitude of administrative changes may exceed the formal margin of error.

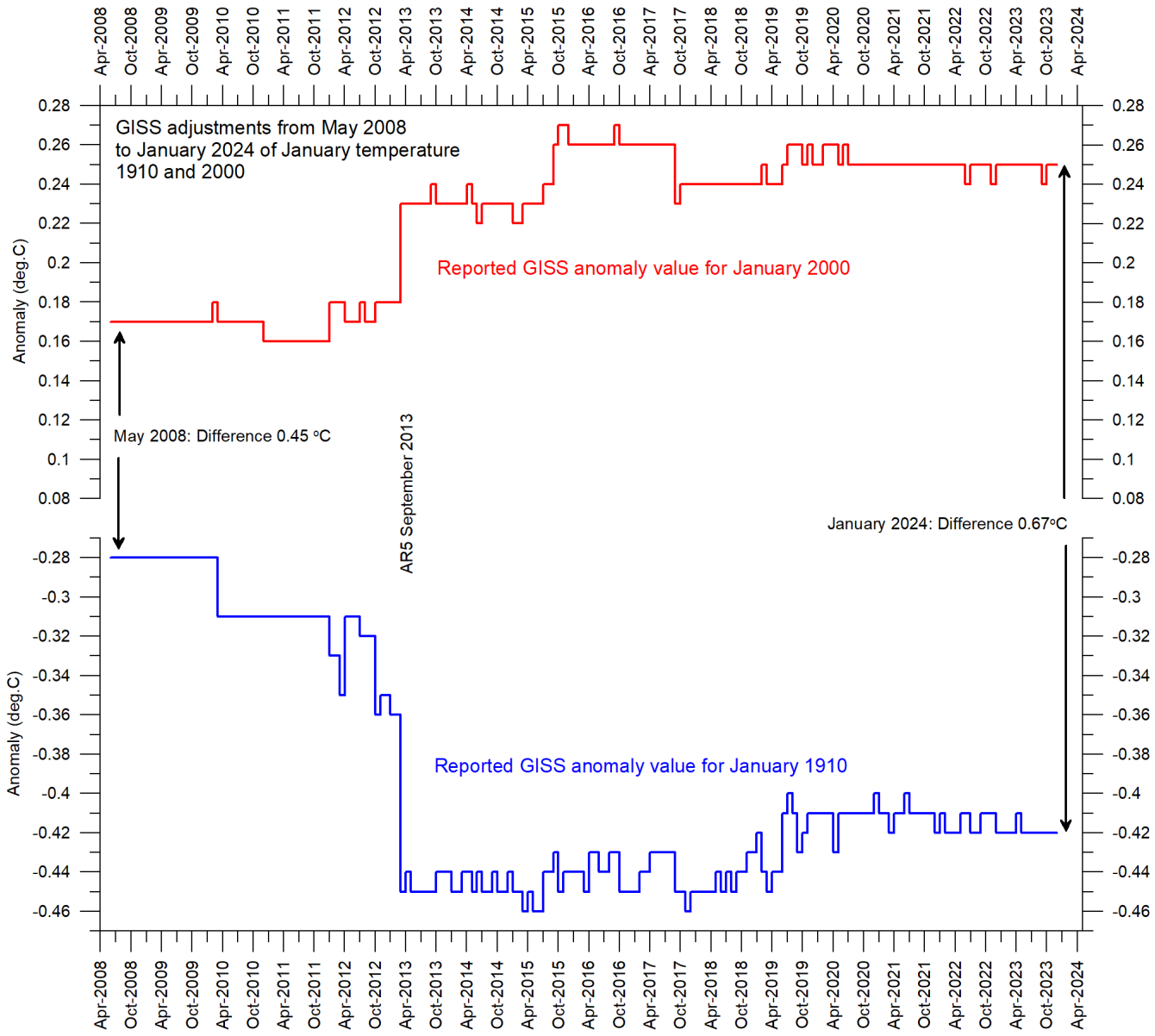

FIGURE 16. Diagram showing adjustments made since May 2008 by the Goddard Institute for Space Studies (GISS) in anomaly values for the months January 1910 and January 2000.

For obvious reasons, as the past does not change, any record undergoing continuing changes cannot describe the past correctly all the time. Frequent and large corrections in a database inevitably signal a fundamental uncertainty about what is likely to represent the correct values. Nevertheless, everybody interested in climate science should gratefully acknowledge the efforts put into maintaining the different temperature databases referred to in the present report. At the same time, however, it is also important to realise that all temperature

records cannot be of equal scientific quality. The simple fact that they to some degree differ shows that they cannot all be completely correct.

Comparing surface air temperatures with lower Troposphere temperatures recorded by satellites

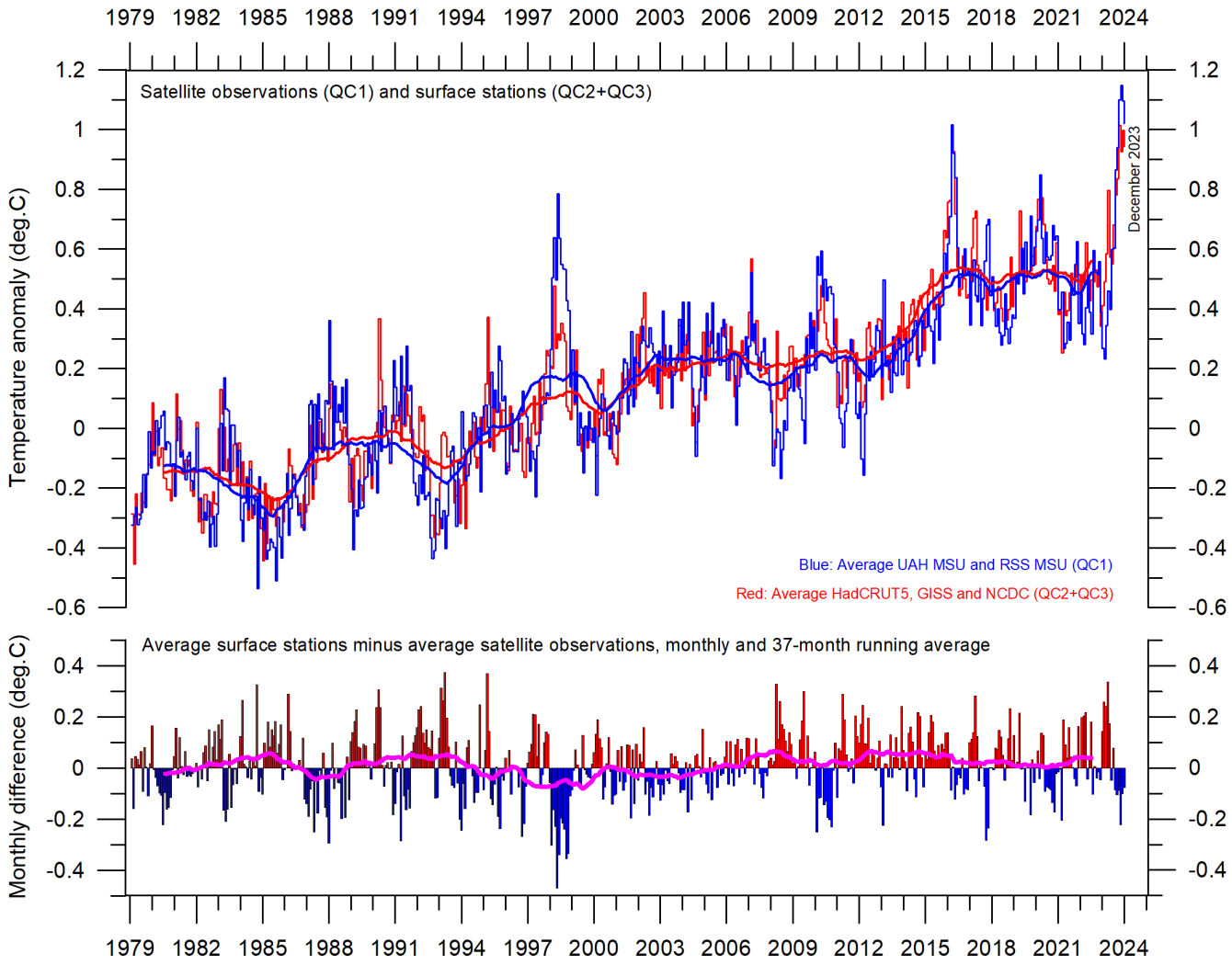

FIGURE 17: Plot showing the average of monthly global surface air temperature estimates (HadCRUT, NCDC and GISS) and satellite-based lower Troposphere temperature estimates (UAH and RSS). The thin lines indicate the monthly value, while the thick lines represent the simple running 37-month average, nearly corresponding to a running 3-year average. The lower panel shows the monthly difference between surface air temperature and satellite temperatures. As the base period differs for the different temperature estimates, they have all been normalised by comparing to the average value of 30 years from January 1979 to December 2008.

In general, there is fair agreement between the average of surface- and satellite records, as shown by figure 17. However, before the major adjustment of the RSS satellite record in 2017 this was different, with the average of surface records then drifting in warm direction, compared to the average of satellite records. Again, this illustrates the importance of ongoing changes of the individual temperature records.

Comparing temperature change over land and oceans; lower Troposphere air temperature

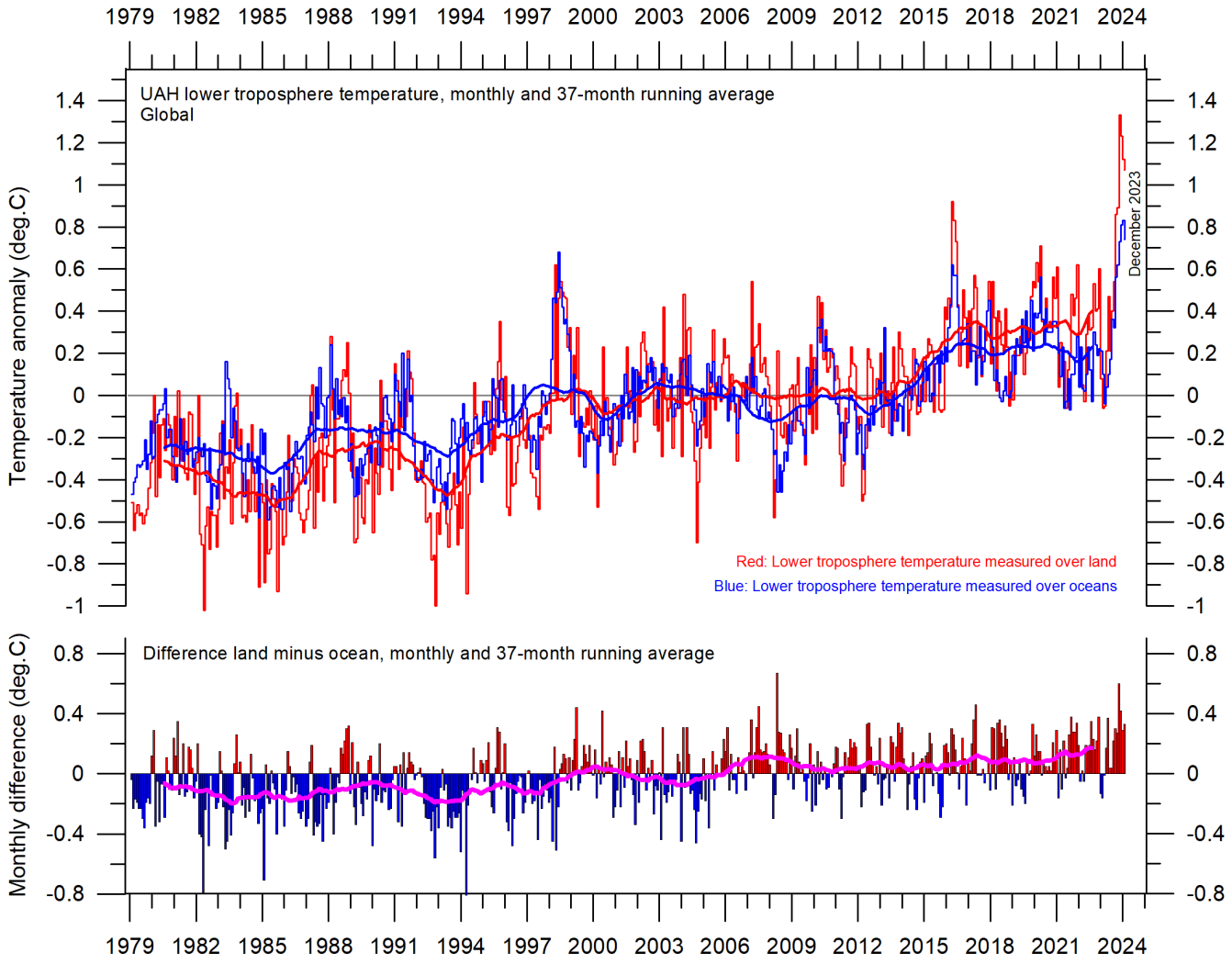

FIGURE 18: Global monthly average lower troposphere temperature since 1979 measured over land and oceans, shown in red and blue, respectively, according to University of Alabama at Huntsville (UAH), USA. The thin lines represent the monthly average, and the thick line the simple running 37-month average, nearly corresponding to a running 3-year average.

Since 1979, the lower troposphere over land has warmed considerably more than over oceans. There may be several reasons for this, such as, e.g., differences in surface heat capacity, variations in incoming solar radiation, cloud cover and land use.

Zonal air temperatures

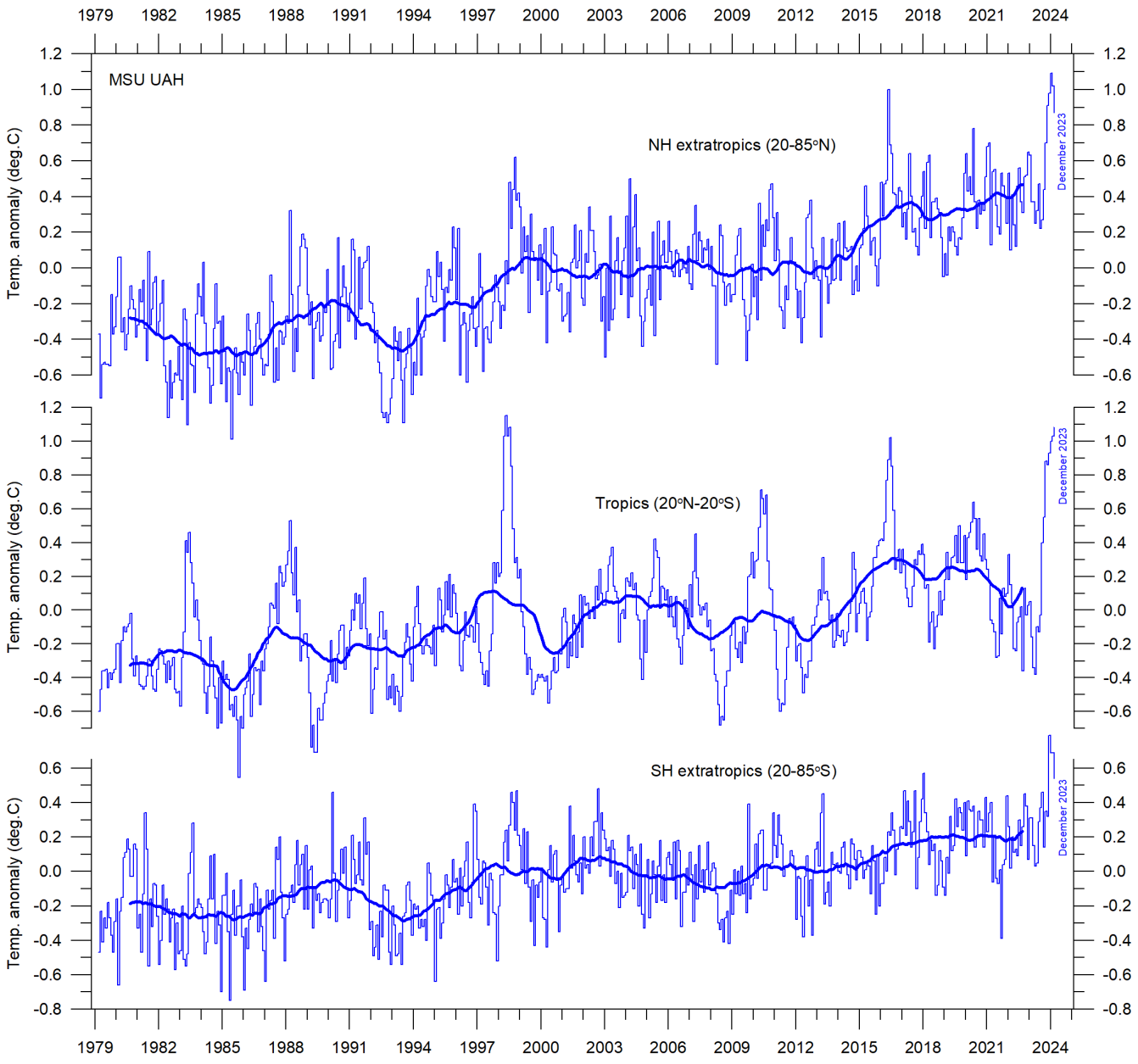

FIGURE 19: Global monthly average lower troposphere temperature since 1979 for the tropics and the northern and southern extratropics, according to University of Alabama at Huntsville, USA. Thick lines are the simple running 37-month average, nearly corresponding to a running 3-year average.

Figure 19 shows that the 'global' warming experienced after 1980 has predominantly been a Northern Hemisphere phenomenon, and mainly played out as two step changes 1994-1999 and 2015-2016. The first of these changes was, however, influenced by the Mt Pinatubo eruption of 1992–93 and the 1997 El Niño episode.

The figure also reveals how the temperature effects of the strong Equatorial El Niños of 1997 and 2015–16, as well as the recent one in 2023, apparently spread to higher latitudes in both hemispheres, although with some delay. The effect was, however, mainly seen in the Northern Hemisphere, and only to lesser degree in the Southern Hemisphere. In general, the temperature variations in the Tropics are with some delay reflected in both hemispheres, especially in the Northern Hemisphere. The Tropical region are clearly of major importance for understanding global meteorological and climatic dynamics.

Polar air temperatures

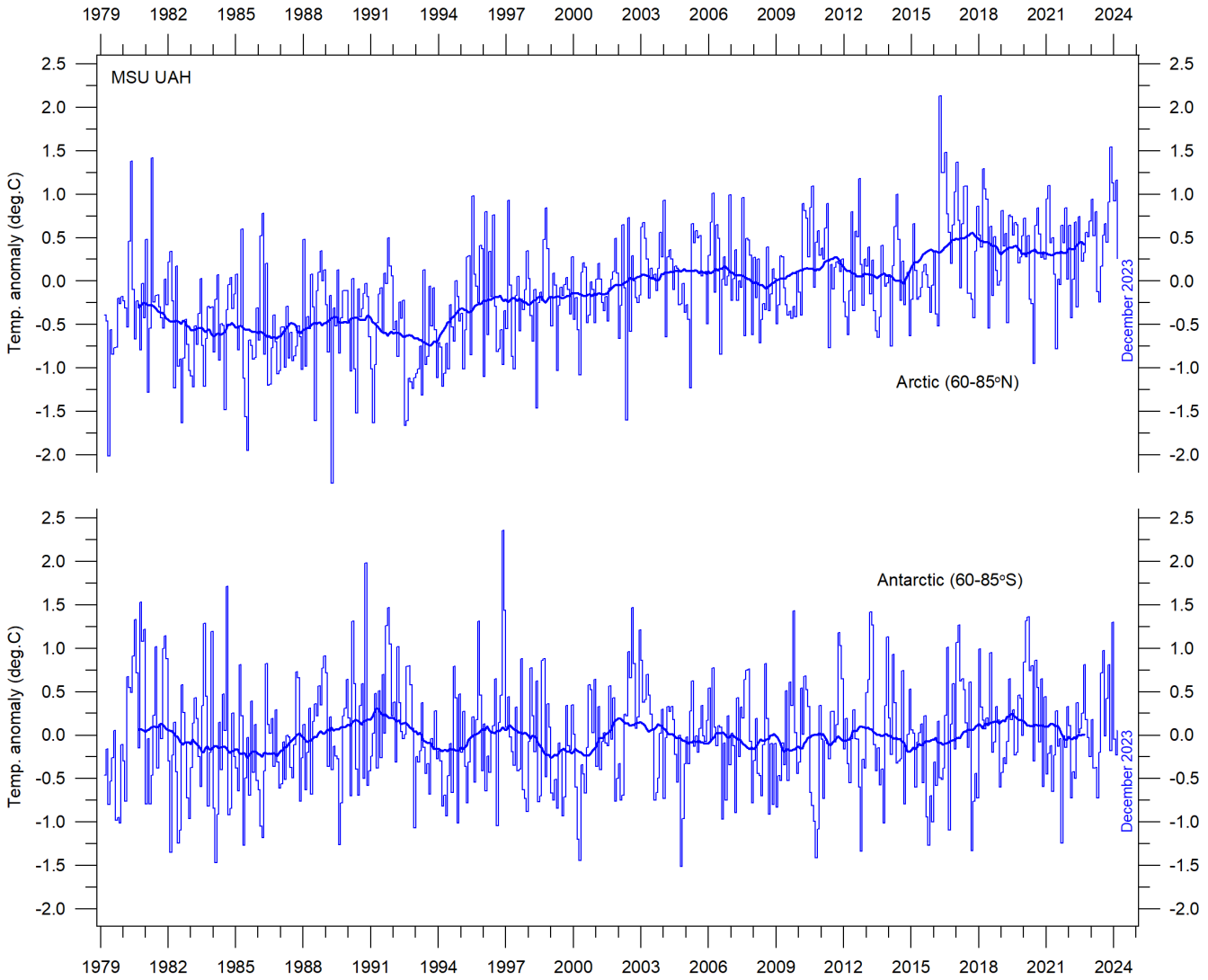

FIGURE 20: Global monthly average lower troposphere temperature since 1979 for the North Pole and South Pole regions, according to University of Alabama at Huntsville, USA. Thick lines are the simple running 37-month average, nearly corresponding to a running 3-year average.

In the Arctic region, warming was rapid in the period 1994–96, but slower subsequently (Figure 20). In 2016, however, temperatures peaked for several months, presumably because of oceanic heat given off to the atmosphere during the 2015-2016 El Niño (Figure 30) and then advected to higher latitudes. A small temperature decrease characterised the Arctic subsequent to 2016, but in 2023 a new temperature peak presumably derived from the ongoing El Niño is seen.

In the Antarctic region, temperatures have essentially remained stable since the onset of the satellite record in 1979. In 2016–17 and in 2023 a small temperature peak is visible in the monthly record and might be interpreted as the subdued effect of El Niño episodes.

Arctic and Antarctic temperature peaks derived from El Niño episodes, as outlined above, are paradoxically due to heat ventilating out from the Pacific Ocean near the Equator. They therefore represent a process cooling the Earth, when considered in a broader context.

The above overall developments are confirmed by considering available long Arctic and Antarctic surface air temperature series, as shown in Figure 21 and 22. On this station level, evidently, also conditions specific for each site are apparent, demonstrating the amount of variation within both polar regions.

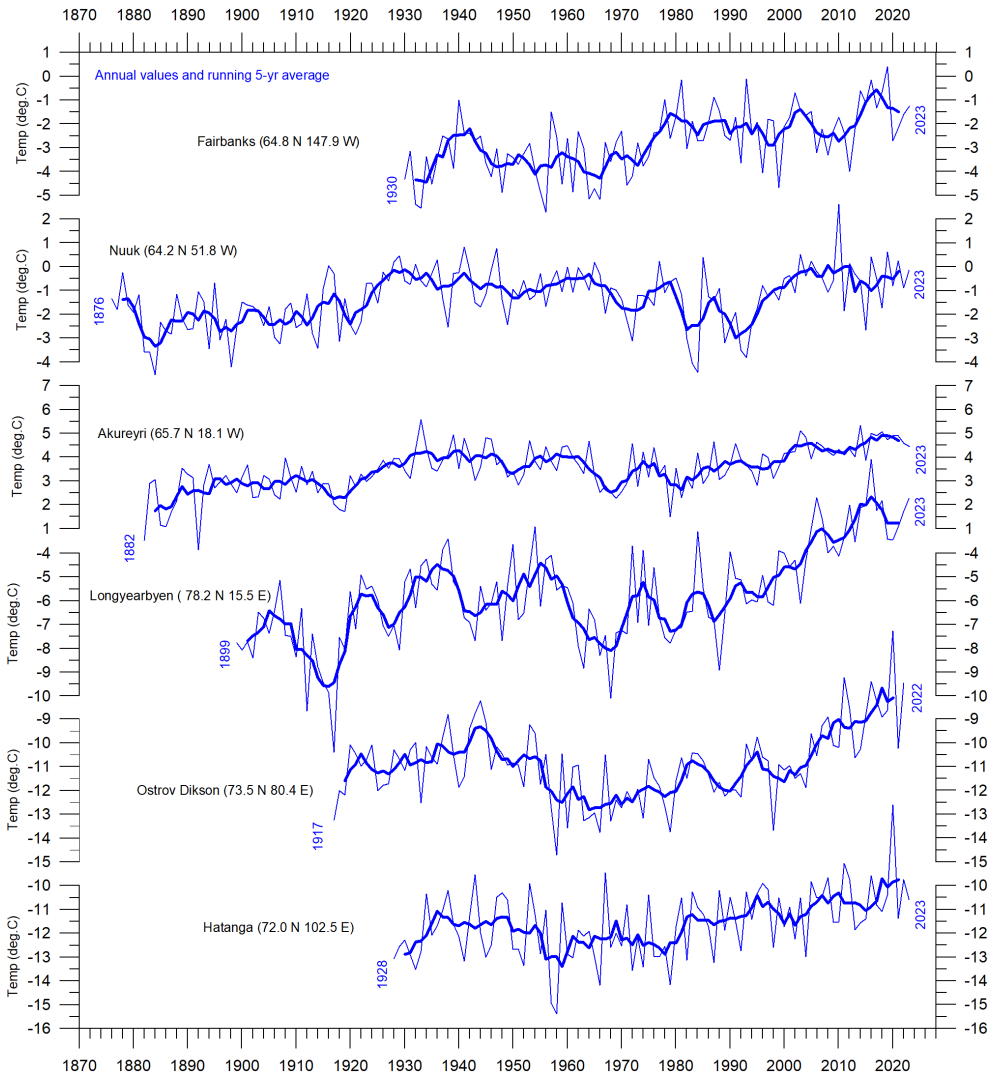

FIGURE 21: Long Arctic surface annual air temperature series. Annual values were calculated from monthly average temperatures. Almost unavoidably, some missing monthly data were encountered in some of the series. In such cases, the missing values were generated as either 1) the average of the preceding and following monthly values, or 2) the average for the month registered the preceding year and the following year. The thin blue line represents the mean annual air temperature, and the thick blue line is the running 5-year average. Data source: Goddard Institute for Space Studies (GISS).

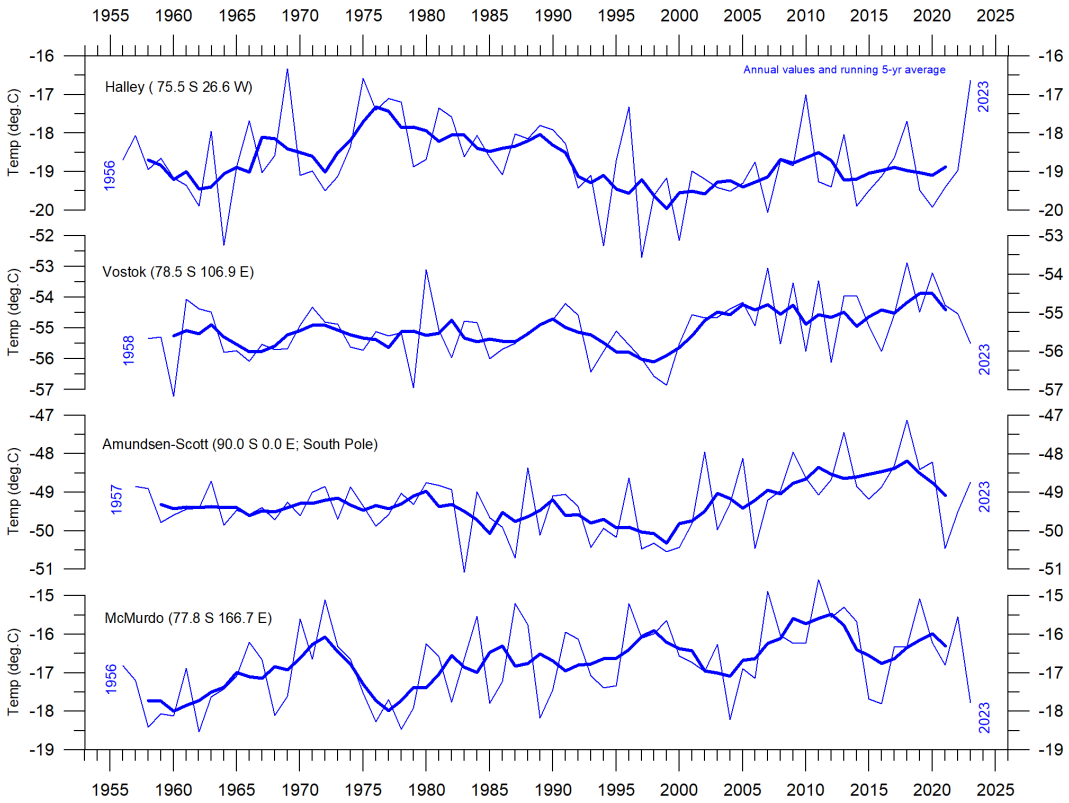

FIGURE 22: Long Antarctic surface annual air temperature series. Annual values were calculated from monthly average temperatures. Almost unavoidably, some missing monthly data were encountered in some of the series. In such cases, the missing values were generated as either 1) the average of the preceding and following monthly values, or 2) the average for the month registered the preceding year and the following year. The thin blue line represents the mean annual air temperature, and the thick blue line is the running 5-year average. Data source: Goddard Institute for Space Studies (GISS).

Comparing atmospheric temperatures from surface to 17 km altitude

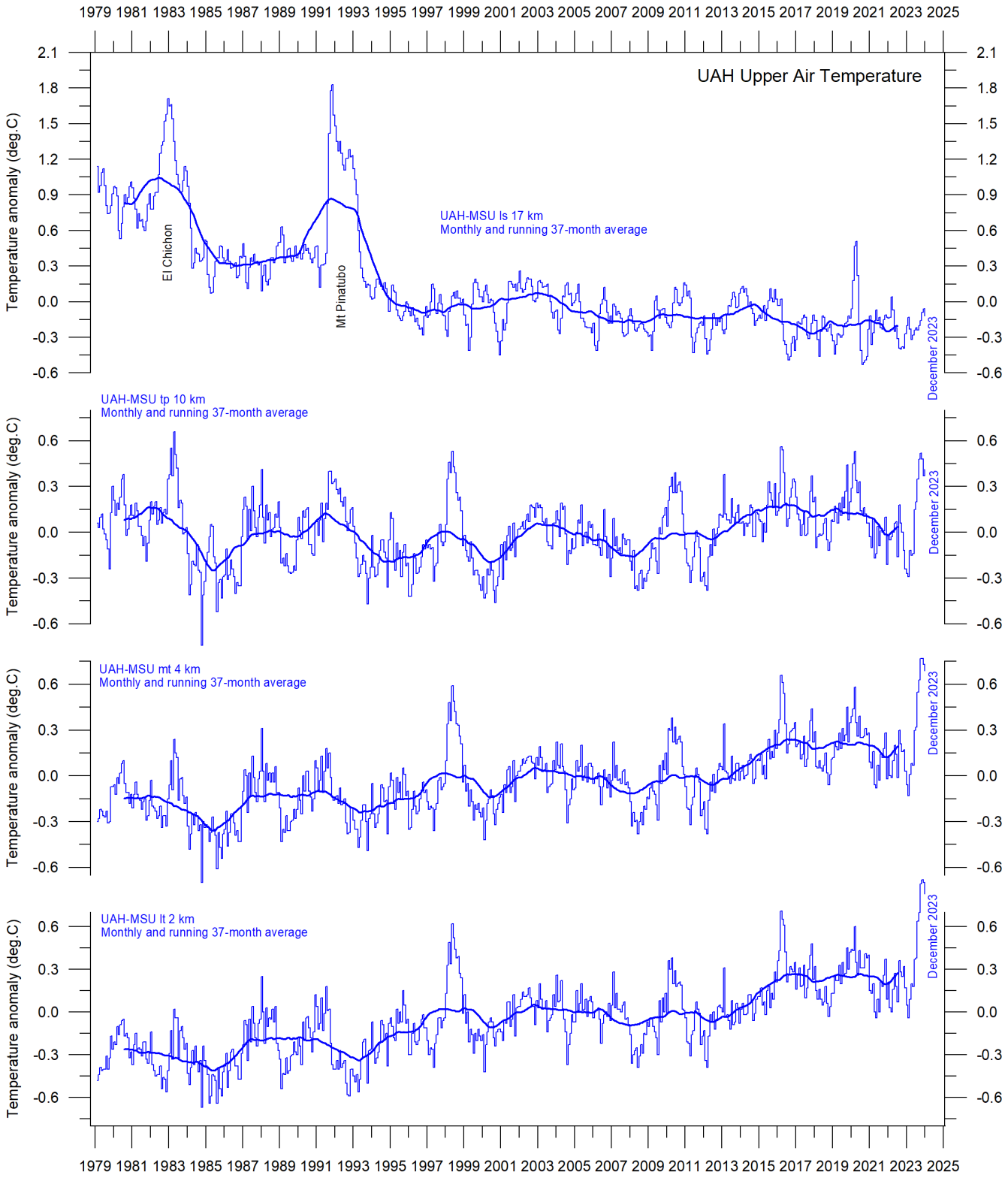

FIGURE 23: Global monthly average temperature in different altitudes according to University of Alabama at Huntsville (UAH), USA. The thin lines represent the monthly average, and the thick line the simple running 37-month average, nearly corresponding to a running 3-year average.

Changes in the vertical temperature profile of the atmosphere are interesting. One reason is that increasing tropospheric temperatures along with decreasing stratospheric temperatures are two central features associated the CO_2 hypothesis ascribing global warming to human-induced atmospheric CO_2 increases.

The temperature variations recorded in the lowermost Troposphere are generally reflected at higher altitudes, up to about 10 km altitude, including many individual troughs and peaks, such as the El Niño induced temperature spike of 2015–16, and the new El Niño beginning in 2023.

At high altitudes, near the Tropopause, the pattern of variations recorded lower in the atmosphere can still be recognised, but for the duration of the record (since 1979) there has been no clear trend towards higher or lower temperatures.

Higher in the atmosphere, in the Stratosphere, at 17 km altitude, two pronounced temperature spikes are visible before the turn of the century. Both can be related to major volcanic eruptions, as indicated in the diagram. The spike in 2020 occurs when major wildfires were playing out in Australia. Ignoring such marked spikes, however, until about 1995 the stratospheric temperature record shows a persistent and marked decline, ascribed by several scientists to the effect of heat being trapped by CO_2 in the Troposphere below. However, the marked Stratospheric temperature decline essentially ends around 1995–96, and a long temperature plateau has characterised the Stratosphere since that time.

Atmospheric greenhouse gasses; water vapour and carbon dioxide

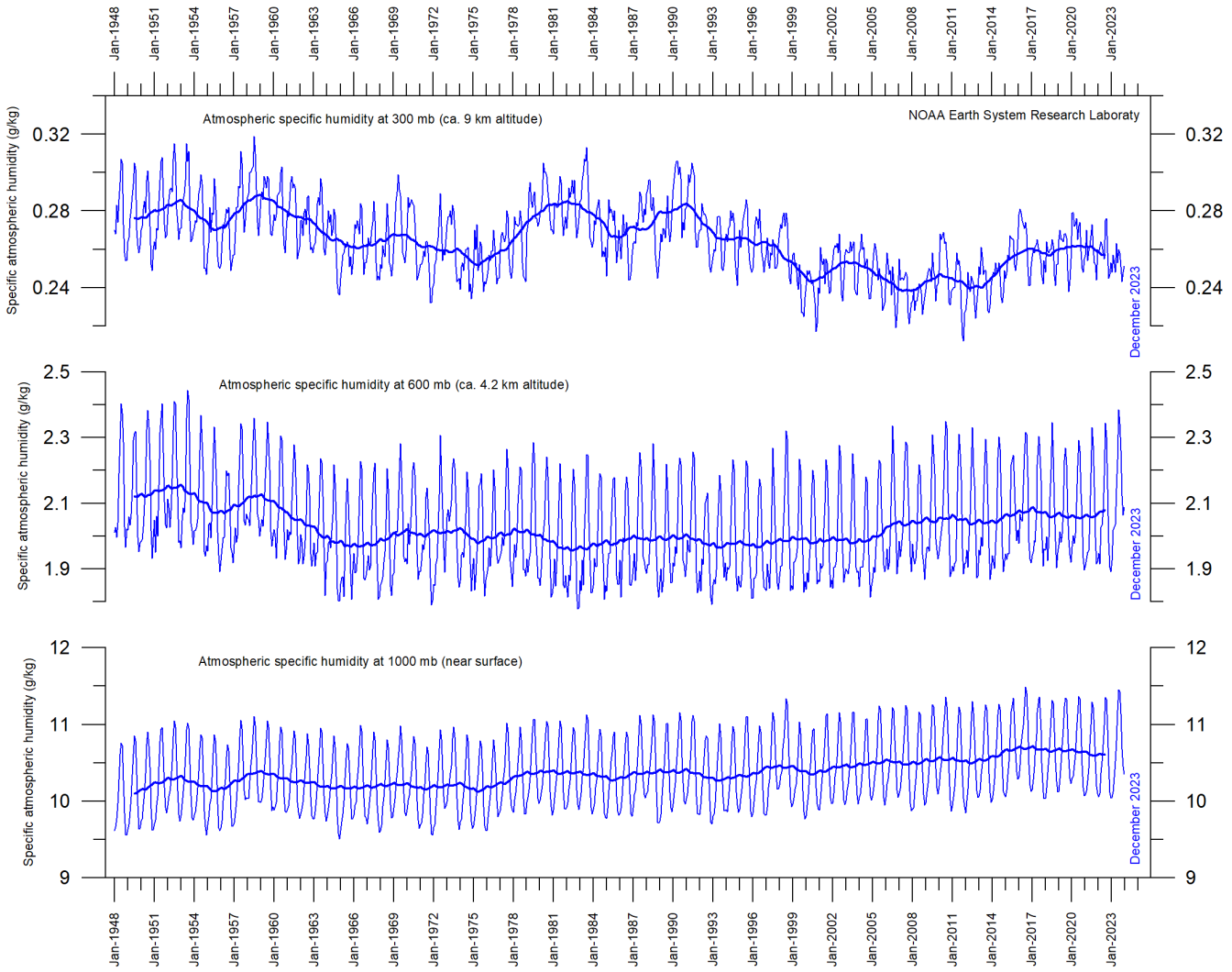

FIGURE 24: Specific atmospheric humidity (g/kg) at three different altitudes in the Troposphere since January 1948. The thin blue lines show monthly values, while the thick blue lines show the running 37-month average (about 3 years). Data source: Earth System Research Laboratory (NOAA).

Water vapor (H_2O) is the most important greenhouse gas in the Troposphere. The highest concentration is found within a latitudinal range from 50°N to 60°S. The two polar regions of the Troposphere are comparatively dry. H_2O is a much more important greenhouse gas than CO_2, both because of its absorption spectrum and its higher concentration.

Figure 24 shows the specific atmospheric humidity to be stable or slightly increasing up to about 4–5 km altitude. At higher levels in the Troposphere (about 9 km), the specific humidity has been decreasing for the duration of the record (since 1948), but with shorter variations superimposed on the falling trend. A Fourier frequency

analysis (not shown here) suggests these changes are influenced, not only by the significant annual variation, but possibly also by a longer variation of about 35-years' duration.

The overall decrease since 1948 in specific humidity at about 9 km altitude is notable, as this altitude roughly corresponds to the level where the theoretical temperature effect of increased atmospheric CO_2 is expected initially to play out.

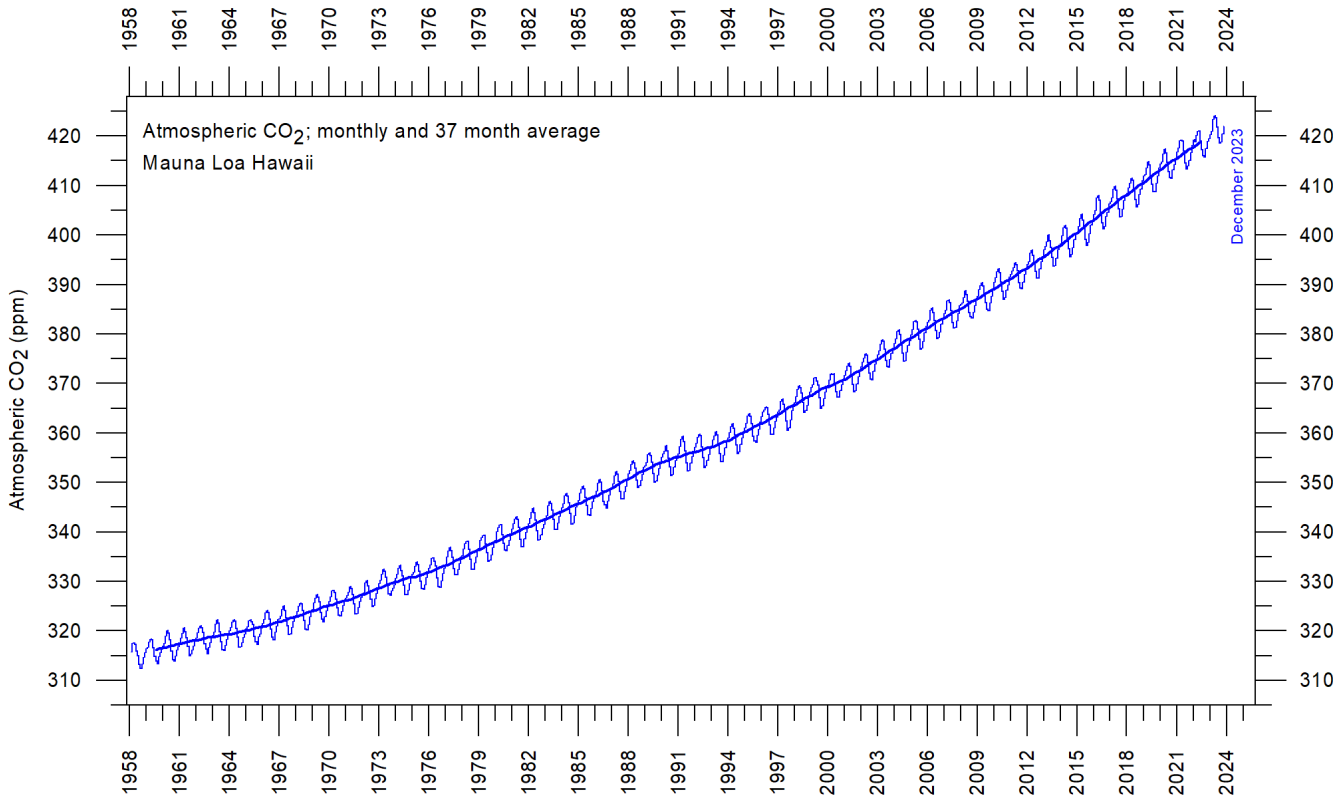

FIGURE 25: Monthly amount of atmospheric CO_2 since March 1958, measured at the Mauna Loa Observatory, Hawaii. The thin line shows the monthly values, while the thick line is the simple running 37-month average, nearly corresponding to a running 3-year average.

Carbon dioxide (CO_2) is an important greenhouse gas, although less important than H_2O. Since 1958, there has been an increasing trend in its atmospheric concentration, with an annual cycle superimposed. At the end of 2023, the amount of atmospheric CO_2 was close to 422ppm (Figure 25). CO_2 is generally considered as a relatively well-mixed gas in the Troposphere.

The 12-month (annual) change in Tropospheric CO_2 (Figure 26) has been increasing from about +1 ppm/year in the early part of the record, to about +2.6 ppm/year towards the end of the record. A Fourier frequency analysis (not shown here) shows the 12-month change of Tropospheric CO_2 to be influenced especially by a significant periodic variation of 3.6-year duration. There is no visible effect of the global COVID-19 lockdown 2020–2021 in the amount of atmospheric CO_2.

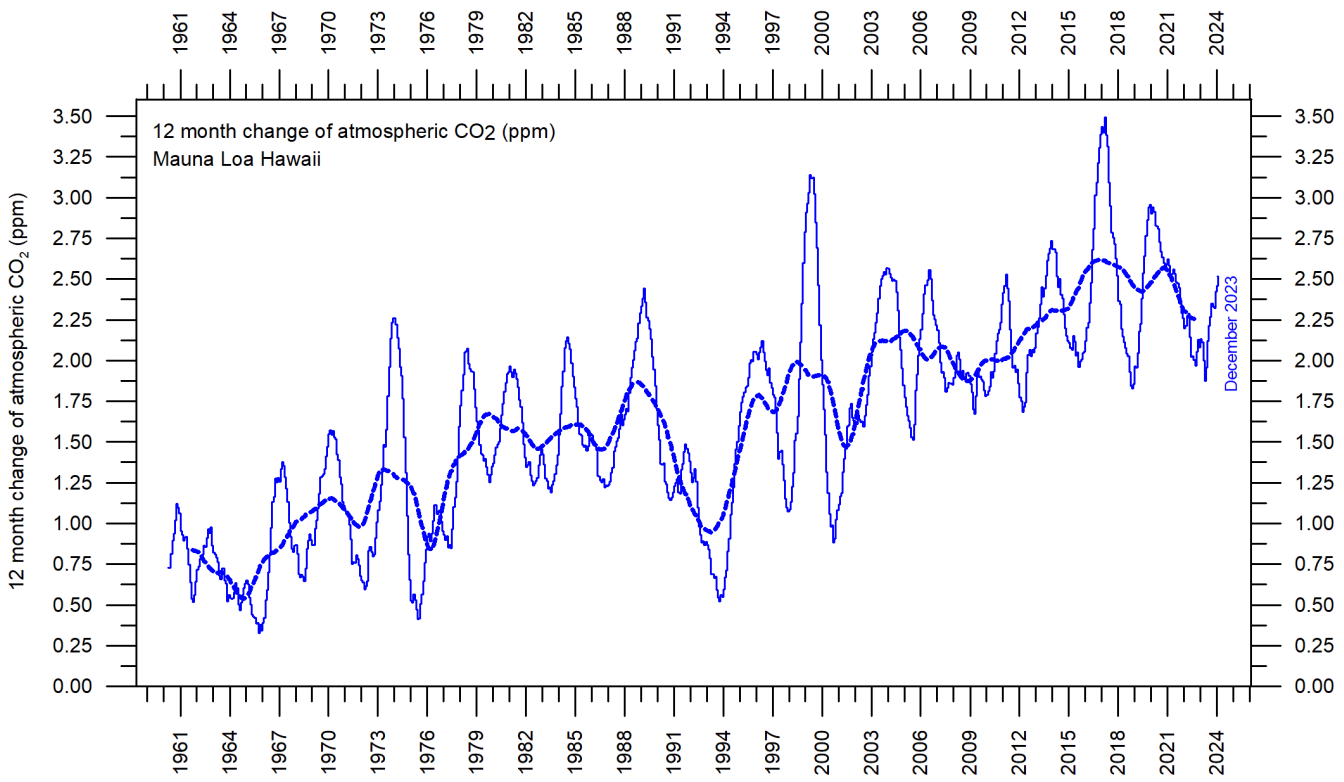

FIGURE 26: Annual (12 month) growth rate (ppm) of atmospheric CO2 since 1959, calculated as the average amount of atmospheric CO2 during the last 12 months, minus the average for the preceding 12 months. The graph is based on data measured at the Mauna Loa Observatory, Hawaii. The thin blue line shows the value calculated month by month, while the dotted blue line represents the simple running 3-year average.

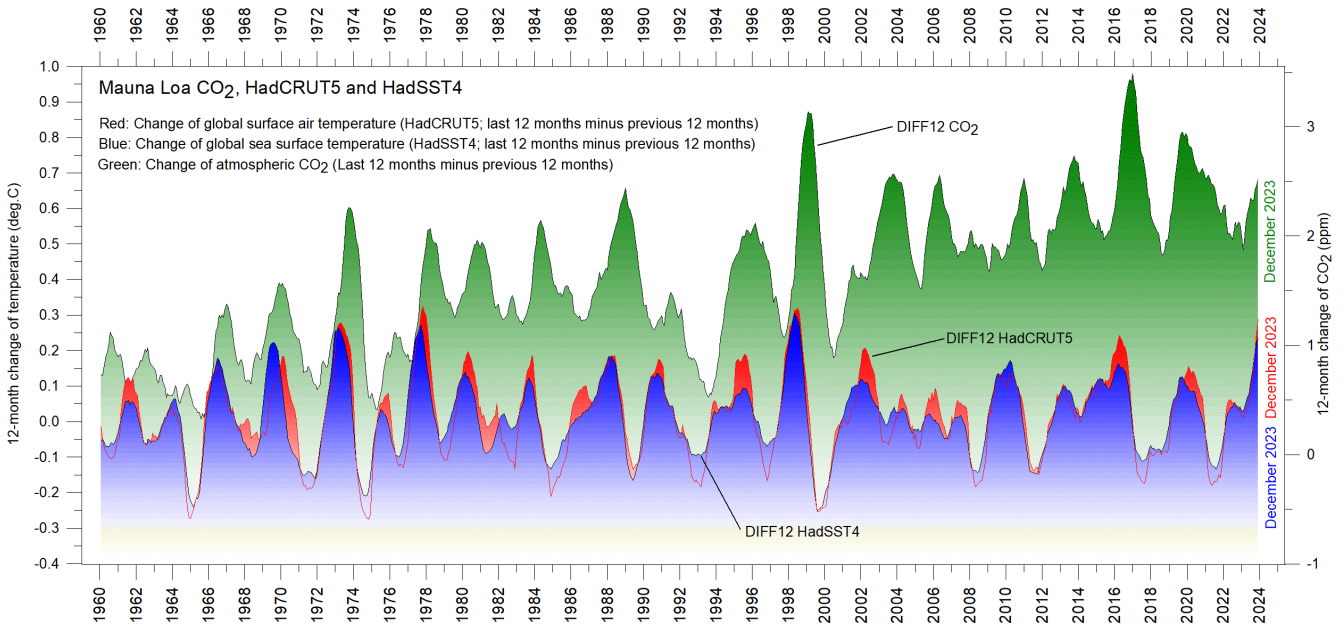

FIGURE 27: Annual (12-month) change of global atmospheric CO_2 concentration (Mauna Loa; green), global sea surface temperature (HadSST4; blue) and global surface air temperature (HadCRUT5; red). All graphs are showing

monthly values of DIFF12, the difference between the average of the last 12 months and the average for the previous 12 months for each data series.

It is informative to consider the variation of the annual change rate of atmospheric CO_2, and global air temperature and global sea surface temperature (Fig. 27). All three change rates clearly vary in concert, but sea-surface temperatures are a few months ahead of the global air temperature, and 11-12 months ahead of changes in atmospheric CO_2. The ocean surface is evidently the starting point for many important climate-related changes.

Figure 28 shows the visual association between annual change of atmospheric CO_2 and La Niña and El Niño episodes, emphasizing the importance of oceanographic dynamics for understanding changes in atmospheric CO_2.

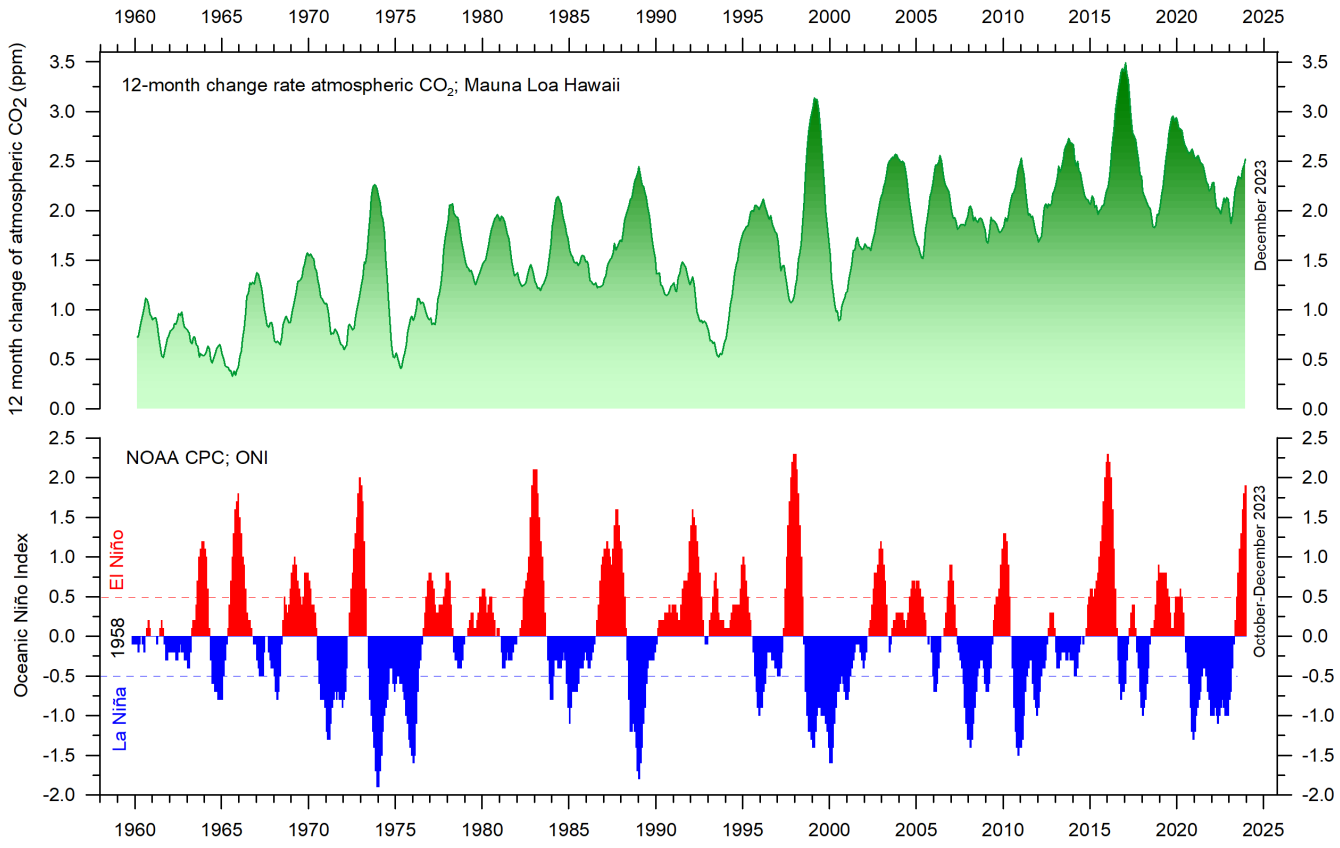

FIGURE 28: Visual association between annual growth rate of atmospheric CO_2 (upper panel) and Oceanic Niño Index (lower panel). See also the diagrams above (Fig. 26 and 27).

Sea surface temperature anomaly at the end of the years 2021, 2022 and 2023

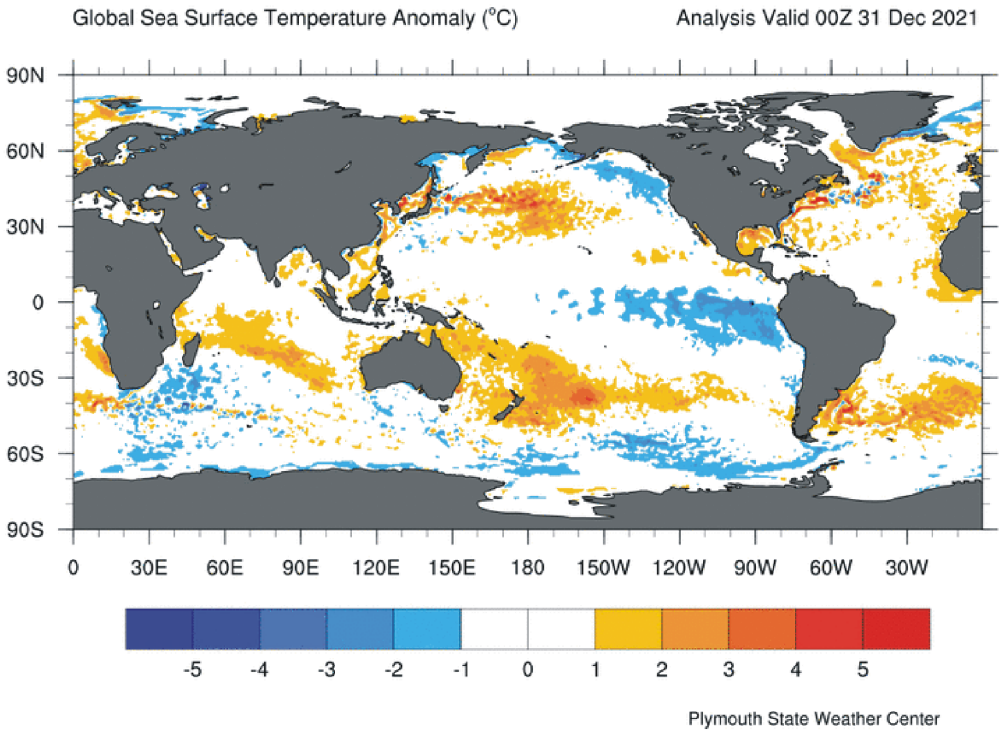

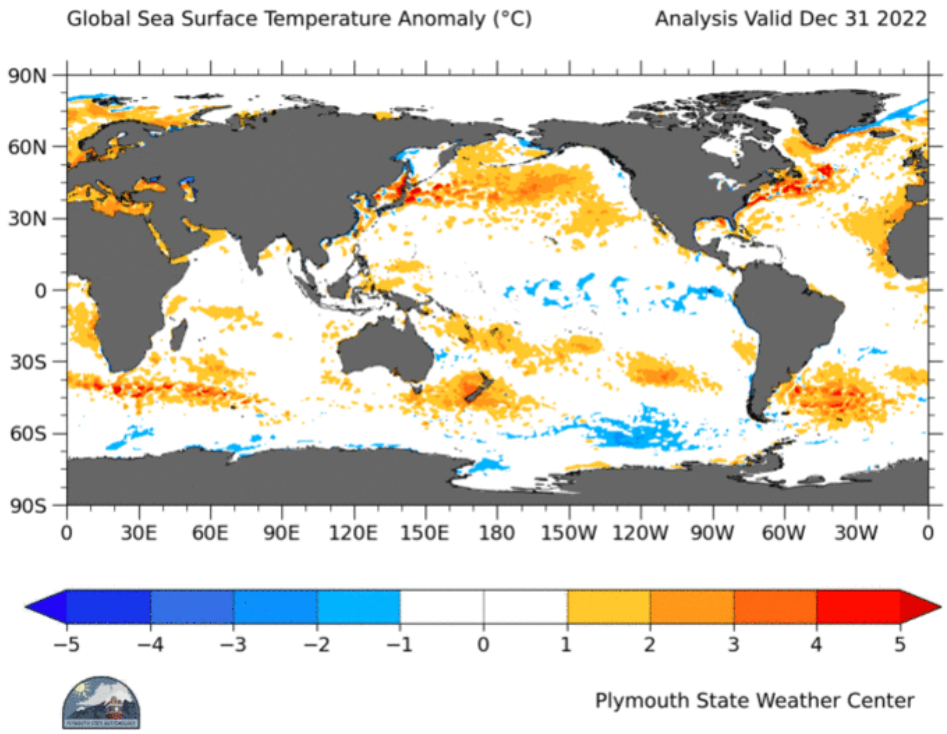

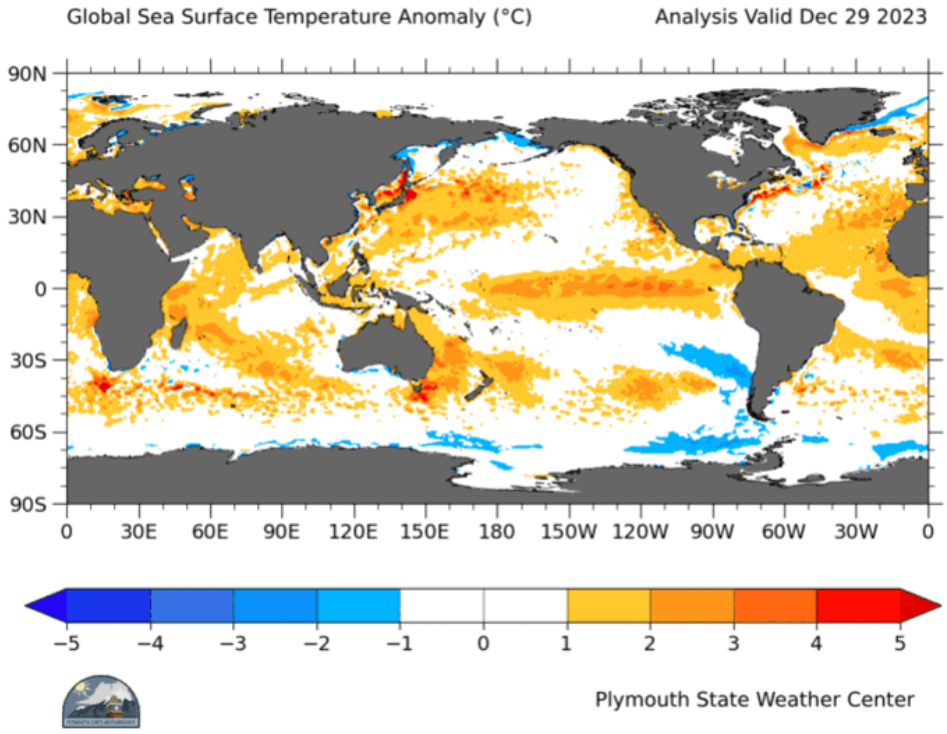

FIGURE 29a-c: Sea surface temperature anomalies at the end of December 2021, 2022, and 2023, respectively (top to bottom, degrees C). The maps show the current anomaly (deviation from reference value) of the surface temperature of Earth's oceans. Reference period: 1977-1991. Dark grey represents land areas. Map source: Plymouth State Weather Center.

.

The three maps in figure 29a-c show the moderate La Niña characterising much of 2021 and 2022, and the ongoing strong El Niño episode at the end of 2023. See also figure 30, where all El Niño and La Niña episodes since 1950 are displayed.

The recent 2015-16 and the ongoing El Niño episode are among the strongest since the beginning of the record in 1950 and matches with the recent global temperature peaks in 2016 and 2023 (Fig.6, 7, 12, 13 and 14). Considering the entire record, however, recent variations between El Niño and La Niña episodes appear quite normal.

A Fourier frequency analysis (not shown here) shows the ONI record to be influenced by a significant 3.6-year cycle, and possibly also by a longer 5.6-year cycle.

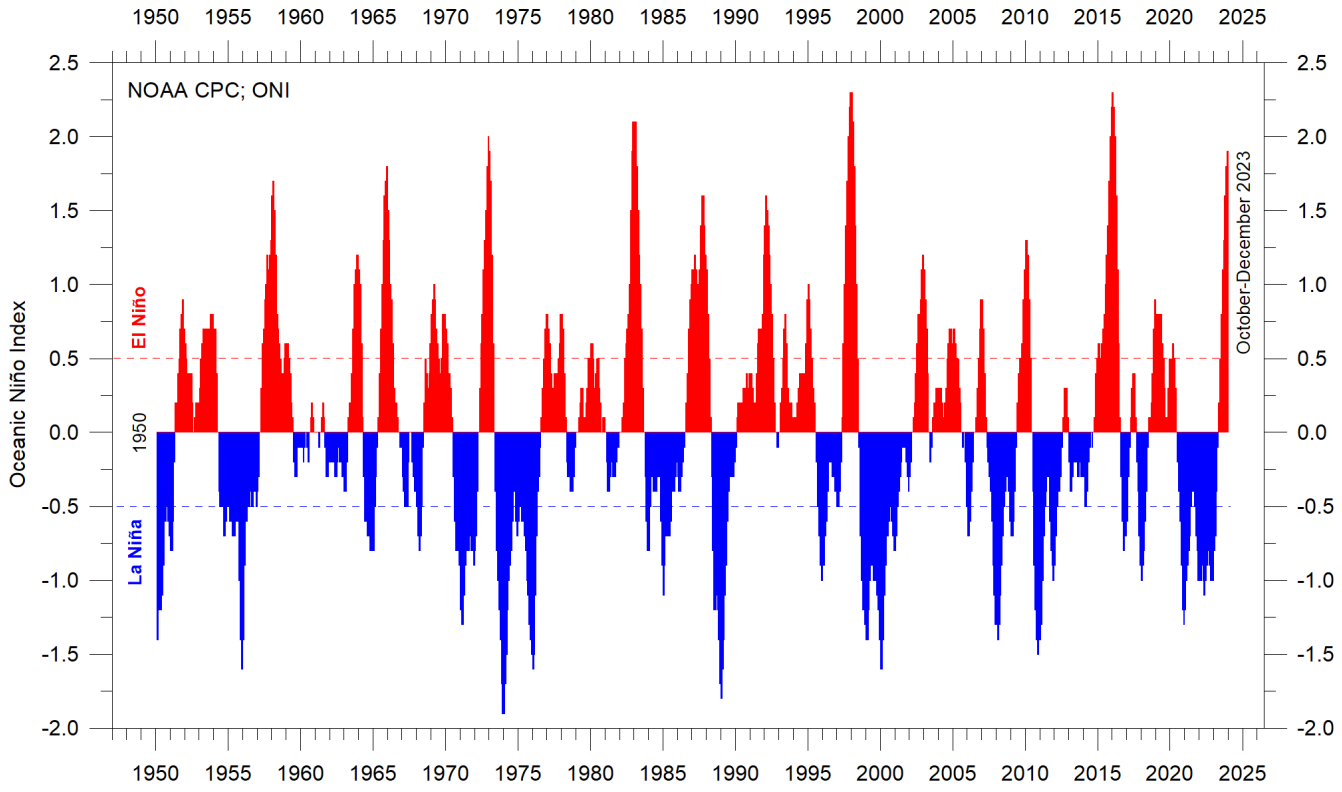

FIGURE 30: Warm and cold episodes for the Oceanic Niño Index (ONI), defined as 3 month running mean of ERSST.v5 SST anomalies in the Niño 3.4 region (5°N-5°S, 120°-170°W). Anomalies are centred on 30-year base periods updated every 5 years.

Global ocean average temperatures to 1900 m depth

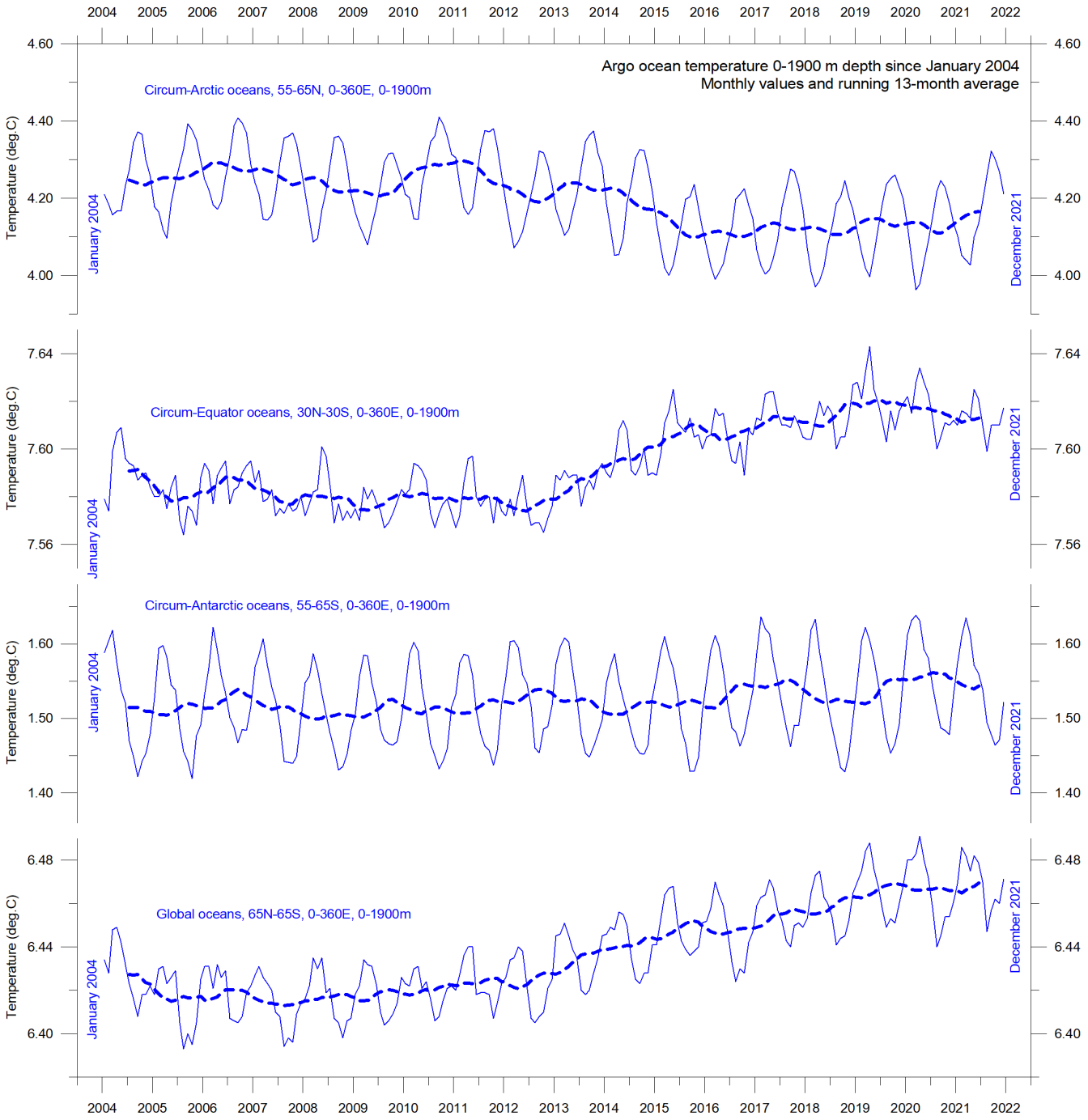

FIGURE 31: Average ocean temperatures January 2004 – December 2021 at 0-1900 m depth in selected latitudinal bands, using Argo-data. The thin line shows monthly values, and the thick stippled line shows the running 13-month average. Source: Global Marine Argo Atlas.

Based on observations by Argo floats (Roemmich and Gilson 2009) the global summary diagram above (Figure 31) shows that, on average, the temperature of the global oceans down to 1900 m depth has been increasing since about 2010. It can also be seen that this increase since 2013 is predominantly due to oceanic changes occurring near the Equator, between 30°N and 30°S. In contrast, for the circum-Arctic oceans, north of 55°N,

depth-integrated ocean temperatures have been decreasing since 2011. Near the Antarctic, south of 55°S, temperatures have essentially been stable. At most latitudes, a clear annual rhythm is seen to play out.

From about 2020 the measurements available may possibly indicate the onset of a new development, with decreasing circum-Equator temperatures, and increasing circum-Arctic temperatures. However more measurements are needed to conclude anything on this ongoing development.

Global ocean temperatures at different depths

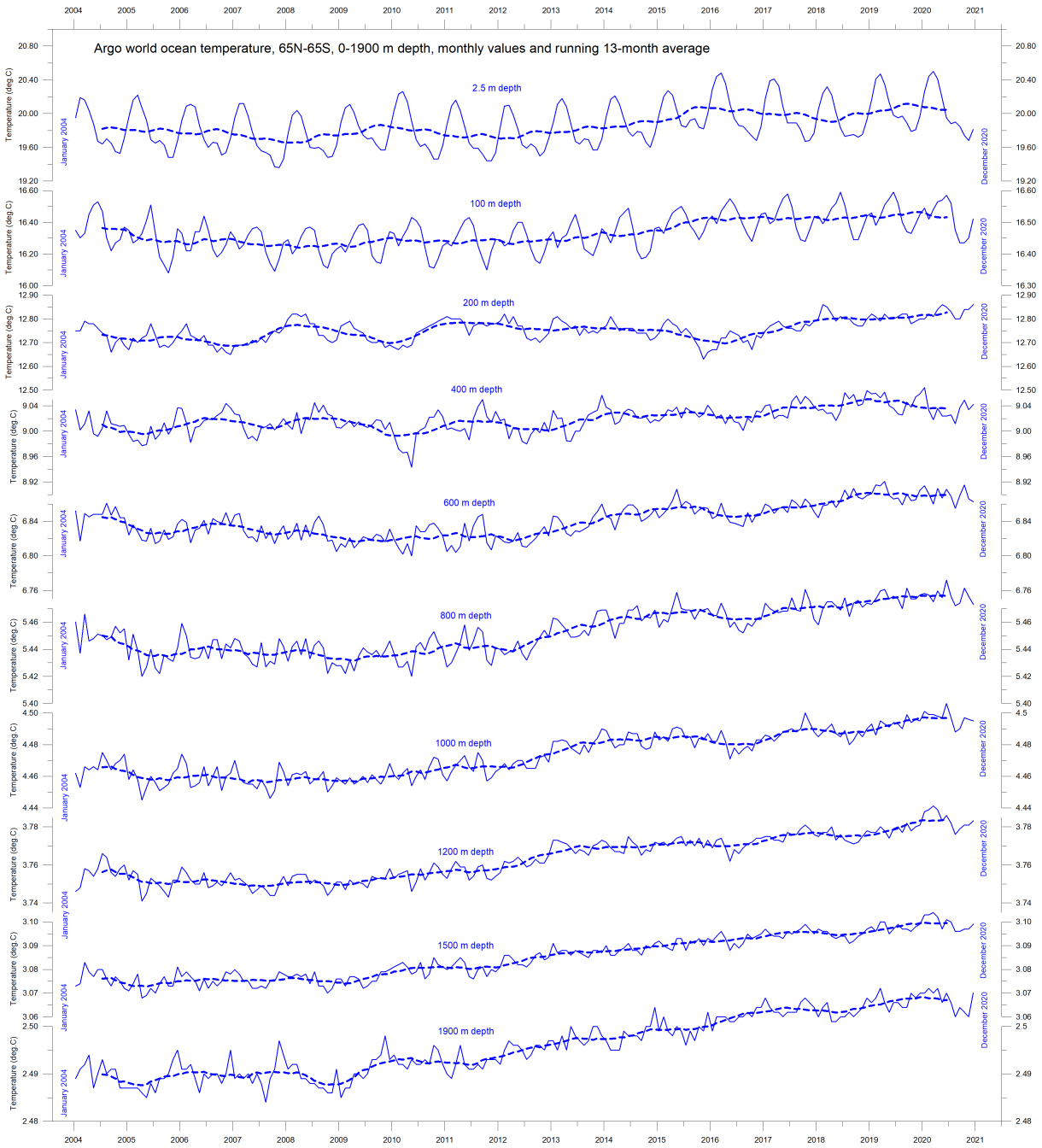

FIGURE 32: Global ocean temperatures January 2004 – August 2020 at different depths between 65°N and 65°S, using Argo-data. The thin line shows monthly values, and the stippled line shows the running 13-month average. Source: Global Marine Argo Atlas.

Figure 32 displays global average oceanic temperatures at different depths. An annual rhythm can be traced to about 100 m depth. In the uppermost 100 m, temperatures have increased since about 2011. At 200–400 m depth, temperatures have exhibited little change during the observational period.

For depths below 400 m, however, temperatures have increased over the observational period. Interestingly, the data suggests that this increase commenced at 1900 m depth in around 2009, and from there has gradually spread upwards. At 600 m depth, the present temperature increase began around 2012; that is, about three years later than at 1900 m depth. The timing of these changes shows that average temperatures in the upper 1900 m of the oceans are not only influenced by conditions playing out at or near the ocean surface, but also by processes operating at greater depths than 1900 m. As a result, part of the current ocean warming appears to be due to circulation changes taking place at depths below 1900 m, and therefore not directly related to processes operating at or near the surface.

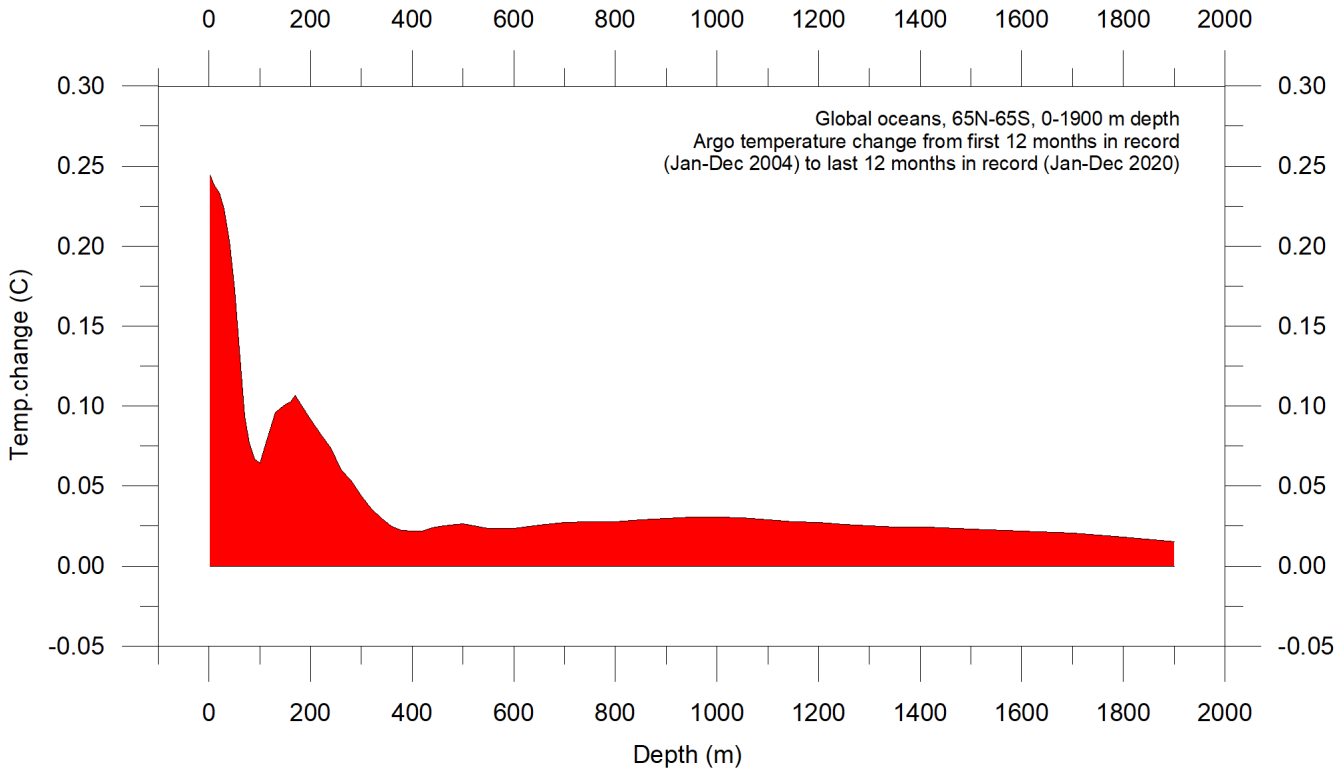

FIGURE 33: Global ocean net temperature change since 2004 from surface to 1900 m depth, using Argo-data. Source: Global Marine Argo Atlas.

This development is also seen in Figure 33, which shows net changes of global ocean temperatures at different depths, calculated as the net difference between two 12-month averages: for January–December 2004 and January-December 2020. The largest net changes are seen to have occurred in the uppermost 200 m of the water column. However, such average values, although important, also hide many interesting regional details. These are considered in the next section.

Regional ocean temperature changes temperatures 0-1900 m depth

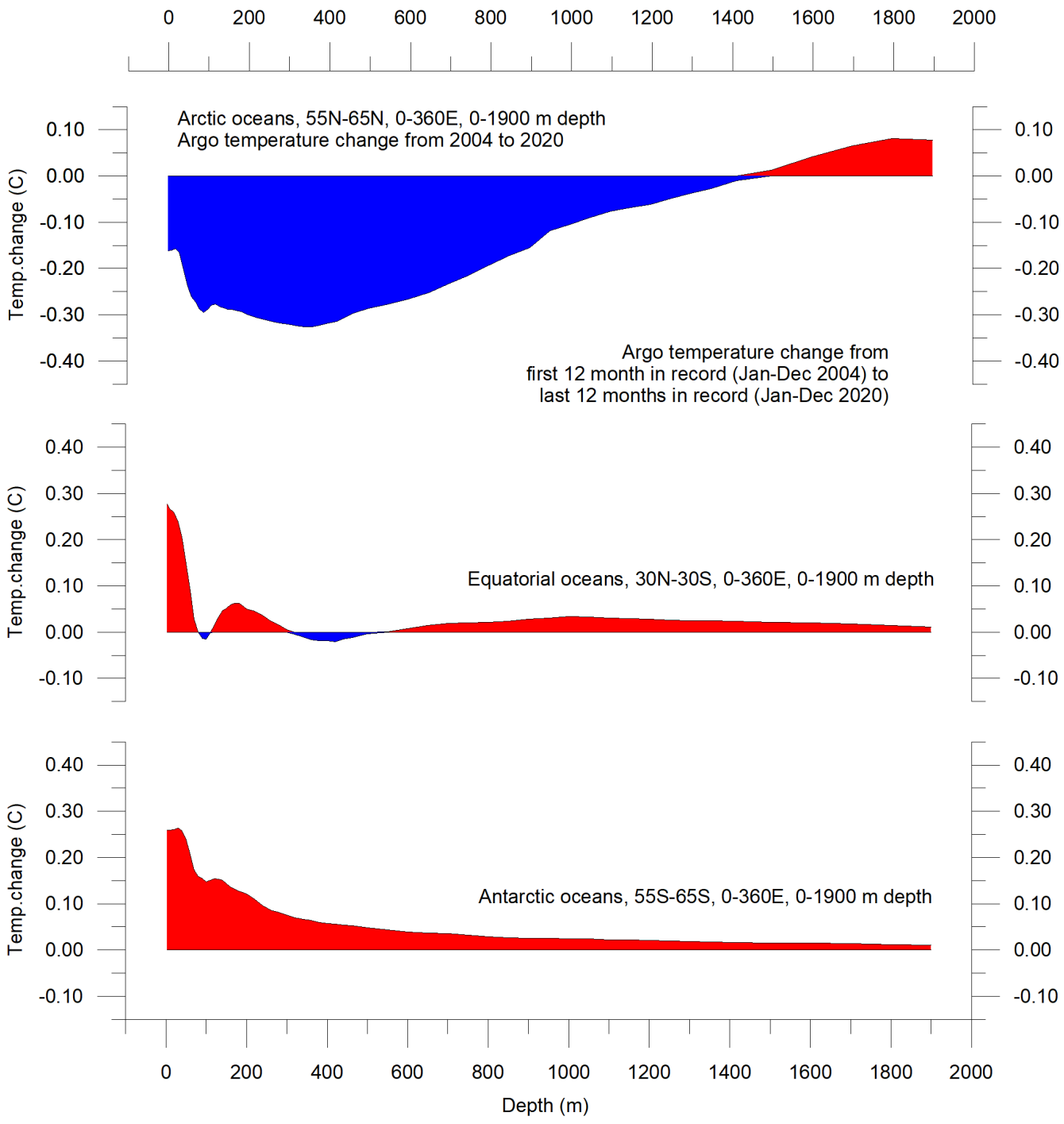

FIGURE 34: Net temperature change since 2004 from surface to 1900 m depth in different parts of the global oceans, using Argo-data. Source: Global Marine Argo Atlas.

Figure 34 shows variation of oceanic temperature net changes between the same two 12-month periods as in the last section, for various depths, and for three different latitudinal bands, representing the Arctic Oceans (55–65°N), Equatorial Oceans (30N-30°S), and Antarctic Oceans (55–65°S), respectively. The global net surface warming seen in Figure 33 can be seen to affect the Equatorial and Antarctic Oceans, but not the Arctic Oceans. In fact, net cooling is pronounced down to 1400 m depth for the northern oceans. However, a major part of Earth's land area is in the Northern Hemisphere, so the surface area (and volume) of 'Arctic' oceans is much smaller than the 'Antarctic' oceans, which are in turn is smaller than the 'Equatorial' oceans. In fact, half of the planet's surface area (land and ocean) is located between 30°N and 30°S.

Nevertheless, the contrast in net temperature changes for the different latitudinal bands is instructive. For the two polar oceans, the Argo data appears to suggest the existence of a bi-polar seesaw, as described by Chylek et al. (2010). It is no less interesting that the near-surface ocean temperature in the two polar oceans contrasts with the overall development of sea ice in the two polar regions (see later in this report).

Ocean temperature net change 2004-2020 in selected sectors

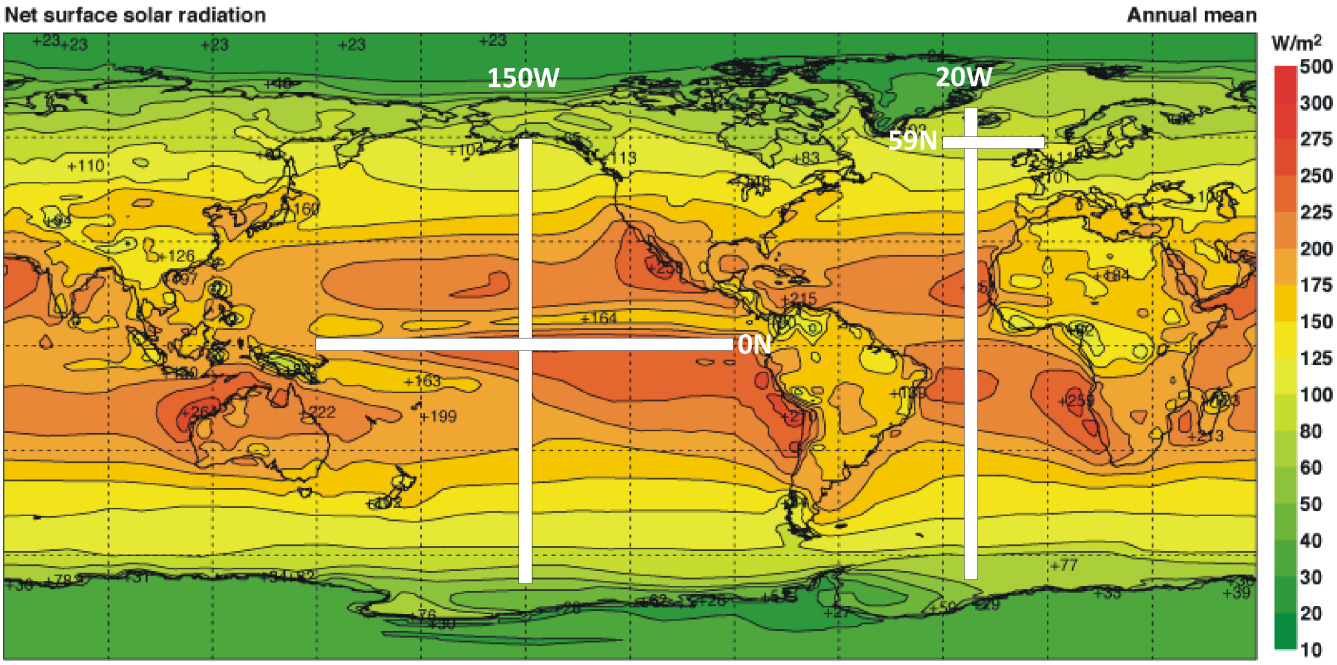

FIGURE 35: Map showing average annual mean net surface solar radiation (W/m²), and the location of four profiles shown and discussed below.

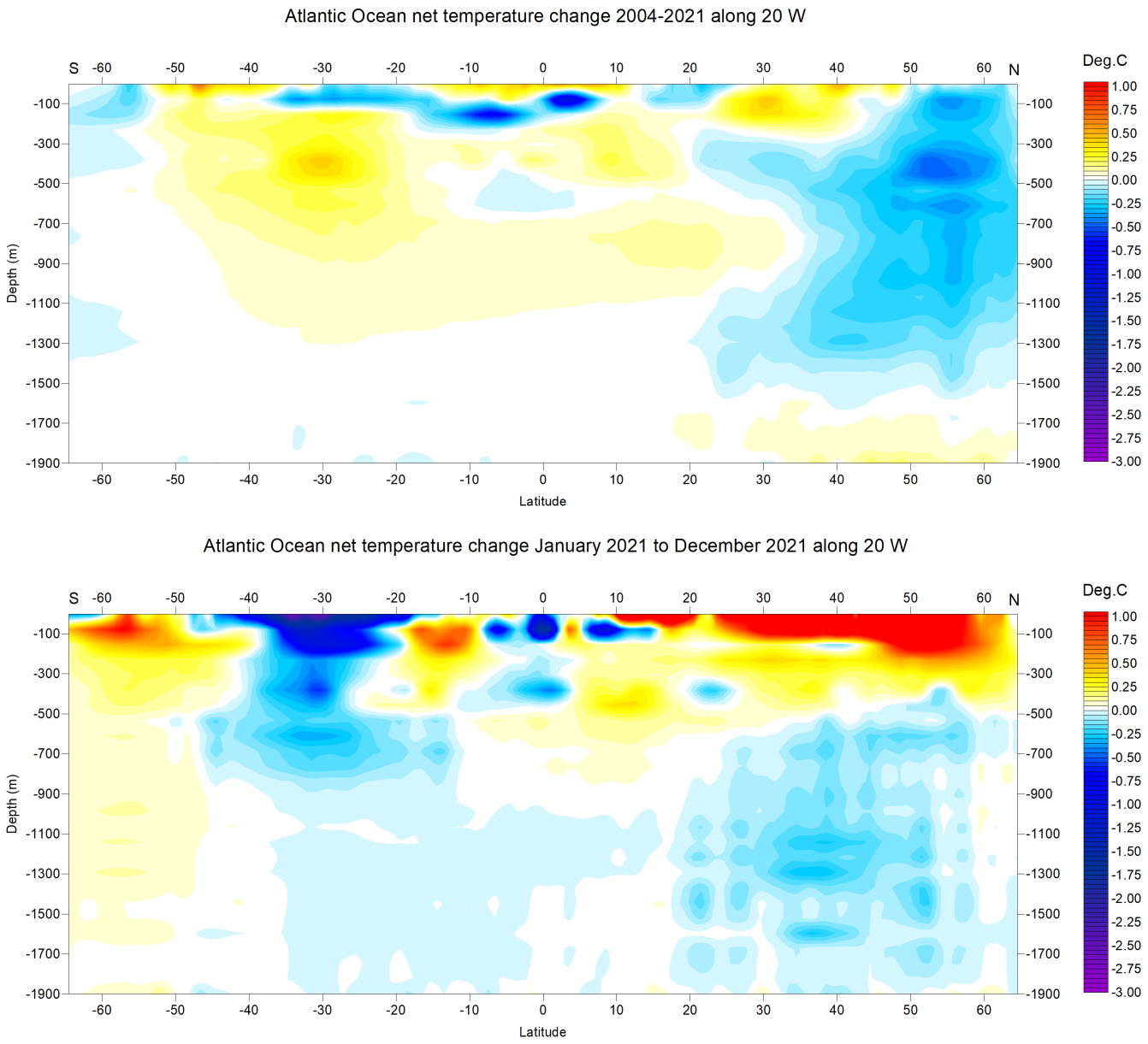

FIGURE 36a-b: *Net temperature changes 2004-2021 and during 2021 from surface to 1900 m depth at 20°W in the Atlantic Ocean, using Argo-data. See Figure 35 for geographical location of transect. Data source: Global Marine Argo Atlas.*

Figure 36a shows net temperature changes during 2004-2021 and during 2021 along 20°W, representing the Atlantic Ocean. To prepare the diagram, 12-month average ocean temperatures for 2021 were compared to annual average temperatures for 2004, representing the initial 12 months in the Argo-record. To give an insight into also the most recent changes, the 12-month net change from January 2021 to December 2021 is shown in the lower diagram (Figure 36b). Warm colours indicate net warming and blue colours indicate cooling. Due to the spherical form of Earth, high latitudes represent smaller ocean volumes than lower ones near the Equator. With this reservation in mind, the data along the Atlantic transect nevertheless reveal several interesting features.

The most prominent feature in the 2004–2021 profile is a marked net cooling north of 35-40°N, affecting depths down to 1500-1600 m. In contrast, warming characterises further south, especially between 20-50°S, down to about 1100 m depth. At 100-150 m depth cooling dominates between 10°N and 40°S.

The temperature development over the last 12 months of the record (Figure 36b) shows a more complicated pattern, especially near the surface. Much of the South Atlantic net warming 2004-2021 is presently undergoing cooling, especially between 20°S and 40°S. In the North Atlantic, the last 12 months display warming north of 10°N, affecting depths down to 200 m.

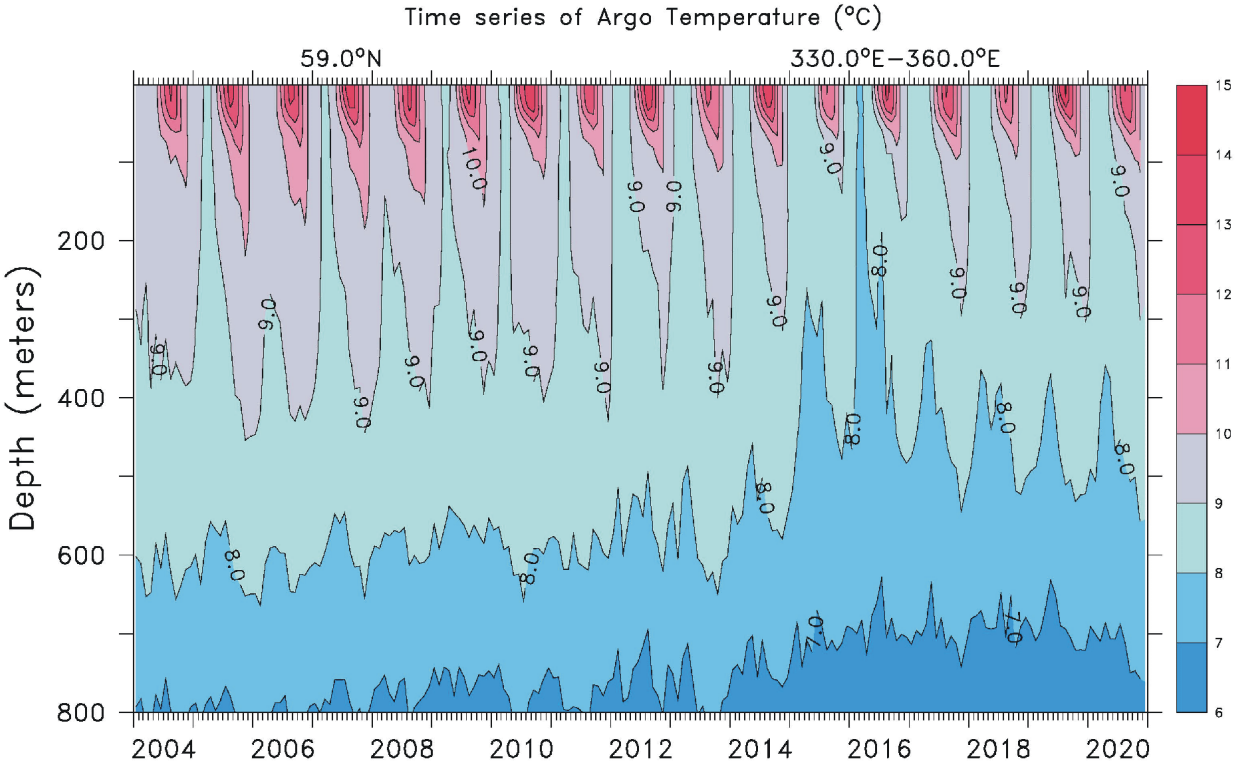

FIGURE 37: Diagram showing time series January 2004 – December 2020 of ocean temperatures at 59°N, 30–0°W, from surface to 800 m depth, using Argo-data. See Figure 35 for geographical location of transect. Source: Global Marine Argo Atlas.

Of particular interest are the temperature dynamics displayed within a 59°N transect across the North Atlantic Current, just south of the Faroe Islands, as this area is important for weather and climate in much of Europe. Figure 37 shows a time series at 59°N, from 30°W to 0°W, and from the surface to 800 m depth. This essentially represents a section across the water masses affected by the North Atlantic Current. Ocean temperatures higher than 9°C are indicated by red colours.

This time series, although still relatively short, display noteworthy dynamics. The prominence of warm water (above 9°C) apparently peaked in early 2006, after which temperatures gradually reduced until 2016. Since then, a partial temperature recovery has taken place. The observed change, from peak to trough, playing out over approximately 11 years, might possibly suggest a 22-year temperature cycle, but we will have to wait until the Argo series is longer before drawing conclusions.

Figure 38 shows the same time series data (59°N, 330–0°W, 0–800 m depth, 2004–2021) as a graph of depth-integrated average ocean temperature.

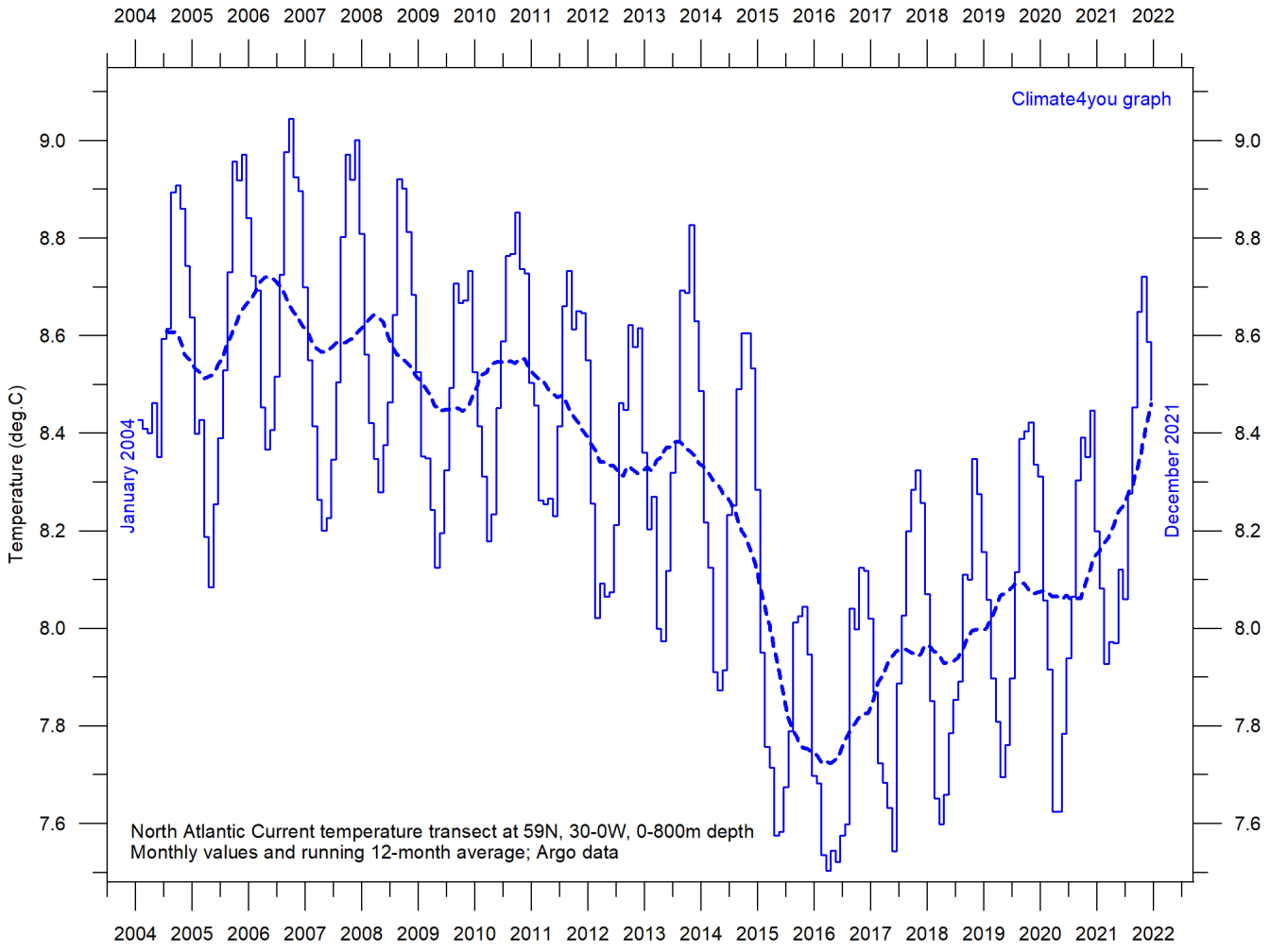

FIGURE 38: Average temperature along 59°N, 30-0W, 0-800 m depth, corresponding to a cross-section of the main part of the North Atlantic Current, using Argo-data. Source: Global Marine Argo Atlas.

Below are shown two Pacific Ocean diagrams (Fig. 39a-b), showing net changes from 2004-2021 and during 2021 along 150°W, using data obtained by Argo-floats, and prepared like the Atlantic diagrams above. Warm colours indicate net warming, and blue colours net cooling. Again, northern, and southern latitudes represent only relatively small ocean volumes, compared to latitudes near the Equator.

One interesting feature for 2004-2021 (Fig. 39a) is net cooling near the Equator (15°S-20°N) down to about 700 m depth. In contrast, two bands (20-40°S and 30-45°N) are characterised by net warming, down to 800-900 m depth. During the last 12 months in the Argo record (Figure 39b) net cooling is prominent apart from surface water 5°S-50°N displaying warming down to 100-200 m depth. This recent (2021) warming at the surface near Equator is probable be the result of a short weakening of the La Niña playing out then (Fig. 30).

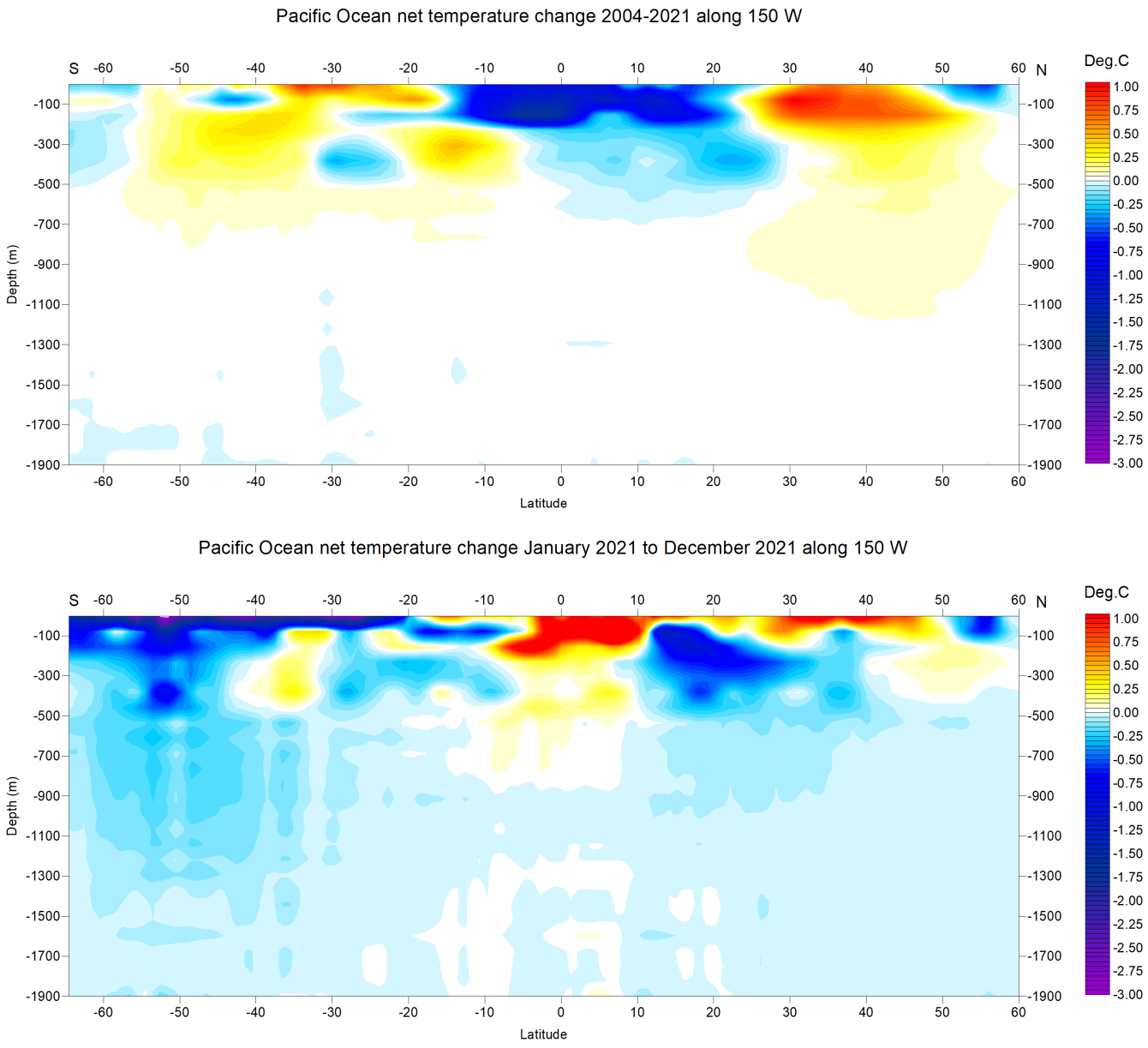

FIGURE 39a-b: *Net temperature changes 2004-2021 and during 2021 from surface to 1900 m depth at 150°W in the Pacific Ocean, using Argo-data. See Figure 35 for geographical location of transect. Data source: Global Marine Argo Atlas.*

Neither the Atlantic or the Pacific longitudinal diagrams reveal the extent to which the net changes displayed are caused by ocean dynamics operating east and west of the two profiles considered. For that reason, they should

not be overinterpreted. They do, however, suggest an interesting contrast, with the Atlantic displaying a more dynamic temperature development than the Pacific, except for depths and latitudes affected by El Niño and La Niña episodes.

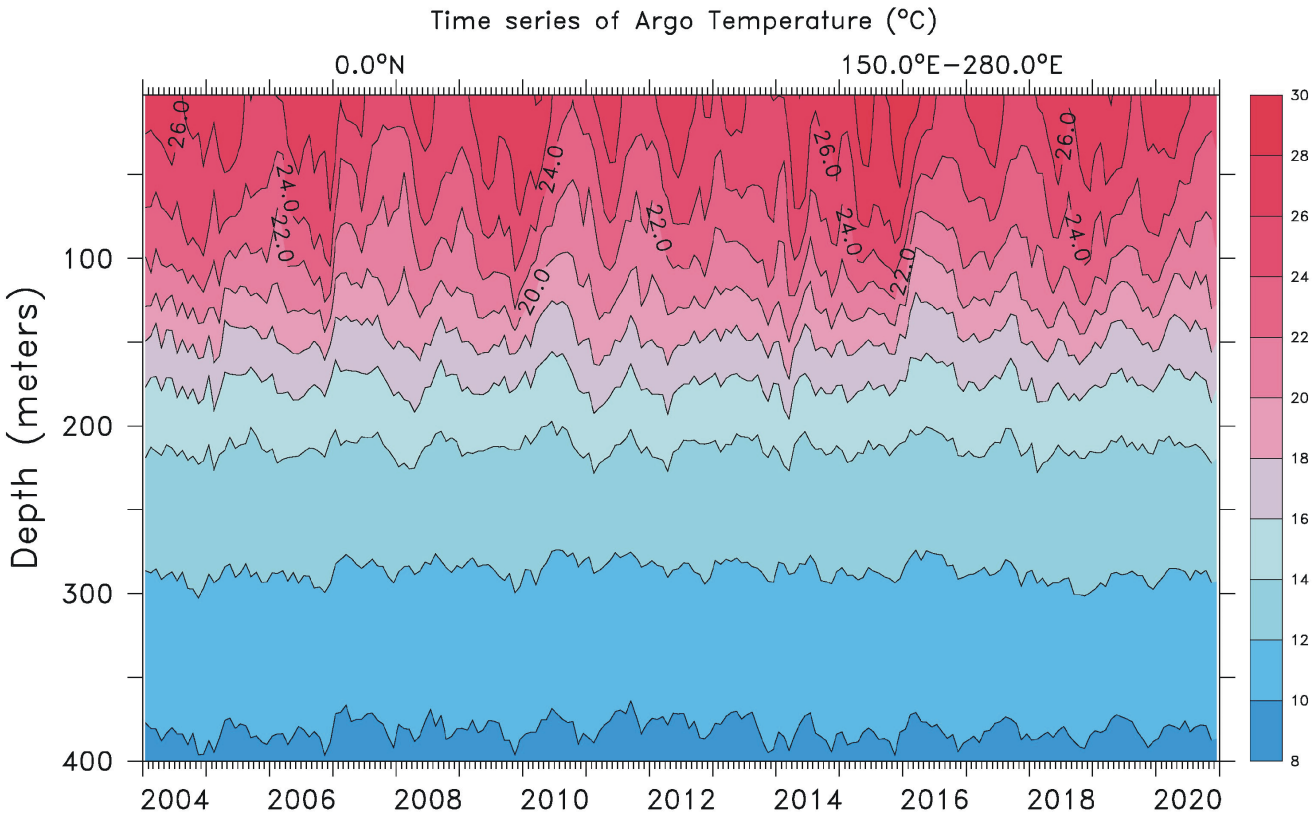

FIGURE 40: Time series showing sea temperature variations with depth January 2004 – December 2020 in the El Niño and La Niña region along the Equator in the Pacific Ocean. See Figure 35 for geographical location of transect. Data source: Global Marine Argo Atlas.

Figure 40 shows a time series of sea temperatures from surface to 400 m depth in the El Niño /La Niña region (Pacific Ocean). By comparing with Figure 30 the individual episodes are easily recognised as temperature variations in the upper 150-200 m of the ocean. Below 200-250 m temperature conditions are essentially constant, demonstrating that El Niño and La Niña episodes are surface phenomenon's, with no influence from greater depths.

Southern Oscillation Index (SOI)

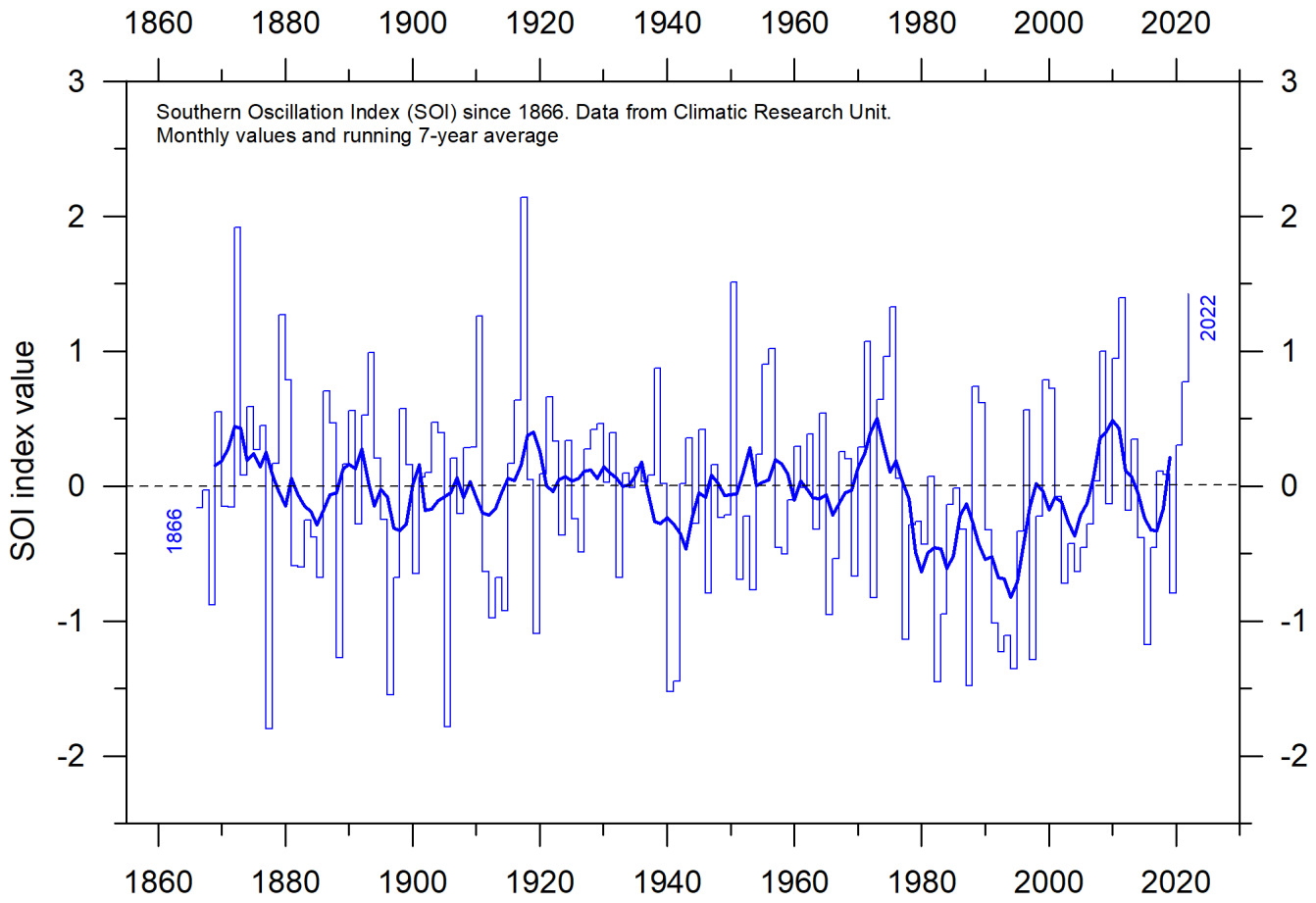

FIGURE 41: Monthly Southern Oscillation Index (SOI) anomaly since 1866, according to the Climatic Research Unit (CRU). The Southern Oscillation Index (SOI) is calculated from the monthly or seasonal fluctuations in the air pressure difference between Tahiti and Darwin. The thin line represents annual values, while the thick line is the simple running 7-year average.

The Southern Oscillation may be considered as the atmospheric component of El Niño/La Niña episodes. Sustained negative values of the SOI (Figure 39) often indicate El Niño episodes. Such negative values are usually accompanied by persistent warming of the central and eastern tropical Pacific Ocean, a decrease in the strength of the Pacific Trade Winds, and a reduction in rainfall over eastern and northern Australia.

Positive values of the SOI are usually associated with stronger Pacific trade winds and higher sea surface temperatures to the north of Australia, indicating La Niña episodes. Waters in the central and eastern tropical

Pacific Ocean become cooler during this time. Eastern and northern Australia usually receives increased precipitation during such periods.

A Fourier frequency analysis (not shown here) shows the SOI record to be influenced by a 3.6-year cycles.

Pacific Decadal Oscillation (PDO)

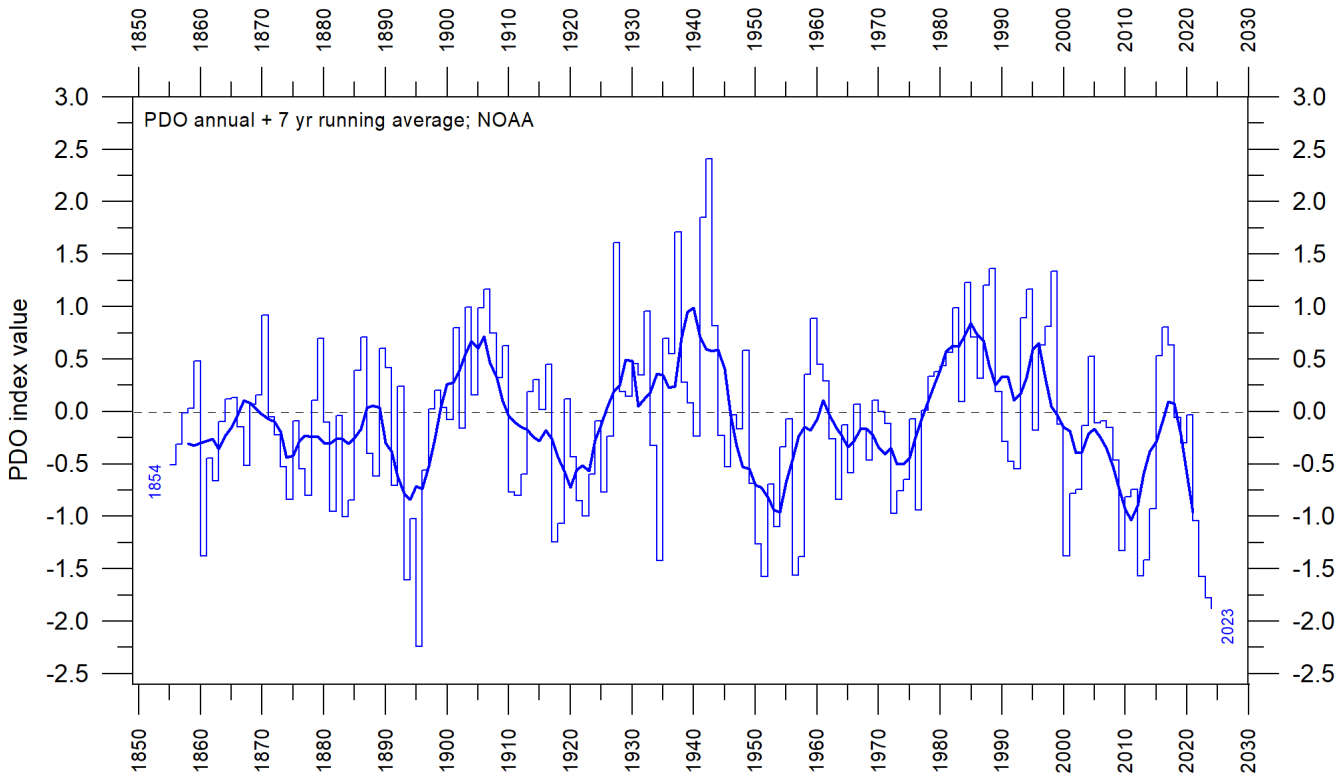

FIGURE 42: Annual values of the Pacific Decadal Oscillation (PDO) according to the Physical Sciences Laboratory, NOOA. The thin line shows the annual PDO values, and the thick line is the simple running 7-year average.

The PDO (Figure 42) is a long-lived El Niño-like pattern of Pacific climate variability, with data extending back to January 1854. Its causes are not currently known, but even in the absence of a theoretical understanding, and understanding its variability improves season-to-season and year-to-year climate forecasts for North America because of its strong tendency for multi-season and multi-year persistence. The PDO also appears to be roughly in phase with global temperature changes. Thus, it is important from a societal-impact perspective, because it shows that 'normal' climate conditions can vary over periods comparable to the length of a human lifetime.

The PDO nicely illustrates how global temperatures are tied to sea-surface temperatures in the Pacific Ocean, the largest ocean on Earth. When sea-surface temperatures are relatively low (negative phase PDO), as they were from 1945 to 1977, global air temperature decreases. When sea-surface temperatures are high (positive phase PDO), as they were from 1977 to 1998, global surface air temperature increases (Figures 12–14).

A Fourier frequency analysis (not shown here) shows the PDO record to be influenced by a significant 5.6-year cycle, and possibly also by a longer 18.6-year long period, corresponding to the length of the lunar nodal tide.

Atlantic Multidecadal Oscillation (AMO)

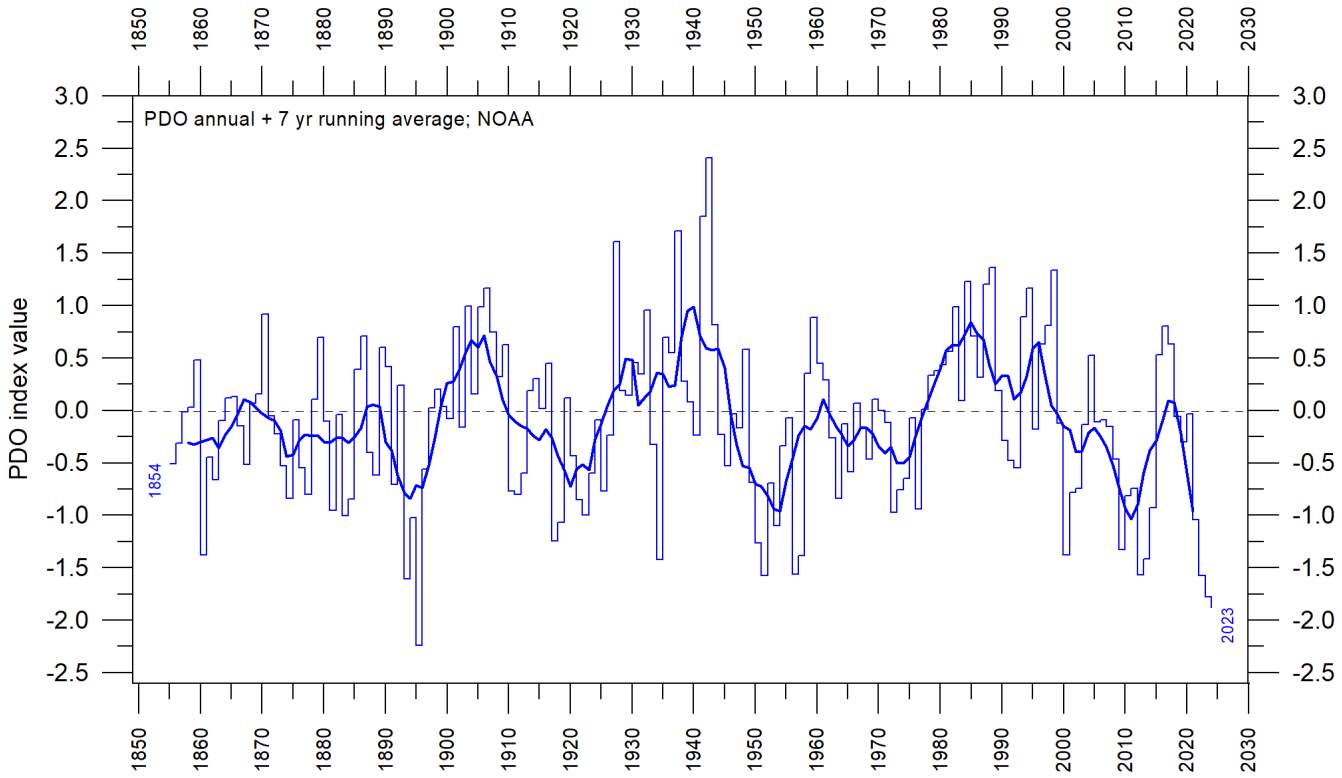

FIGURE 43: Annual Atlantic Multidecadal Oscillation (AMO) detrended and unsmoothed index values since 1856. The thin blue line shows annual values, and the thick line is the simple running 11-year average. Data source: Earth System Research Laboratory, NOAA, USA.

The Atlantic Multidecadal Oscillation (AMO; Figure 43) is a mode of variability occurring in the North Atlantic Ocean sea-surface temperature field. The AMO is essentially an index of North Atlantic sea-surface temperatures (SST).

The AMO index appears to be correlated to air temperatures and rainfall over much of the Northern Hemisphere. The association appears to be high for northeastern Brazil, African Sahel rainfall and North American and European summer climate. The AMO index also appears to be associated with changes in the frequency of North American droughts and is reflected in the frequency of severe Atlantic hurricanes.

As one example, the AMO index may be related to the past occurrence of major droughts in the US Midwest and the Southwest. When the AMO is high, these droughts tend to be more frequent or prolonged, and vice-versa

for low values. Two of the most severe droughts of the 20th century in the US – in the 1950s and 1930s' 'Dust Bowl' – occurred during a time of peak AMO values, which lasted from 1925 to 1965. On the other hand, Florida and the Pacific Northwest tend to experience an opposite effect, high AMO in these areas being associated with relatively high precipitation.

A Fourier-analysis (not shown here) shows the AMO record to be influenced by an about 70-year long cycle.

Sea-level

In general

Global, regional, and local sea levels always change. During the last glacial maximum, about 20–25,000 years ago, global sea levels were around 120 m lower than modern ones. Since the end of the so-called Little Ice Age, about 100–150 years ago, global sea levels have on average increased 1–2 mm/year, according to tide gauge data.

Global (or eustatic) sea-level change is measured relative to an idealised reference level, the geoid, which is a mathematical model of planet Earth's surface (Carter et al. 2014). Global sea-level is a function of the volume of the planet surface the ocean basins and the volume of water they contain. Changes in global sea-level are caused by – but not limited to – four main mechanisms:

1. Changes in local and regional air pressure and wind, and tidal changes introduced by the Moon.
2. Changes in ocean basin volume by tectonic (geological) forces.
3. Changes in ocean water density caused by variations in currents, water temperature and salinity.
4. Changes in the volume of water caused by changes in the mass balance of terrestrial glaciers.

There are also some other mechanisms influencing sea level: storage of ground water, storage in lakes and rivers, evaporation, and so on.

Ocean basin volume changes occur too slowly to be significant over human lifetimes and it is therefore the mechanisms 3 and 4 that drive contemporary concerns about sea-level rise.

Higher temperature in itself is only a minor factor contributing to global sea-level rise, because seawater has a relatively small coefficient of expansion and because, over the timescales of interest, any warming is largely confined to the upper few hundred metres of the ocean surface.

The growth or decay of sea ice has no influence on sea level. However, the melting of land-based ice – including both mountain glaciers and the ice sheets of Greenland and Antarctica – is a more significant As already noted, sea-levels were about 120 m lower during the last glacial maximum, and during the most recent interglacial, about 120,000 years ago, global temperatures and thus sea levels were higher than today, because significant parts of the Greenland ice sheet melted.

On a regional and local scale, however, factors relating to changes in air pressure, wind and geoid must also be considered. As an example, changes in the volume of the Greenlandic Ice Sheet will affect the geoid in the regions adjacent to Greenland. Should overall mass in Greenland diminish, the geoid surface will be displaced

towards the centre of the Earth, and sea level in the region will drop correspondingly. This will happen even though the overall volume of water in the global oceans increases as glacier ice is lost.

In northern Europe, another factor must also be considered when estimating the future sea level. Norway, Sweden, Finland, and Denmark were all totally or partly covered by the European ice sheet 20–25,000 years ago. Even today, the effect of this ice load is seen in the ongoing isostatic land rise in the area, of several millimetres per year. At many sites this more than compensates for the slow global sea-level rise, so a net sea-level fall in relation to the land is recorded.

The enormous mass transfer associated with the growing Ice Sheets in North America and Europe resulted in viscoelastic mantle flow and elastic effects in the upper crust. Thus, outside the margin of the large Ice the planet surface was bulging up in concert with the isostatic depression taking place below the Ice Sheets. Such regions today slowly are sinking back, resulting in apparent above-normal sea level rise rates. Several locations along the east coast of USA are an example of this.

The relative movement of sea level in relation to land is what matters for coastal planning, and this is termed the ‘relative sea level change’. This is what is recorded by tide gauges.

Sea-level from satellite altimetry

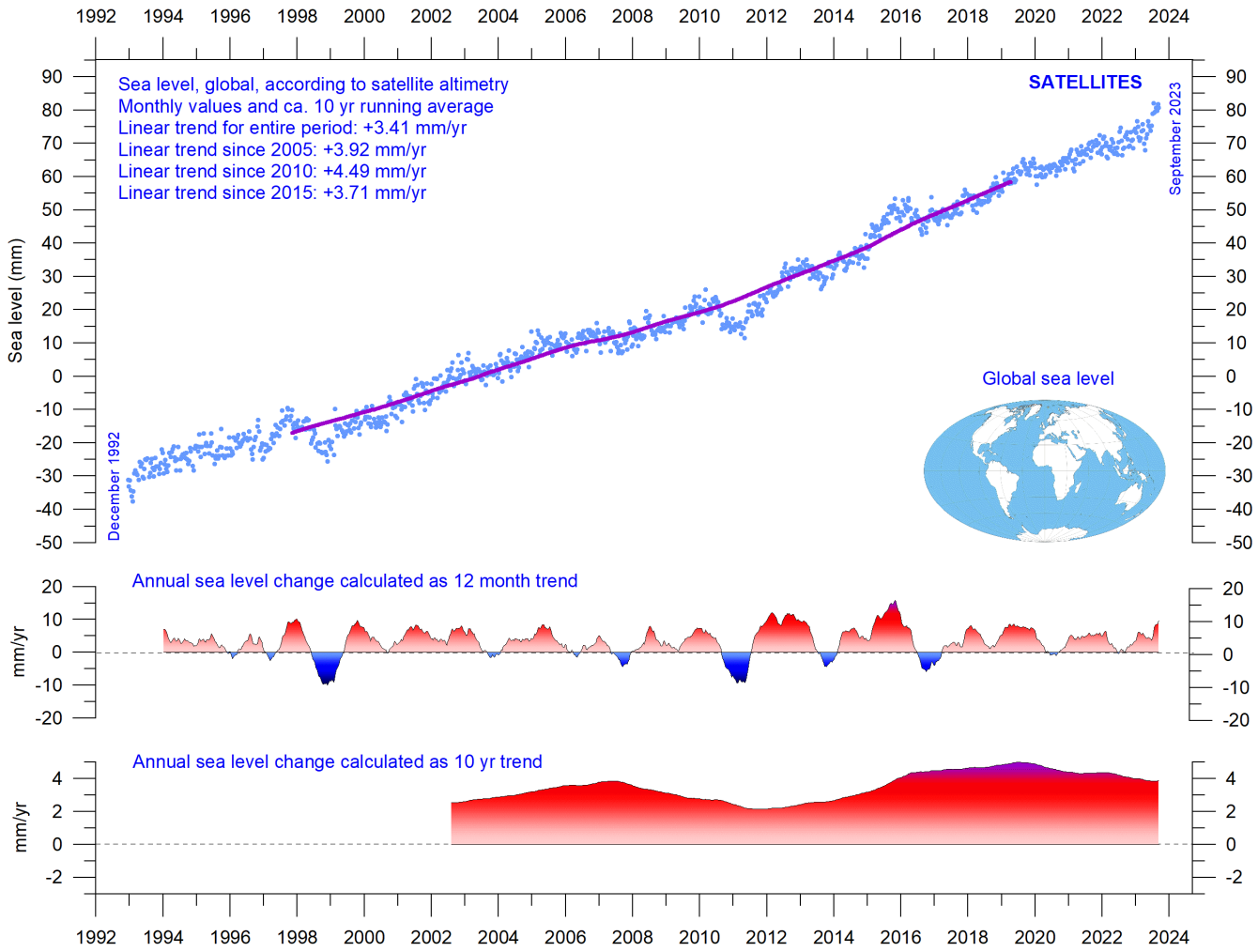

FIGURE 44: Global sea level change since December 1992 according to the Colorado Center for Astrodynamics Research at University of Colorado at Boulder. The blue dots are the individual observations (with seasonal signals and calculated GIA effect removed), and the purple line represents the running 121-month (ca. 10-year) average. The two lower panels show the annual sea level change, calculated for 1 and 10-year time windows, respectively. These values are plotted at the end of the interval considered.

Satellite altimetry is a relatively new type of measurement, providing unique and valuable insights into changes in the detailed surface topography of the oceans, with nearly global coverage. However, it is probably not a precise tool for estimating absolute changes in global sea level due to interpretation issues surrounding the original satellite data.

The most important is the Glacial Isostatic Adjustment (GIA), a correction for the large-scale, long-term mass transfer from the oceans to the land that results from the waxing and waning of the large Quaternary ice sheets in North America and northern Europe. This enormous mass transfer causes changes in surface load, resulting in viscoelastic mantle flow and elastic effects in the upper crust. It is hard to correct the satellite data for this effect, since no single technique or observational network can give enough information. Researchers therefore must resort to modelling, and the answer they get depends upon the type of deglaciation model (for the last glaciation)

and upon the type of crust-mantle model that is assumed. Because of this (and other factors), estimates of global sea-level change based on satellite altimetry vary somewhat.

In the above case (Figure 44) the global sea-level rise estimate is about 3.4 mm/year (since 1992), with the estimated GIA effect removed. Linear trends calculated since 2005, 2010 and 2015 do not suggest any recent acceleration, and the lower panel in Figure 44 instead suggests that a sea-level rise peak was reached in around 2019.

Sea level from tide-gauges

Tide-gauges are located at coastal sites and record the net movement of the local ocean surface in relation to land. These measurements (see, for example, Figure 43) are key information for local coastal planning, and are directly applicable for planning coastal installations, in contrast to satellite altimetry.

At any specific coastal site, the measured net movement of the local coastal sea-level comprises two local components:

- the vertical change of the ocean surface
- the vertical change of the land surface

For example, a tide-gauge may record an apparent sea-level increase of 3 mm/year. If geodetic measurements show the land to be sinking by 2 mm/year, the real sea-level rise is only 1 mm/year (3 minus 2 mm/year). In a global sea-level change context, the value of 1 mm/year is relevant, but in a local coastal planning context the 3 mm/year tide-gauge value is the one that is useful for local planning authorities.

To construct a time series of sea-level measurements at each tide-gauge, the monthly and annual means must be reduced to a common datum. This reduction is performed by the Permanent Service for Mean Sea Level (PSMSL), making use of data provided by the national authorities. The Revised Local Reference (RLR) datum at each station is defined to be approximately 7000 mm below mean sea level, with this arbitrary choice made many years ago to avoid negative numbers in the resulting RLR monthly and annual mean values.

Few places on Earth are completely stable, and most tide-gauges are located at sites exposed to tectonic uplift or sinking (the vertical change of the land surface). This widespread vertical instability has several causes and affects the interpretation of data from the individual tide-gauges. Much effort is therefore put into correcting for local tectonic movements.

As a result, data from tide-gauges located at tectonic stable sites is of special interest. One example of a long, continuous record from such a stable site is from Korsør, Denmark (Figure 45). This record indicates a stable sea-level rise of about 0.83 mm per year since 1897, without any sign of recent acceleration.

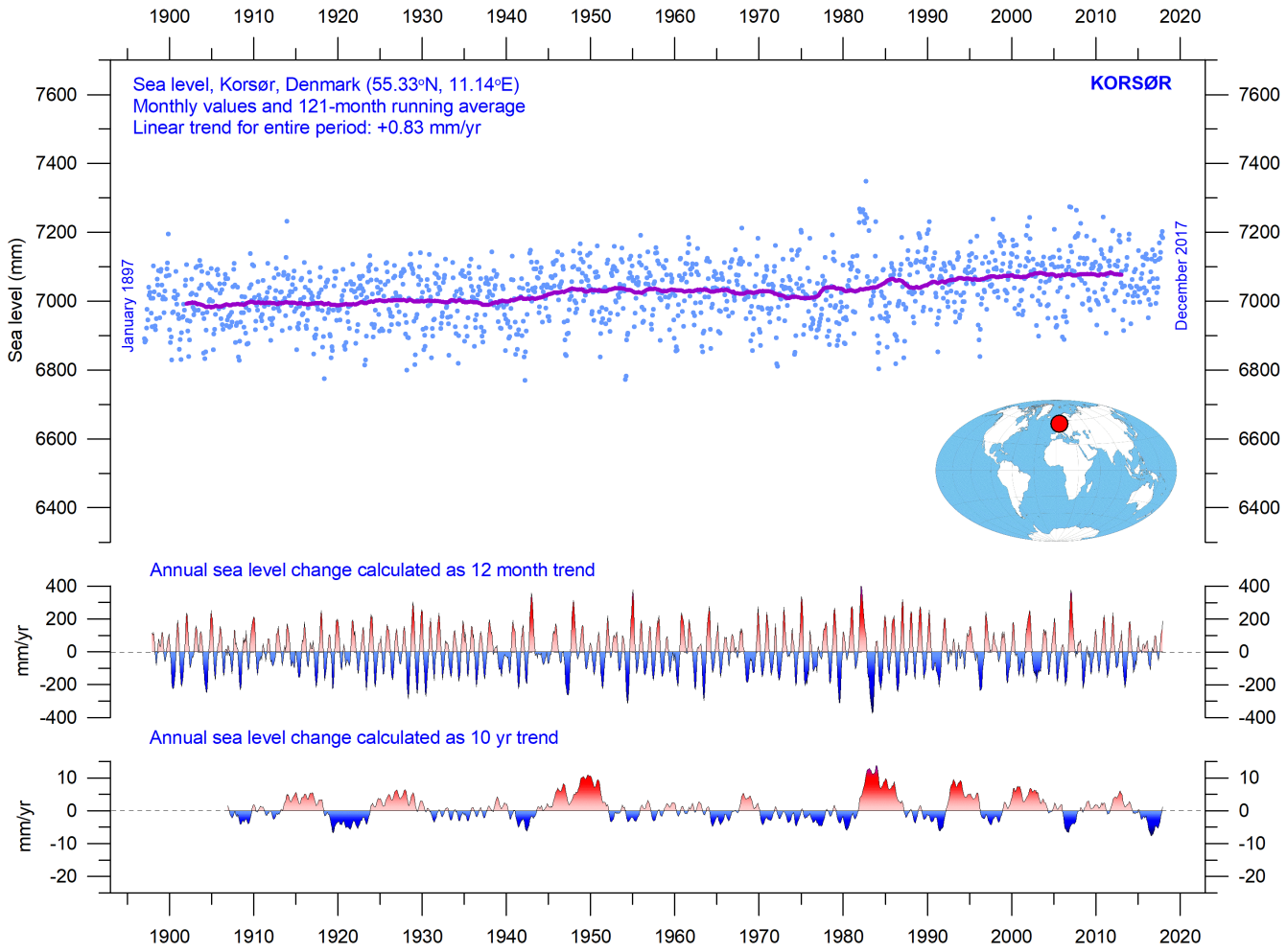

FIGURE 45. Korsør (Denmark) monthly tide gauge data from PSMSL Data Explorer. The blue dots are the individual monthly observations, and the purple line represents the running 121-month (ca. 10-year) average. The two lower panels show the annual sea level change, calculated for 1 and 10-year time windows, respectively. These values are plotted at the end of the interval considered.

Evidently, of interest are also attempts to compare tide-gauge records from different places on planet Earth. Holgate (2007) suggested nine specific stations to capture the global variability found in a larger number of stations over the last half century. However, some of the stations suggested by Holgate has not reported values for several years, leading to the southern hemisphere now being seriously underrepresented in his original data set. Therefore, in the diagram below (Figure 46) several other long tide-gauge series have been included, to provide a more balanced representation of both hemispheres (15 stations in total).

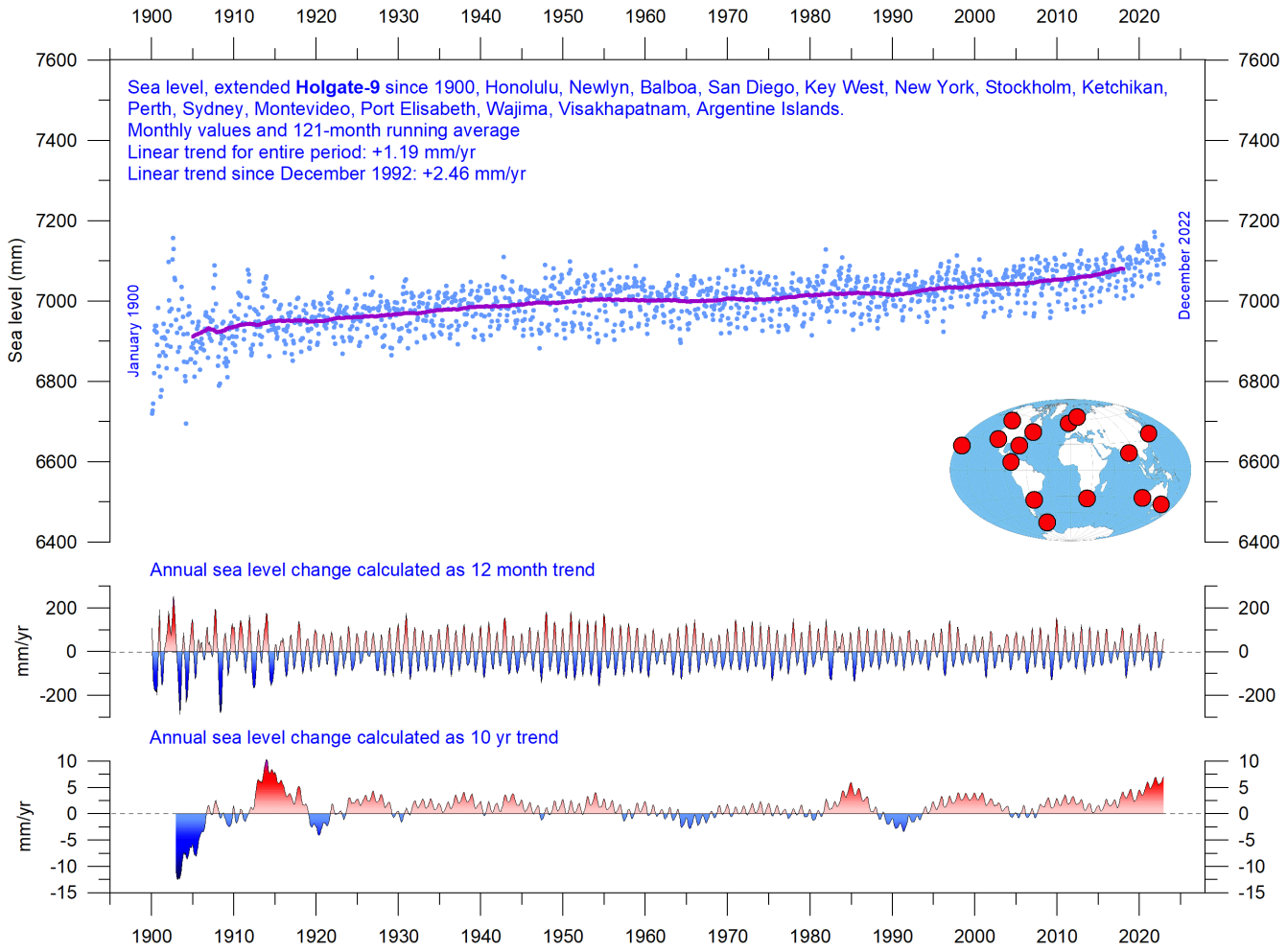

FIGURE 46. Extended Holgate-9 monthly tide-gauge data from PSMSL Data Explorer. Holgate (2007) suggested nine stations to capture the global variability found in a larger number of stations over the last half century studied previously. However, some of the stations suggested by Holgate has not reported values for several years, leading to the southern hemisphere now being seriously underrepresented in his original data set. Therefore, in the above diagram several other long tide-gauge series have been included, to provide a more balanced representation of both hemispheres (15 stations in total). The blue dots are the individual average monthly observations, and the purple line represents the running 121-month (ca. 10 year) average. The two lower panels show the average annual sea level change, calculated for moving 1 and 10-year windows, respectively. These values are plotted at the end of the time window considered, month by month.

Data from tide-gauges all over the world suggest an average global sea-level rise of 1-2 mm/year (Figure 46), while the modern satellite-derived record (Figure 44) suggest a rise of about 3.4 mm/year, or more. The difference between the two data sets is remarkable. It is however known that satellite observations are facing several complications in areas near the coast. Vignudelli et al. (2019) provide an updated overview of the current limitations of classical satellite altimetry in coastal regions. Since 2015 an increased sea level rate may be suggested by the above composite record (Figure 46), but it remains to be seen if this is the result of one of the recurrent variations displayed in the lower panel of the diagram.

Sea level modelled for the future

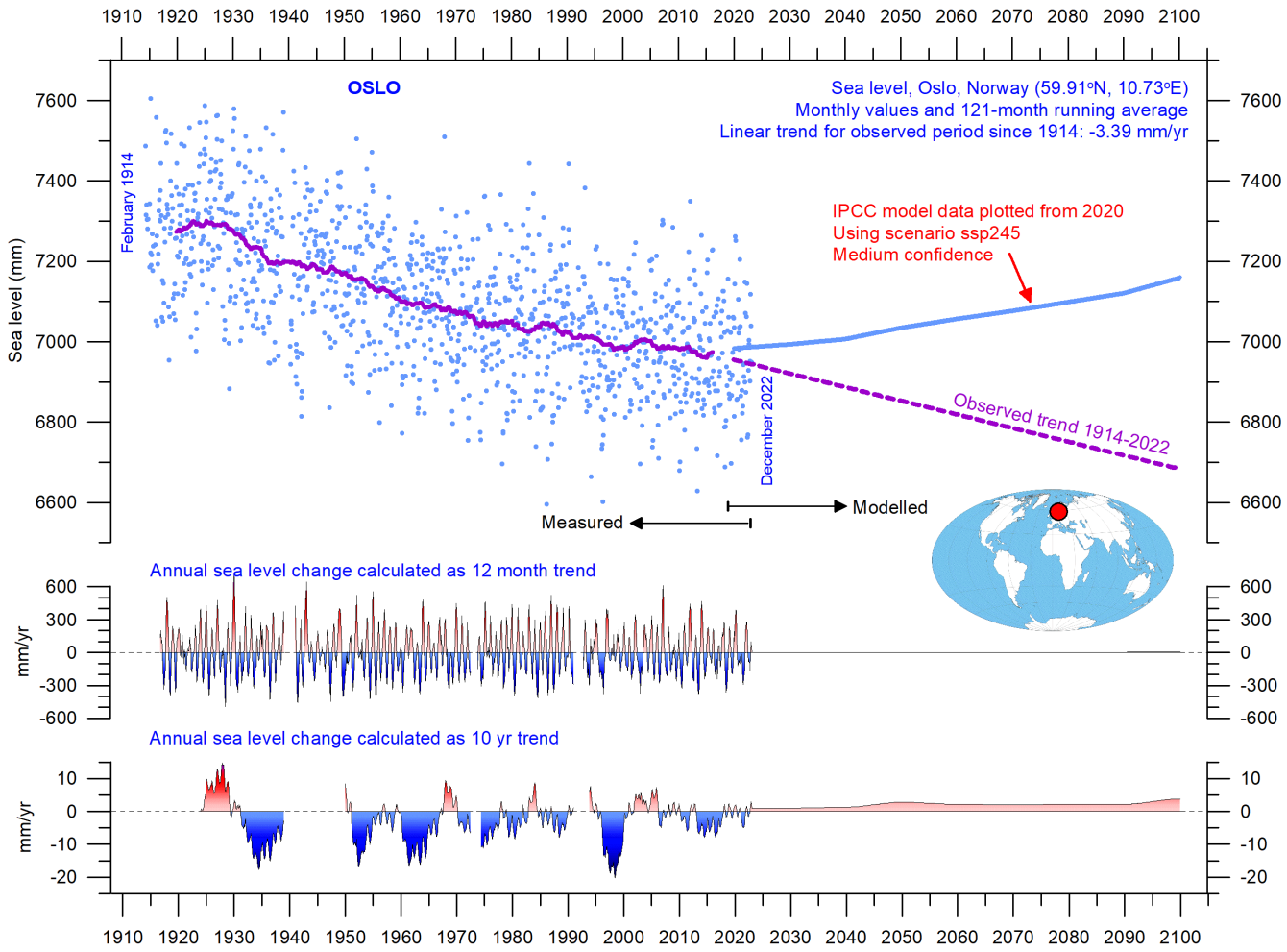

FIGURE 47: Observed and modelled sea level at Oslo (Norway). The blue dots are the individual monthly tide gauge observations (PSMSL Data Explorer) 1914-2019, and the purple line represents the running 121-month (ca. 10-year) average. The modelled data for the future is shown by a solid blue line 2020-2100, using the moderate SSP2-4.5 scenario (IPCC 2020). The two lower panels show the annual sea level change, calculated for 1 and 10-year time windows, respectively. These values are plotted at the end of the interval considered.

The issue of sea-level change, and particularly the identification of a hypothetical human contribution to that change, is a complex topic. Given the scientific and political controversy that surrounds the matter, the great public interest in this area is entirely understandable.

A recent IPCC publication, the 6th Assessment Report from Working Group I, was released on August 9th, 2021. Modelled data for global and regional sea-level projections 2020–2150 are available from the IPCC AR6 Sea Level Projection Tool (see link at the end of this report). The IPCC models future development of several

factors, such as glacier mass change, vertical land movement, water temperature and -storage. Modelled sea-level projections for different emissions scenarios are calculated relative to a baseline defined by observations for 1995–2014.

It is enlightening to compare the modelled data with observed sea-level data. Figure 47 shows this for one location, namely Oslo, in Norway. Northern Europe was covered by the European Ice Sheet 20–25,000 years ago, with more than 2 km of ice over the location of modern Oslo at the maximum glaciation. Today, the effect of this ice load is clearly demonstrated by the fact that southern Norway experiences an ongoing isostatic land rise of several millimetres per year. At many sites affected by the last (Weichselian/Wisconsin) glaciation, this ongoing isostatic movement more than compensates for the slow global sea-level rise, so a net sea-level decrease in relation to land is recorded.

As Oslo was covered by thick ice during the last glaciation, it is affected by a marked isostatic land rise today. If the observed sea-level change rate at Oslo continues (based on about 110 years of observations), by 2100, the relative sea-level (in relation to land) will have dropped by about 27 cm relative to 2020 (Figure 45). However, according to the IPCC, it will have increased about 17.5 cm. IPCC projects a rather sudden increase around 2020, which contrasts with to the stable sea-level decline of about -3.39 mm/year observed since 1914. Observed (measured) and modelled data now have an overlap of 3 years (Figure 47). The overlap period is still short, but it seems to suggest an unbroken sea-level decrease at Oslo since 2020, in contrast to the model projection (blue line in Figure 47).

A few reflections might be appropriate at this point. The step change in relative sea-level dynamics for Oslo (and many other coastal sites) in 2020 appears rather implausible and suggests that the modelled data is not describing the real-world dynamics adequately. This is remarkable, as the modelled sea-level projections for different SSP scenarios are calculated relative to a baseline defined by observations 1995–2014, for each station. The modelers must therefore have seen the observed data.

According to the 6th Assessment Report, human activities are estimated to have caused approximately 1.0°C of global warming above pre-industrial levels, with a likely range of 0.8–1.2°C (Summary for Policymakers, A.1.3). It is therefore particularly surprising that the modelled effect of this change should first affect sea levels in the shape of a step change in 2020. Had the modelers instead calibrated their sea-level data from an earlier date, say 1950, which would have been completely possible, the contrast between observed and modelled data would immediately have become apparent.

Global, Arctic and Antarctic sea ice extent

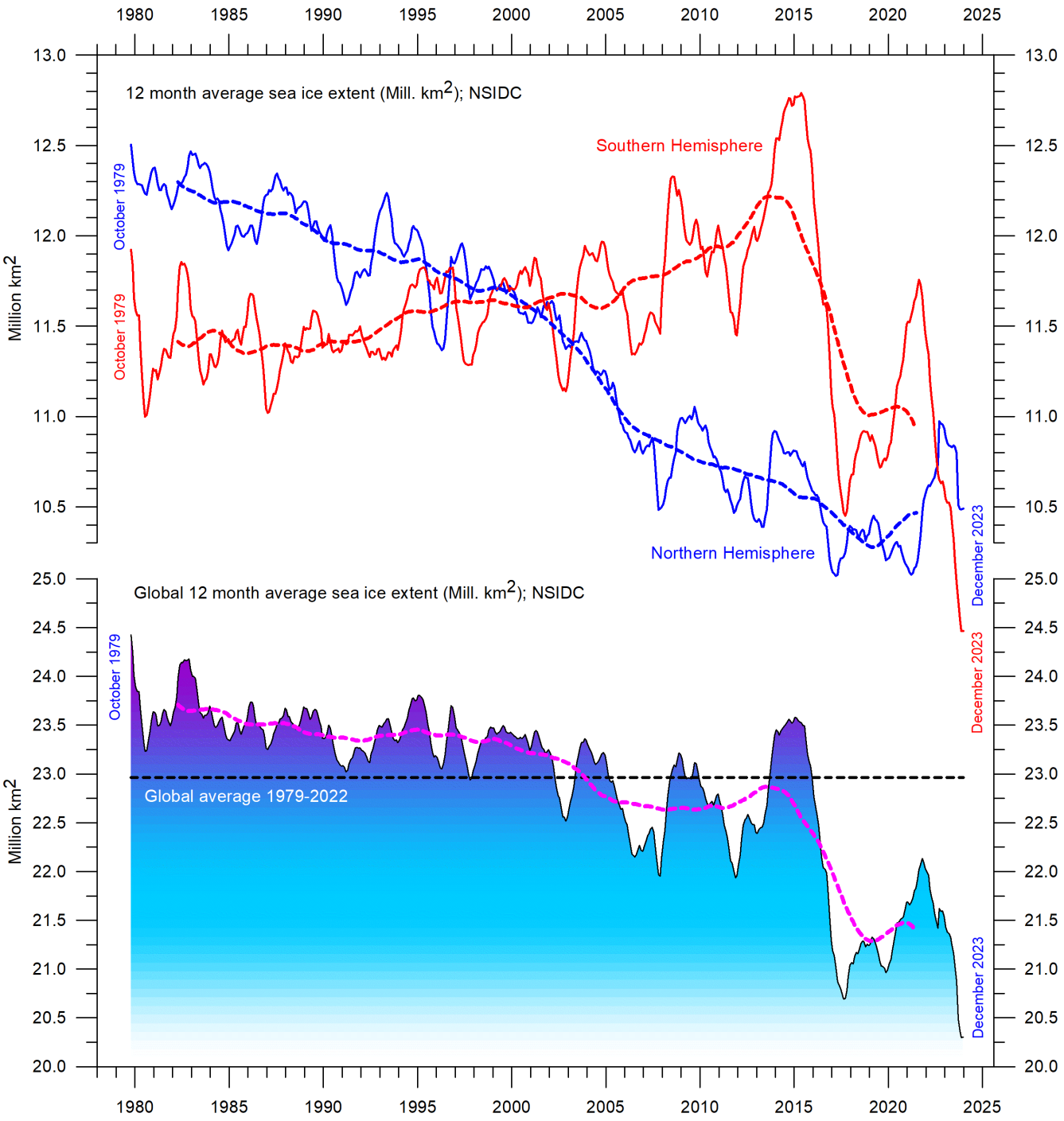

FIGURE 48: Global and hemispheric 12-month running average sea ice extent since 1979, the satellite-era. The October 1979 value represents the monthly average of November 1978 - October 1979, the November 1979 value represents the average of December 1978 - November 1979, etc. The stippled lines represent a 61-month (ca.5 years) average. Last month included in the 12-month calculations is shown to the right in the diagram. Data source: National Snow and Ice Data Center (NSIDC).

The two 12-month average sea-ice extent graphs in Figure 48 display a contrasting development between the two poles over the period 1979–2020. The Northern Hemisphere sea-ice trend towards smaller extent is clearly displayed by the blue lined, and so is the simultaneous increase in the Southern Hemisphere until 2016. In many respects, this and previous observations presented in this report suggest that the years 2016-2021 may well mark an important shift in the global climate system (see, e.g., ocean temperatures in Figure 31).

The Antarctic sea-ice extent decreased extraordinary rapidly during the Southern Hemisphere spring of 2016, much faster than in any previous spring during the satellite era (since 1979). A strong ice retreat occurred in all sectors of the Antarctic, but was greatest in the Weddell and Ross Seas. In these sectors, strong northerly (warm) surface winds pushed the sea ice back towards the Antarctic continent. The background for the special wind conditions in 2016 has been discussed by various authors (e.g. Turner et al. 2017 and Phys.org 2019), and appears to be a phenomenon related to natural climate variability. The satellite sea-ice record is still short, and does not fully represent natural variations playing out over more than a decade or two.

What can be discerned from the still short record is nevertheless instructive. The two 12-month average graphs in Figure 48 show recurring variations superimposed on the overall trends. These shorter variations are influenced by a 4.3-year periodic variation for the Arctic sea ice, while for the Antarctic sea ice a periodic variation of about 3.3 years is important.

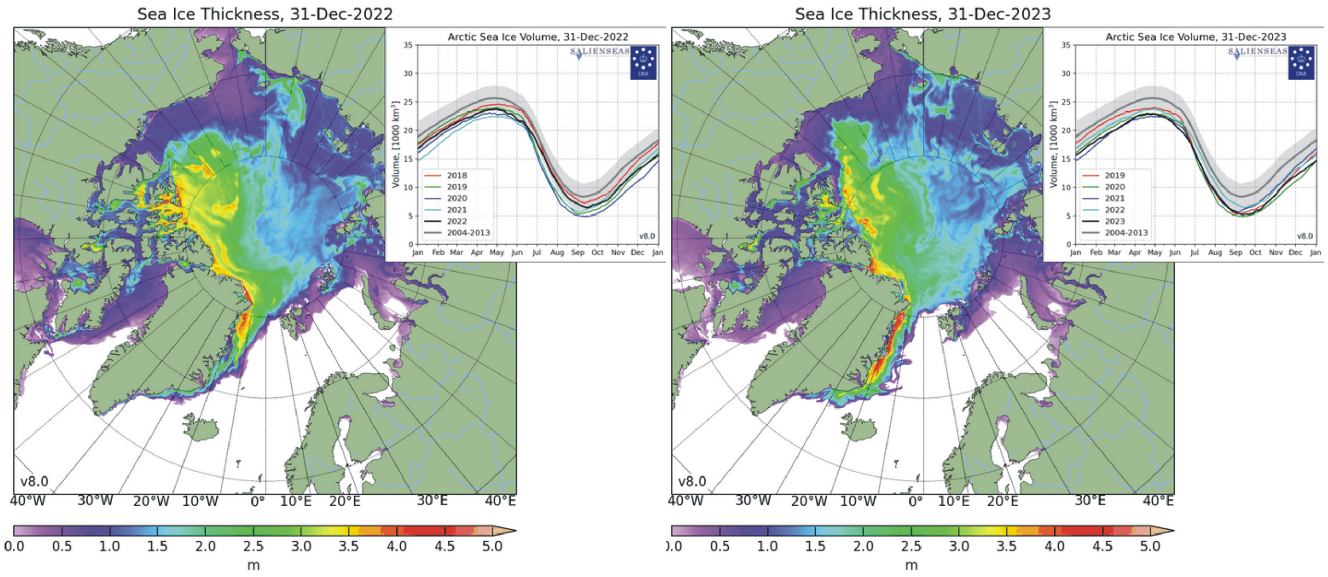

FIGURE 49: Diagrams showing Arctic sea ice extent and thickness 31 December 2022 (left) and 2023 (right) and the seasonal cycles of the calculated total arctic sea ice volume, according to the Danish Meteorological Institute (DMI). The mean sea ice volume and standard deviation for the period 2004-2013 are shown by grey shading in the insert diagrams.

Figure 49 illustrates the overall extent and thickness of the Arctic sea-ice from the end of 2022 to the end of 2023. Sea-ice thickness has decreased somewhat along the coast of the Canadian Archipelago. Presumably, this is the result of strong melting in this region during summer 2023, while both thickness and extent have been increasing along the east coast Greenland during 2023. These developments are detailed in Figure 50.

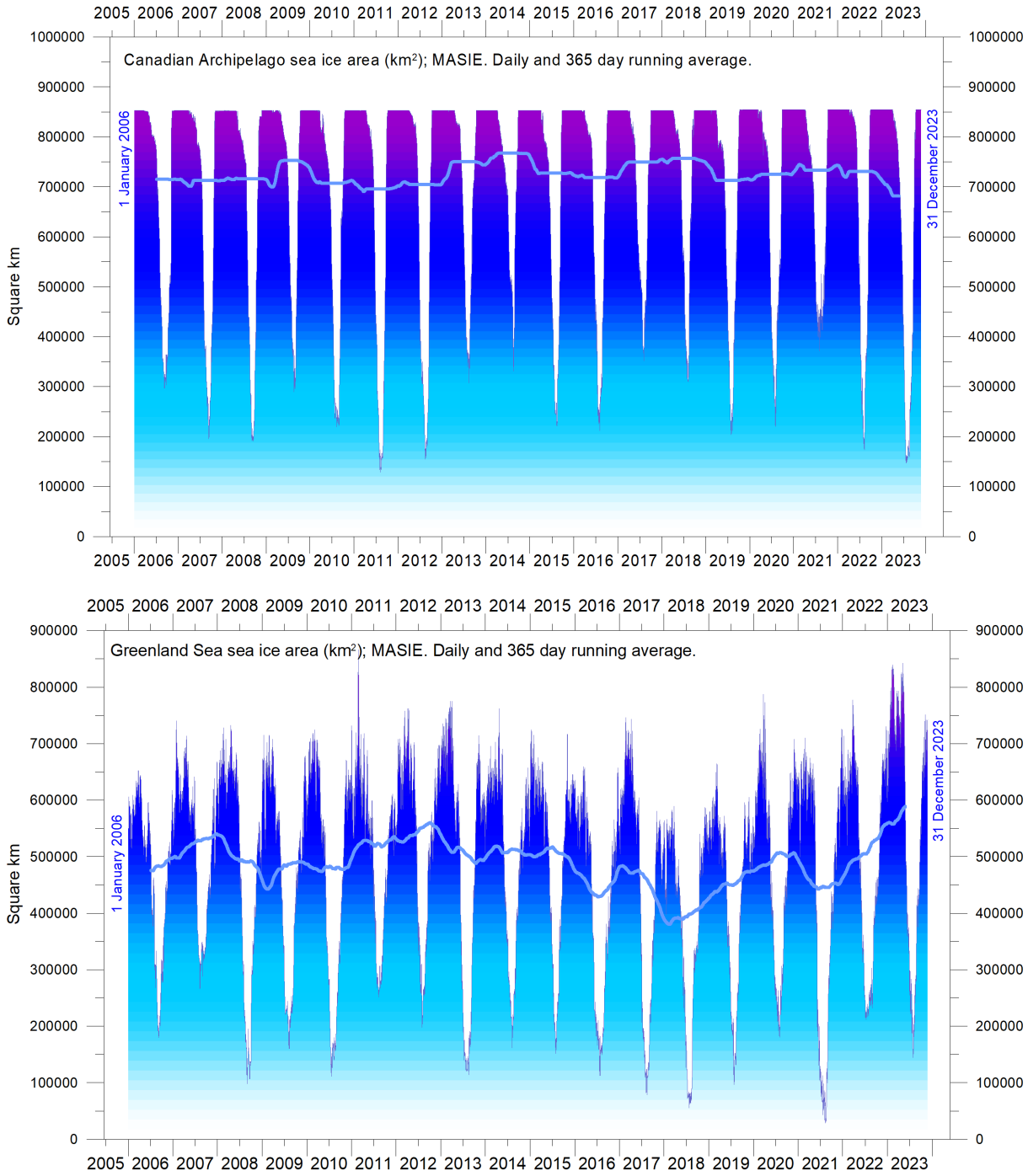

FIGURE 50a-b: Daily sea ice extension (km^2) in the Canadian Archipelago and in the Greenland Sea since 2006 according to the Multisensor Analyzed Sea Ice Extent (MASIE).

Northern Hemisphere snow cover extent

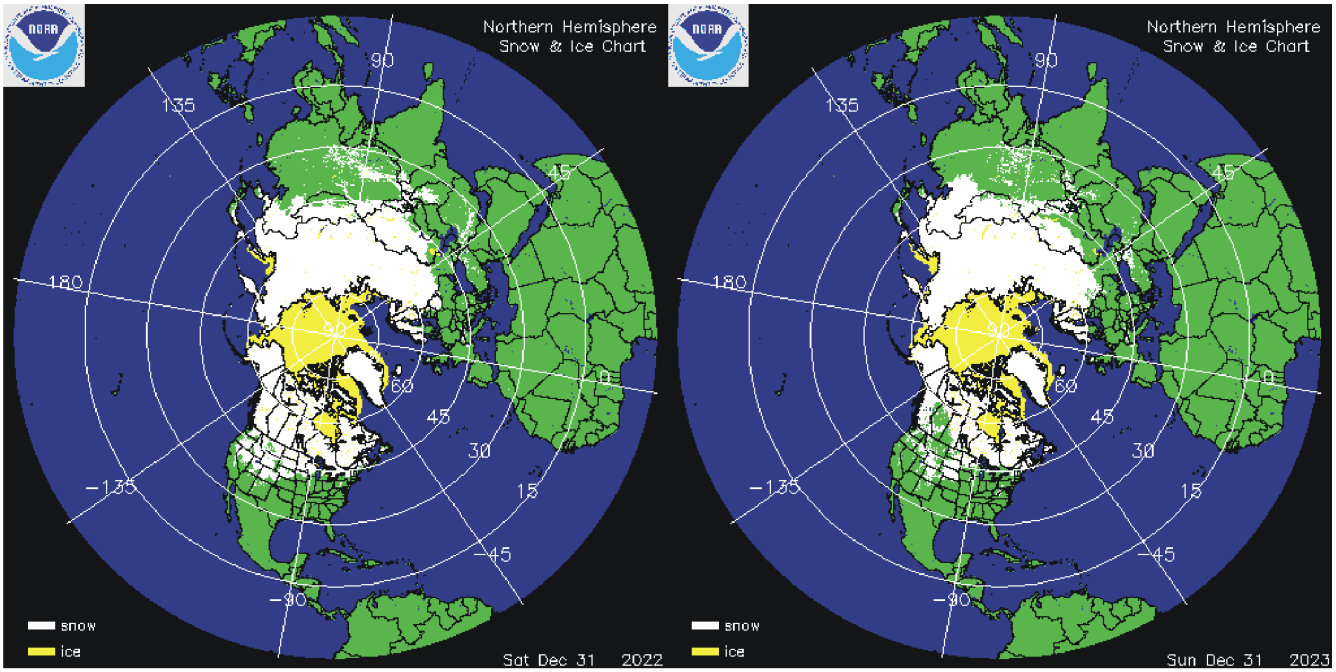

FIGURE 51: Northern hemisphere snow cover (white) and sea ice (yellow) 31 December 2022 (left) and 2023 (right). Map source: National Ice Center (NIC).

Variations in the global snow cover are mainly the result of changes playing out in the Northern Hemisphere (Figure 51), where all the major land areas are located. The Southern Hemisphere snow cover is essentially controlled by the Antarctic ice sheet, and therefore relatively stable.

Northern Hemisphere snow cover is exposed to large local and regional variations from year to year. However, the overall tendency (since 1972) is towards quasi-stable conditions, as illustrated by Figure 51. During the Northern Hemisphere summer, the snow cover usually shrinks to about 2,400,000 km^2 (principally controlled by the size of the Greenland ice sheet), but during the winter it increases to about 50,000,000 km^2, representing no less than 33% of planet Earth's total land area. Northern Hemisphere snow cover maximum extension usually occurs in February, and the minimum in August (Figure 52).

A Fourier-analysis (not shown here) shows the Northern Hemisphere record to be influenced not only by the annual cycle, but probably also by a longer about 6.5-year long cycle.

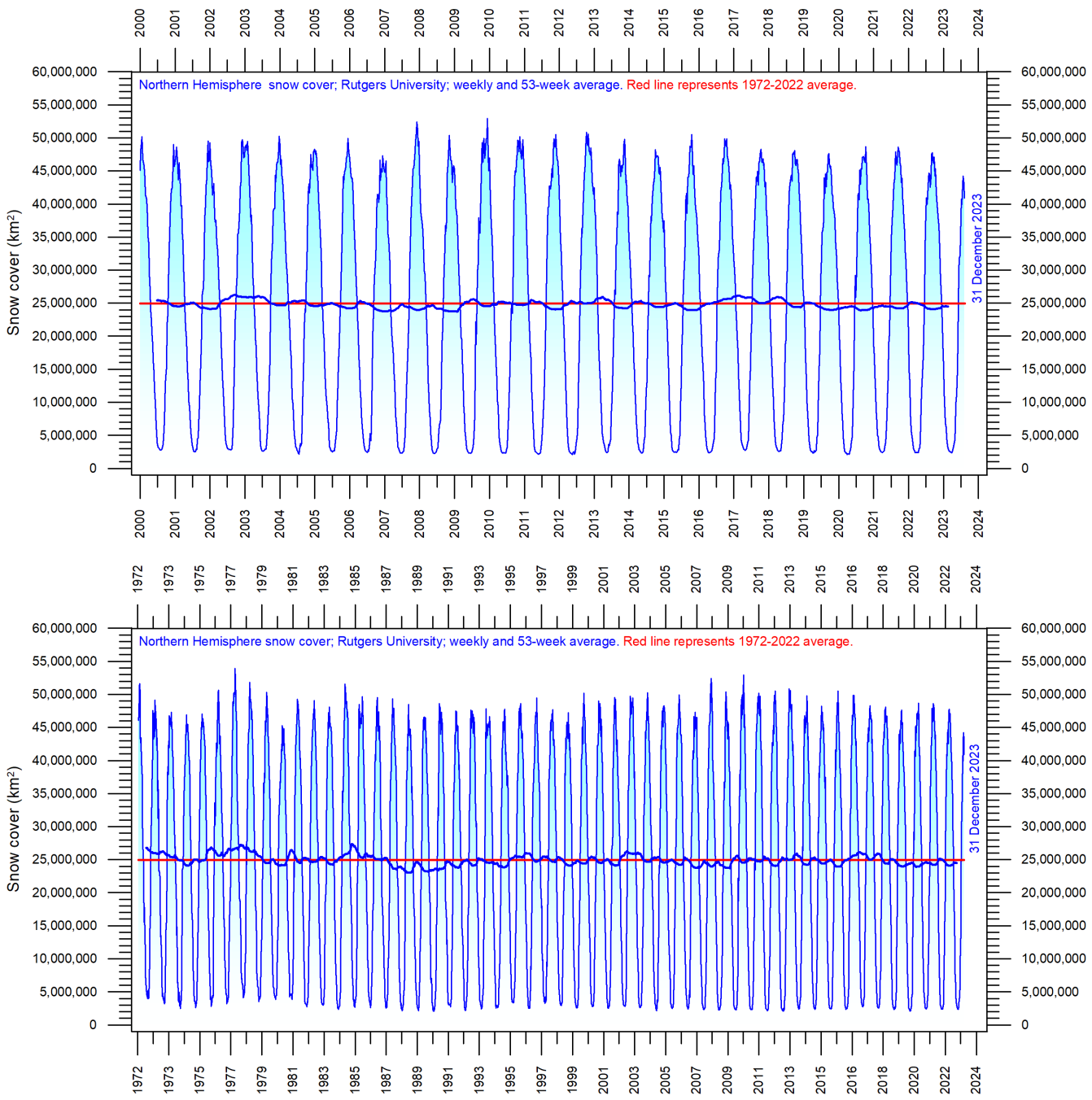

FIGURE 52a-b: Northern hemisphere weekly snow cover extent since January 2000 (upper diagram) and 1972 (lower diagram) according to Rutgers University Global Snow Laboratory. The thin blue line is the weekly data, and the thick blue line is the running 53-week average (approximately 1 year). The horizontal red line is the 1972-2022 average.

Considering seasonal changes (Figure 53), the Northern Hemisphere snow cover has slightly increased during autumn, is stable at mid-winter, and is slightly decreasing in spring. In 2023, the Northern Hemisphere snow cover extent was close to the 1972–2022 average (Figure 52).

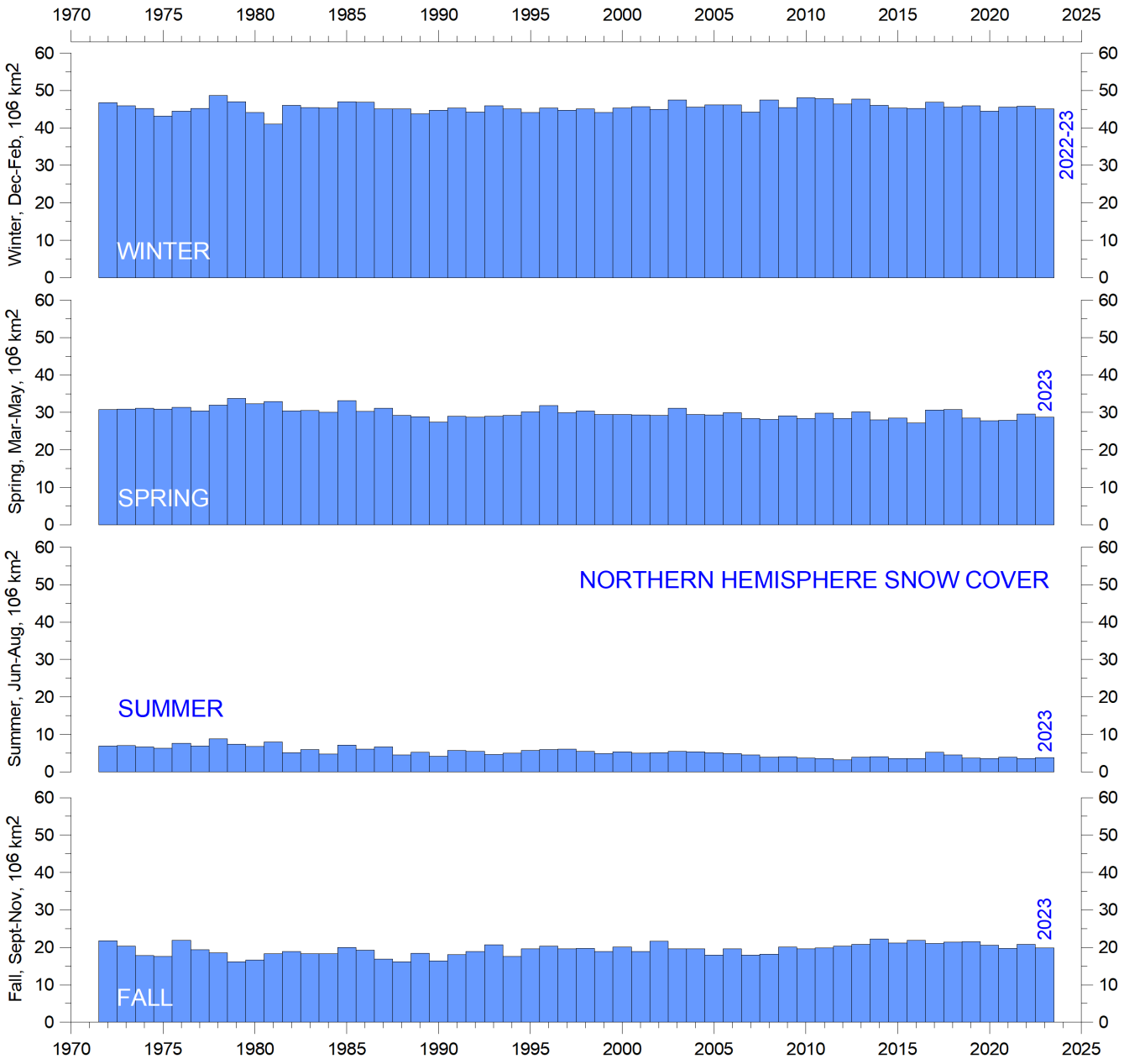

FIGURE 53: Northern Hemisphere seasonal snow cover since 1972 according to Rutgers University Global Snow Laboratory.

Global precipitation

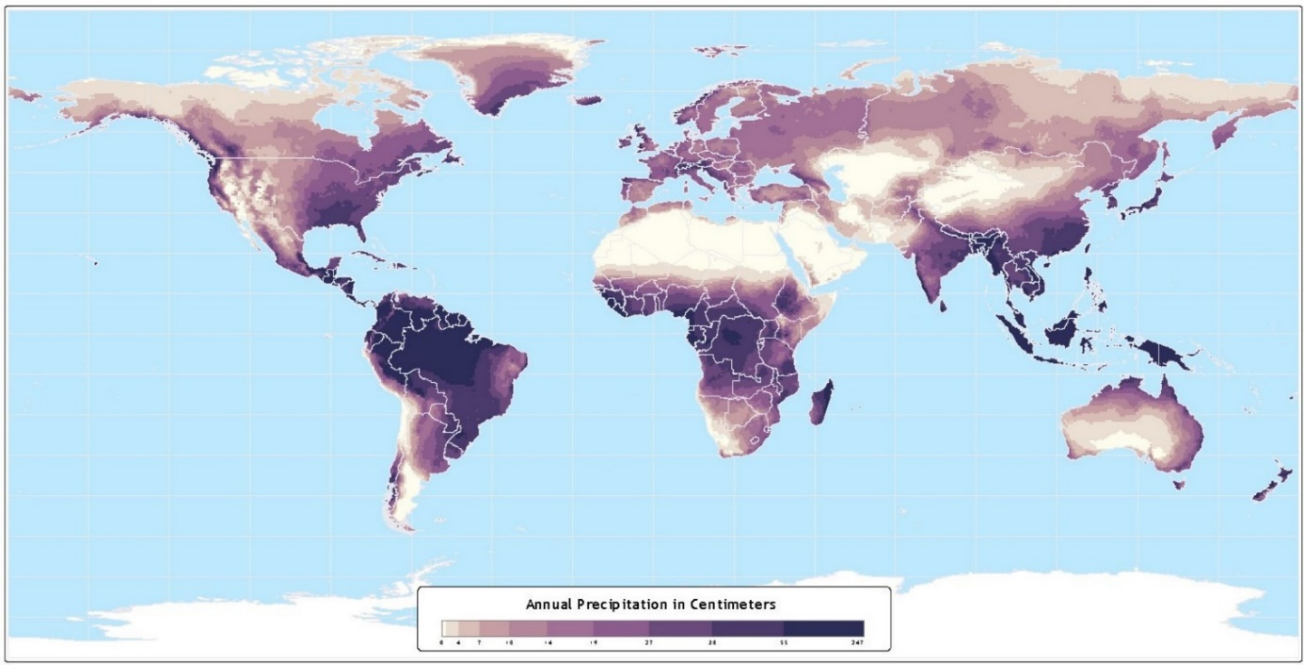

FIGURE 54: Annual precipitation in Centimeters. 30-year (1960 to 1990) average annual precipitation on land Picture source: NASA/Atlas of the Biosphere.

Annual regional precipitation (rain, snow) varies from more than 3000 mm/year to almost nothing (Figure 54). The global average precipitation undergoes variations from one year to the next, and the calculated annual anomaly in relation to the 1901-2021 average is shown in Figure 55. Annual variations in the global average precipitation up to ±30 mm/year are not unusual. The global precipitation was especially high around 1956, 1973 and 2010, and especially low around 1941, 1965, 1987 and 1992.

A Fourier frequency analysis (not shown here) shows the global precipitation anomaly (Figure 55) to be influenced by a significant 5.6-year cycle, and possibly also by a 3.6-year cycle. The 3.6 and 5.6-year cycles are also found in the data describing variations of SOI and PDO (Figure 41-42), respectively.

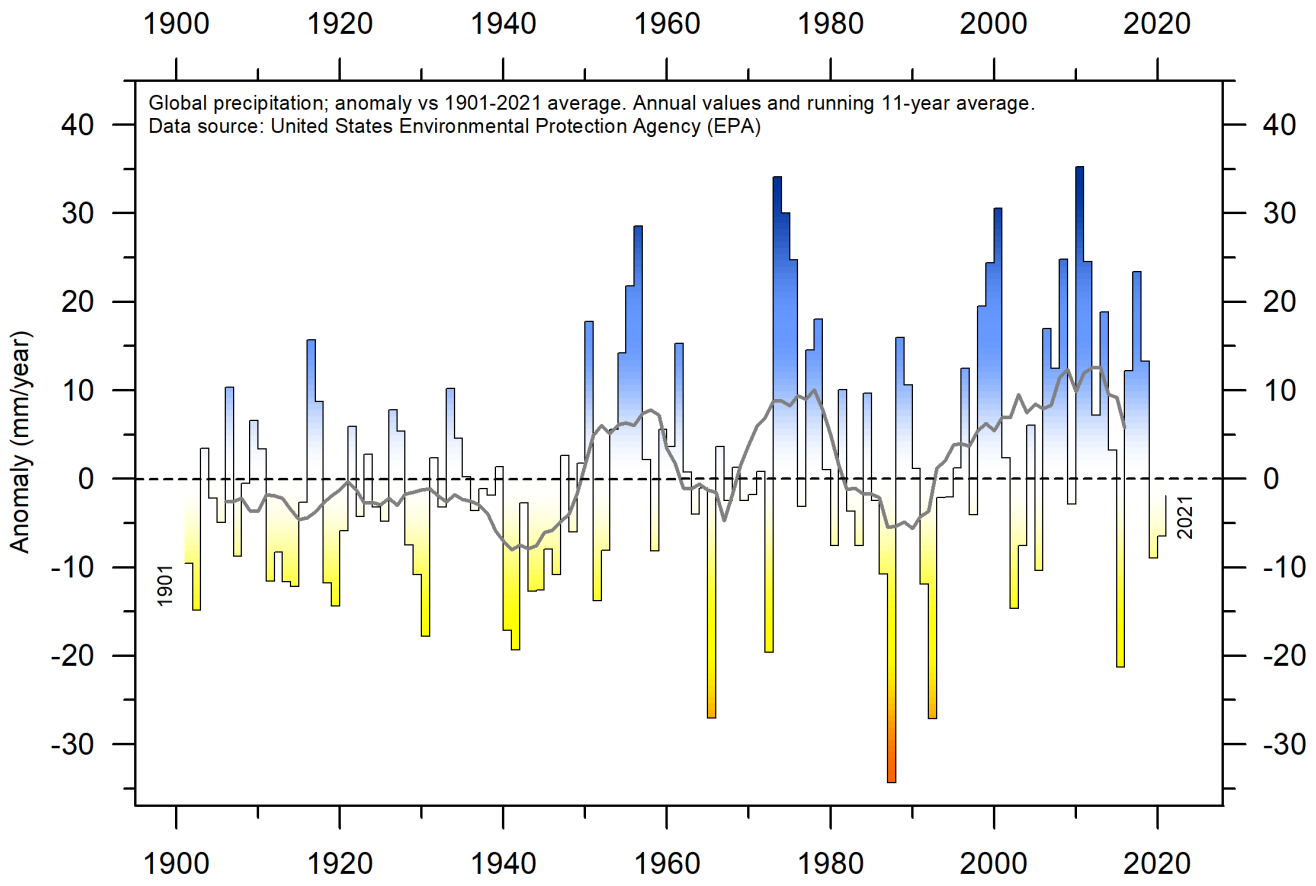

FIGURE 55: Variation of annual anomalies in relation to the global average precipitation from 1901 to 2021 based on rainfall and snowfall measurements from land-based weather stations worldwide. Data source: United States Environmental Protection Agency (EPA).

Tropical storm and hurricane accumulated cyclone energy (ACE)

Accumulated cyclone energy (ACE) is a measure used by the National Oceanic and Atmospheric Administration (NOAA) to express the activity of individual tropical cyclones and entire tropical cyclone seasons. ACE is calculated as the square of the wind speed every six hours, and is then scaled by a factor of 10,000 for usability, using a unit of 10^4 knots^2. The ACE of a season is the sum of the ACE for each storm, and therefore encapsulates the number, strength, and duration of all the tropical storms in the season. The ACE data and ongoing cyclone dynamics are detailed in Maue (2011).

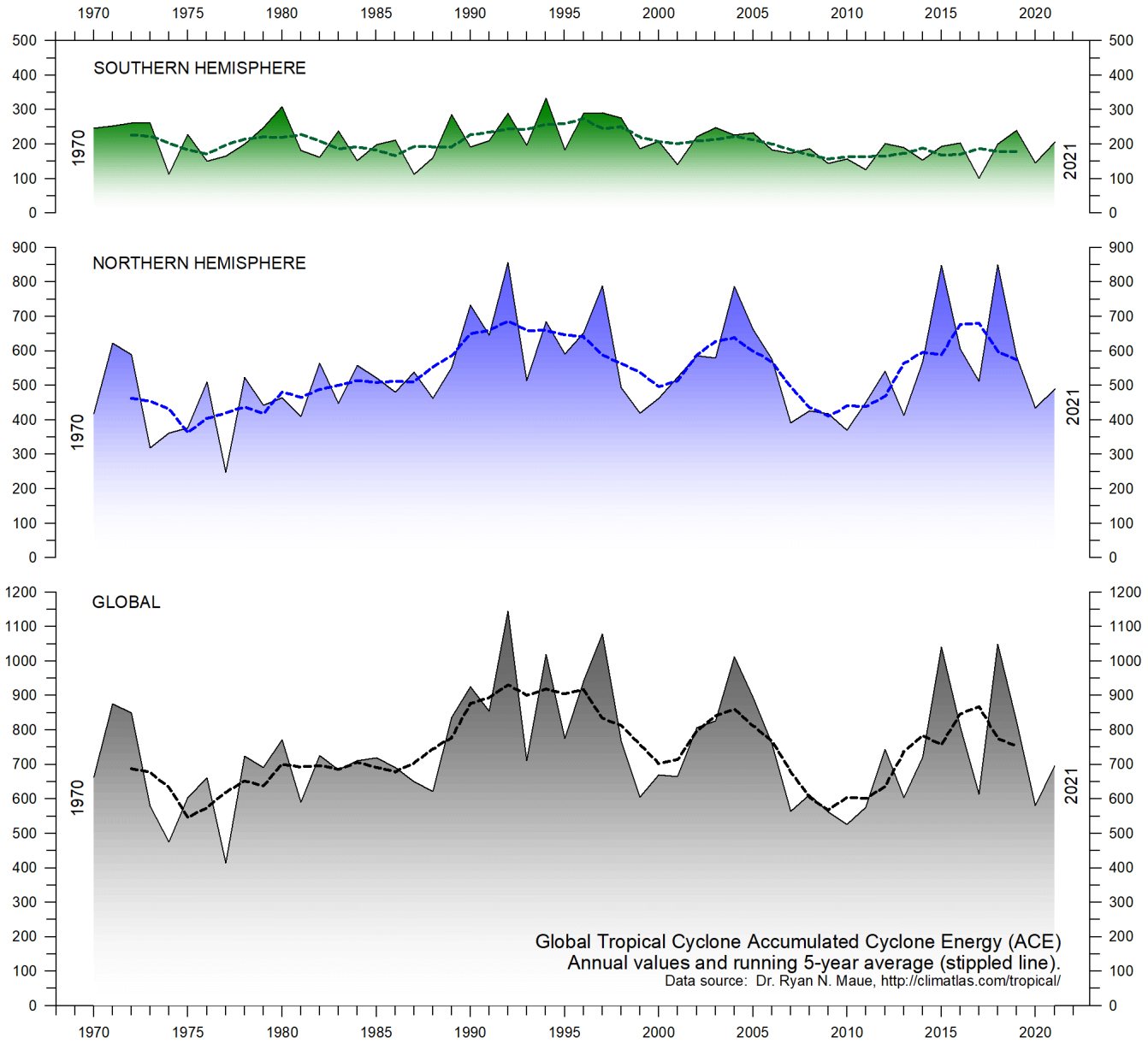

FIGURE 56: The diagram above shows the annual global tropical storm and hurricane accumulated cyclone energy (ACE) 10^4 Knots^2, since 1970. Data source: Maue ACE data.

The damage potential of a hurricane is proportional to the square or cube of the maximum wind speed, and thus ACE is not only a measure of tropical cyclone activity, but also a measure of the damage potential of an individual cyclone or a season. Existing records (Figure 56) do not suggest any abnormal cyclone activity in recent years.

The global ACE data since 1970 display a variable pattern over time, but without any clear trend, as are the diagrams for the Northern- and Southern Hemisphere (panels in Figure 56). A Fourier analysis (not shown here) indicates oscillations of about 11.5- and 3.6-years' duration for the global data, and also suggests a longer one, of about 33-years', but the data series is too short to draw firm conclusions on this.

The period 1989–1998 was characterised by high values. Other peaks were seen 2004, 2015 and 2018, and the periods 1973–1988, 1999–2003 and 2006–2014 were characterised by comparatively low activity. The peaks in

1997/98 and 2016 coincide with strong El Niño events in the Pacific Ocean (Figure 30). Northern Hemisphere ACE values (central panel in Figure 56) dominate the global signal (lower panel) and therefore the peaks and lows are similar to the global data, without any clear trend over the length of the record. The Northern Hemisphere's main cyclone season is June–November. The Southern Hemisphere ACE values (upper panel in Figure 56) are generally lower than for the Northern Hemisphere, and the main cyclone season is December–April.

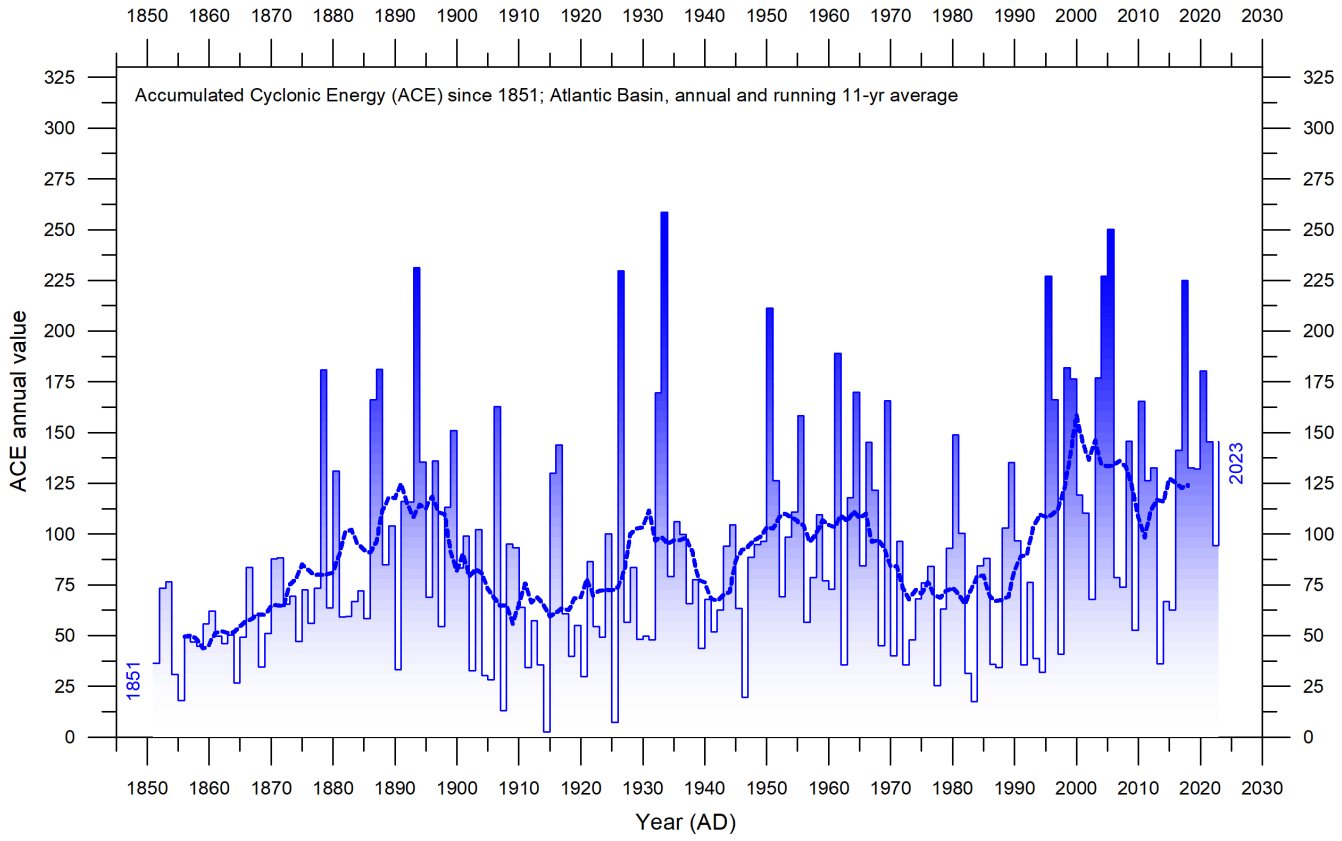

FIGURE 57: Accumulated cyclonic energy (ACE; Atlantic basin) per year since 1851 AD. Thin lines show annual ACE values, and the thick line shows the running 7-year average. There is probably an undercount bias of storms before the satellite era (prior to the mid–1960s), due to the difficulty in identifying storms from available information. Data source: ACE data.

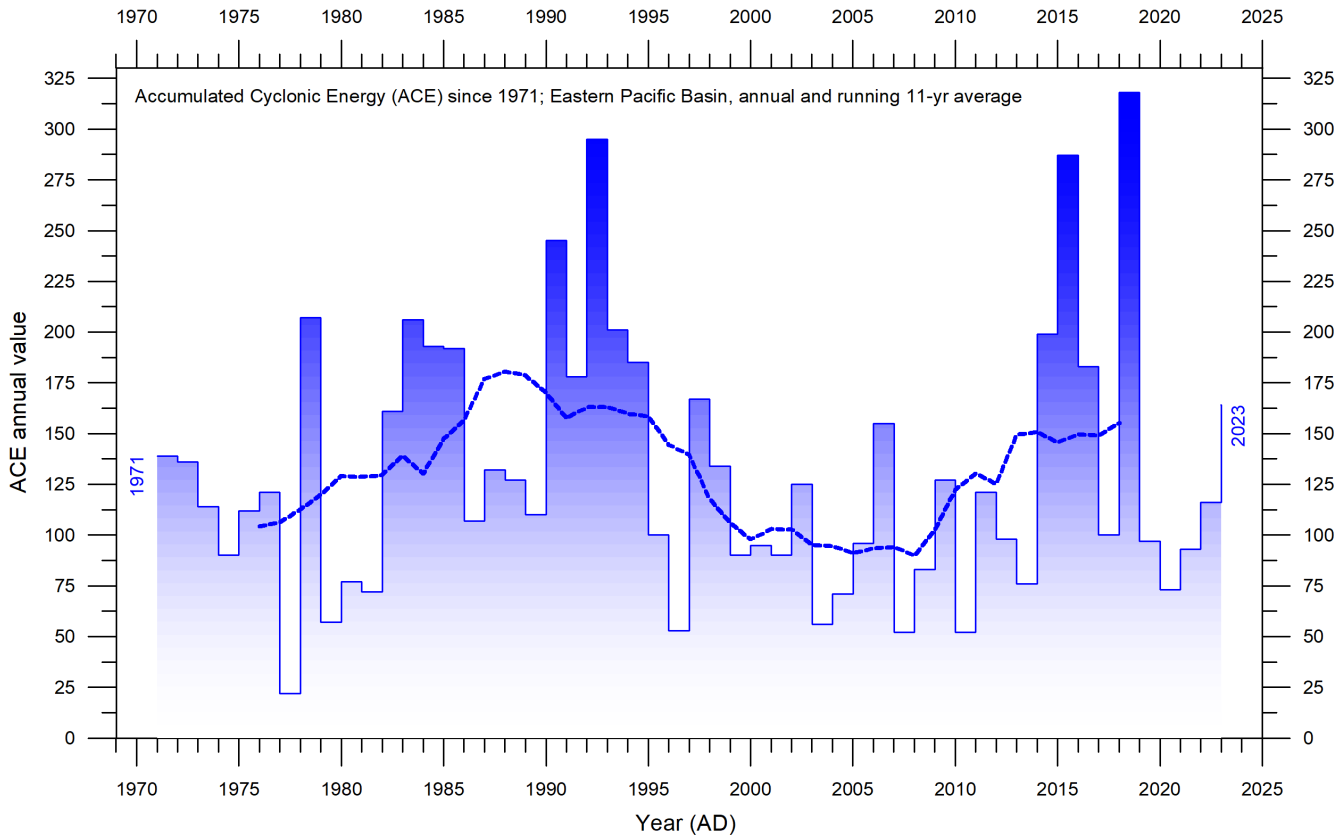

FIGURE 58: Accumulated cyclonic energy (ACE; Eastern Pacific Basin) per year since 1971 AD. Thin lines show annual ACE values, and the thick line shows the running 7-year average. Pacific Basin ACE-data is not considered reliable before the 1971 season, and therefore not shown here. Data source: ACE data.

The Atlantic Oceanographic and Meteorological Laboratory ACE data series goes back to 1850. A Fourier analysis (not shown here) for the Atlantic Basin (Figure 57) shows the ACE series to be influenced by a important periodic variation of 61.5 years' duration, and possibly also by a 5.6-year period. The Atlantic Basin hurricane season often shows above-average activity when La Niña conditions are present in Pacific during late summer (August–October), as was the case in 2017 (Johnstone and Curry, 2017). The Eastern Pacific Basin data series is much shorter, starting in 1971, and is influenced by an important cycle of 2.4-years' duration, and possibly also by a longer about 28-year period. An ACE peak was apparently reached during 2015-18, but future observations will decide if this conjecture is true or not.

Other storm and wind observations

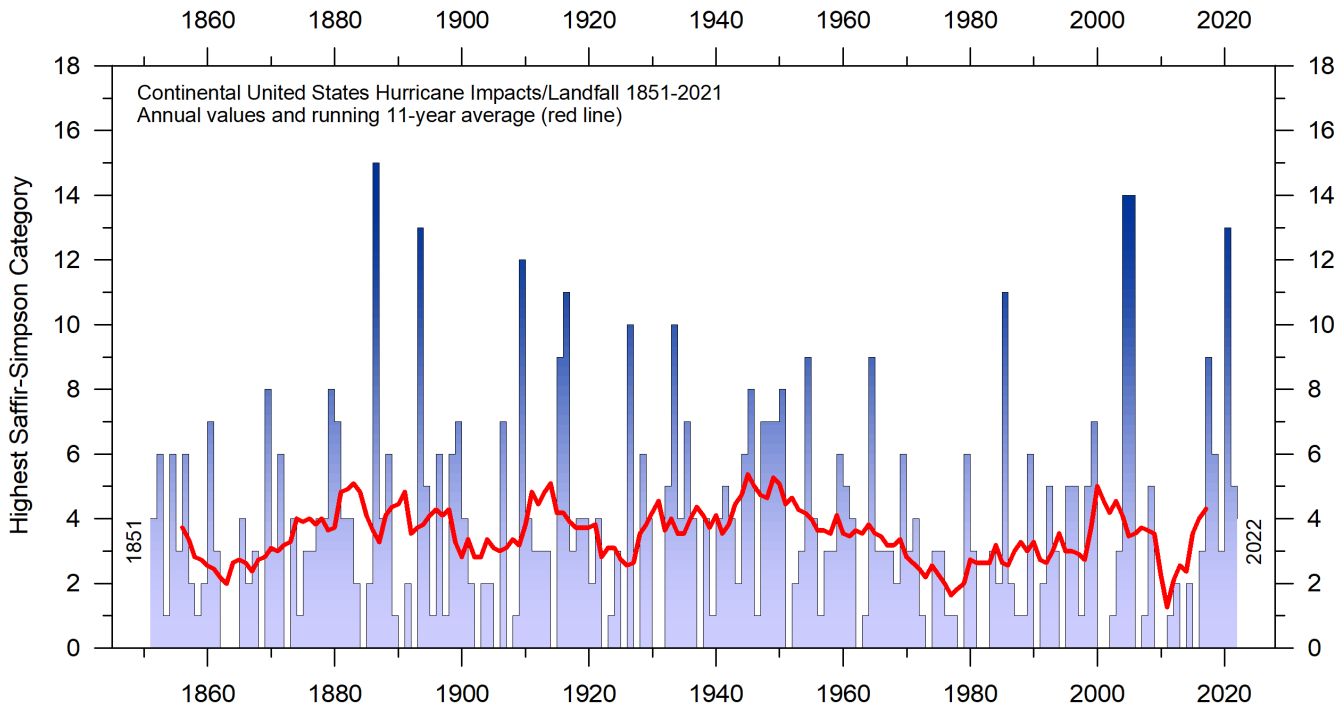

FIGURE 59: Number of Continental United States Hurricane Impacts/Landfalls 1851-2022. The highest Saffir-Simpson Hurricane Scale impact in the United States is based upon estimated maximum sustained surface winds produced at the coast. Data source: Hurricane Research Division, NOAA.

The number of hurricane landfalls in the continental United States is shown in Figure 59. The series shows considerable variations from year to year, but it is not possible to detect any clear trend over time. A Fourier analysis (not shown here) reveals a statistically significant period of about 3.2 years.

An insight into changes in prevailing wind conditions may be obtained from the inspection of observations carried out at coastal meteorological stations situated at particularly wind-exposed places. One example is Lista Lighthouse, in southernmost Norway. It sits on an exposed cape at the extreme southwestern edge of the mainland of Norway, well suited to register wind conditions in the adjoining North Sea and the European sector of the North Atlantic. It has a monthly wind record going back to January 1931, as displayed in Figure 60. This shows that peak wind strengths were recorded shortly after World War II and have since declined somewhat, to some degree mirroring the record of US hurricane landfalls (Figure 59); that is, on the opposite shore of the North Atlantic.

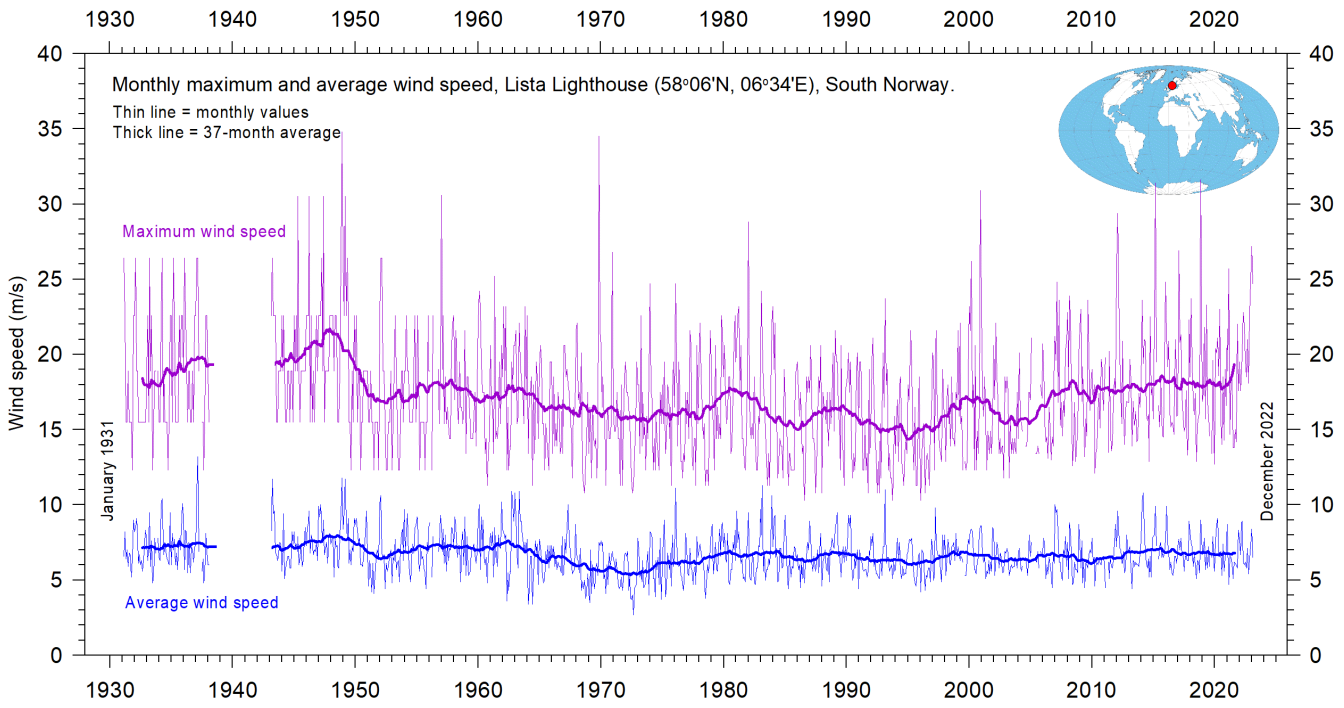

FIGURE 60: Monthly maximum and average wind speed since January 1931 measured at Lista Lighthouse, South Norway. Lista Lighthouse is situated on an exposed cape located at the extreme southwestern edge of mainland Norway, in a position to register wind conditions in the adjoining North See and the European sector of the North Atlantic. Data source: SeKlima.

Written references:

Carter R.M., de Lange W., Hansen, J.M., Humlum O., Idso C., Kear, D., Legates, D., Mörner, N.A., Ollier C., Singer F. & Soon W. 2014. *Commentary and Analysis on the Whitehead& Associates 2014 NSW Sea-Level Report.* Policy Brief, NIPCC, 24. September 2014, 44 pp. http://climatechangereconsidered.org/wp-content/uploads/2014/09/NIPCC-Report-on-NSW-Coastal-SL-9z-corrected.pdf

Chylek, P., Folland, C. K., Lesins, G., and Dubey, M. K. 2010. Twentieth century bipolar seesaw of the Arctic and Antarctic surface air temperatures. *Geophysical Research Letters*, 37, L08703, doi:10.1029/2010GL042793

Holgate, S.J. 2007. On the decadal rates of sea level change during the twentieth century. *Geophys. Res. Letters*, 34, L01602, doi:10.1029/2006GL028492

Johnstone, J. and Curry, J. 2017. *Causes and Predictability of the Exceptionally Active 2017 Atlantic Hurricane Season*. Climate Forecast Applications Network (CFAN), 9 pages. https://curryja.files.wordpress.com/2017/11/hurricane_review_2017-final.pdf

Maue, R.L. 2011. Recent historically low global tropical cyclone activity. *Geophysical Research Letters*, Vol. 38, L14803, doi:10.1029/2011GL047711

Roemmich, D. and J. Gilson, 2009. The 2004-2008 mean and annual cycle of temperature, salinity, and steric height in the global ocean from the Argo Program. *Progress in Oceanography*, 82, 81-100.

Turner et.al. 2017. Unprecedented springtime retreat of Antarctic sea ice in 2016. Geophysical Research Letters, Vol.44(13), p. 6868-6875. https://doi.org/10.1002/2017GL073656

Vignudelli et al. 2019. Satellite Altimetry Measurements of Sea Level in the Coastal Zone. *Surveys in Geophysics, Vol.* 40, p. 1319–1349. https://link.springer.com/article/10.1007/s10712-019-09569-1

Links to data sources, accessed January-February 2024:

ACE data: https://en.wikipedia.org/wiki/Accumulated_cyclone_energy

AMO, Earth System Research Laboratory, NOAA, USA: https://www.esrl.noaa.gov/psd/data/timeseries/AMO/

Atlantic Oceanographic and Meteorological Laboratory, Hurricane research Division: http://www.aoml.noaa.gov/hrd/tcfaq/E11.html

NASA, Atlas of the Biosphere: https://www.jpl.nasa.gov/edu/teach/activity/precipitation-towers-modeling-weather-data/ Credit: Center for Sustainability and the Global Environment, University of Wisconsin - Madison; Climate Research Unit, University of East Anglia.

Continental United States Hurricane Impacts/Landfalls: https://www.aoml.noaa.gov/hrd/hurdat/All_U.S._Hurricanes.html

Colorado Center for Astrodynamics Research: http://sealevel.colorado.edu/

Danish Meteorological Institute (DMI): http://ocean.dmi.dk/arctic/icethickness/thk.uk.php

United States Environmental Protection Agency (EPA): https://www.epa.gov/climate-indicators/climate-change-indicators-us-and-global-precipitation

Earth System Research Laboratory (ESRL): https://www.esrl.noaa.gov/psd/map/clim/olr.shtml

SeKlima: https://seklima.met.no/observations/

GISS temperature data: https://data.giss.nasa.gov/gistemp/

Global Marine Argo Atlas: http://www.argo.ucsd.edu/Marine_Atlas.html

Goddard Institute for Space Studies (GISS): https://www.giss.nasa.gov/

HadCRUT temperature data: http://hadobs.metoffice.com/

Hurricane Research Division, NOAA: http://www.aoml.noaa.gov/hrd/tcfaq/E23.html

Hurricane Research Division, Continental United States Hurricane Impacts/Landfalls: https://www.aoml.noaa.gov/hrd/hurdat/All_U.S._Hurricanes.html

Multisensor Analyzed Sea Ice Extent (MASIE): https://nsidc.org/data/masie

National Ice Center (NIC). http://www.natice.noaa.gov/pub/ims/ims_gif/DATA/cursnow.gif

National Snow and Ice Data Center (NSIDC): http://nsidc.org/data/seaice_index/index.html

NCDC temperature data: https://www.ncdc.noaa.gov/monitoring-references/faq/

Ocean temperatures from Argo floats: http://www.argo.ucsd.edu/

Oceanic Niño Index (ONI): http://www.cpc.ncep.noaa.gov/products/analysis_monitoring/ensostuff/ensoyears.shtml

Outgoing long wave radiation (OLR): https://www.esrl.noaa.gov/psd/map/clim/olr.shtml

PDO, NOAA Physical Sciences Laboratory: https://psl.noaa.gov/pdo/

Permanent Service for Mean Sea Level: http://www.psmsl.org/

Phys.org 2019: https://phys.org/news/2019-01-antarctica-sea-ice-climate.html

Plymouth State Weather Center: http://vortex.plymouth.edu/sfc/sst/

PSMSL Data Explorer: http://www.psmsl.org/data/obtaining/map.html

Rutgers University Global Snow Laboratory: http://climate.rutgers.edu/snowcover/index.php

RSS temperature data: http://www.remss.com/measurements/upper-air-temperature

Sea level from satellites: https://sealevel.colorado.edu/data/2020rel1-global-mean-sea-level-seasonal-signals-retained

Sea level from tide-gauges: http://www.psmsl.org/data/obtaining/map.html

Sea level modelled: IPCC AR6 Sea Level Projection Tool: https://sealevel.nasa.gov/data_tools/17

Sea ice extent Danish Meteorological Institute (DMI): http://ocean.dmi.dk/arctic/icethickness/thk.uk.php

Southern Oscillation Index (SOI): http://crudata.uea.ac.uk/cru/data/soi/

Maue ACE data: climatlas.com/tropical/

UAH temperature data: http://www.nsstc.uah.edu/data/msu/v6.0/tlt/uahncdc_lt_6.0.txt